



DISSERTATION

Implementing model-based building systems control methods in the lighting and shading domain

ausgeführt zum Zwecke der Erlangung des akademischen Grades eines

Doktors der technischen Wissenschaften

unter der Leitung von

Univ. Prof. Dipl.-Ing. Dr. techn. A. Mahdavi

E 259-3 Abteilung für Bauphysik und Bauökologie

Institut für Architekturwissenschaften

eingereicht an der

Technischen Universität Wien

Fakultät für Architektur

Von

MSc Sokol Dervishi

Matrikelnr. 0426897

Wien, Oktober 2010

Kurzfassung

Tageslicht als effiziente natürliche und nachhaltige Energiequelle hat seit jeher eine besondere Bedeutung für das tägliche Leben. Ein effizientes tageslichtorientiertes Design und die lichttechnische Gebäudesteuerung können durch lichttechnische Simulationsprogramme unterstützt und verbessert werden. Die vorliegende Arbeit präsentiert neue Entwicklungen im Bereich simulationsbasierter Gebäudelichtsteuerungssysteme für Beleuchtung und Beschattung.

Essentieller Bestandteil der simulationsbasierten Lichtsteuerung ist das benötigte Himmelsstrahlungsmodell. Unterschiedliche Methoden zur Generierung von Himmelsstrahlungsmodellen werden gezeigt. Diese Modelle können für Simulationen zur Bestimmung von Beleuchtungsstärke und Strahlungsdichte unterschiedlich ausgerichteter Flächen benutzt werden. In dieser Arbeit werden vier Strahlungsdichten von vertikalen Flächen berechnet und mit den zugehörigen Messungen verglichen.

Zur Bestimmung der möglichen Tageslichtnutzung in Räumen benötigen die Simulationen Leuchtdichtedaten des Himmels. Da diese Daten üblicherweise nicht für alle Standorte zur Verfügung stehen, sind Methoden auf Basis von Globalstrahlung unter Verwendung von „Lichtausbeute-Modells“ nötig. Vier dieser Modelle werden verglichen und anhand von Messdaten validiert.

Ein detailliertes Himmelsstrahlungsmodell unter Verwendung eines „Lichtausbeute-Modells“ wird in einer prototypischen Implementierung einer simulationsbasierten Lichtsteuerung integriert. Diese Steuerung verfügt über die Möglichkeit Verschattung und Leuchten auf Basis von Echtzeit-Messungen und numerischen Simulationen des Raummodells zu steuern. Das Raummodell beinhaltet eine detaillierte Beschreibung der Geometrie, Einrichtung, Fenster, Leuchten und der entsprechenden Reflexions- und Transmissionsgrade der Oberflächen, sowie die Lage virtueller Sensoren. Diese virtuellen Sensoren werden zur Aufzeichnung der unterschiedlichen Leistungsindikatoren wie Beleuchtungsstärke, Lichtverteilung und Blendung benötigt.

Abstract

Daylight has always played a dominant role in human life. It is an efficient, natural, renewable source of energy. Advanced lighting simulation tools can provide active support in daylight design and systems control in buildings. The present thesis presents advances in simulation-assisted lighting systems control in the lighting and shading domain.

For the implementation of simulation-assisted lighting systems control detailed sky luminance models are needed. Given this context, alternative methods to derive sky model generation are presented. These sky models can be used in simulation applications to compute illuminance and irradiance values on arbitrarily oriented surfaces. In the present contribution, computed irradiance values on four vertical surfaces with corresponding measurements were compared based on availability of the monitoring data. On the other side, for the daylight availability inside the space, the simulation tools need illuminance data as an input for the generation of the sky luminance models. This data is not commonly measured for most locations. However, the illuminance data can be derived based on more widely available global irradiance data using proper luminous efficacy models. The present thesis compares four global luminous efficacy models for the derivation of illuminance data.

The detailed sky luminance mapping and the luminous efficacy models are applied in a prototypical implementation of a simulation-assisted lighting system control. The control application can control the position of movable window blinds and the dimming level of the luminaires using real-time sensing and numeric simulation. The room model contains detailed description of the geometry, furniture, location and size of windows, reflectance and transmittance properties of surfaces, as well as the position of virtual sensors which monitor different performance indicators such as illuminance levels, light distribution uniformity, or glare indices.

Acknowledgements

The research presented in the dissertation was supported, in part, by a grant from the Austrian Science Foundation (FWF), project number L219-N07. project number: 808563-8846.

Part of the text in the dissertation are adopted from papers, written in relation to the project, and co-authored with Prof. Mahdavi and project-team members

First and foremost, I would like to deeply thank Prof. Mahdavi for his encouragement, advice and continuous support. I also truly appreciate his patience, generosity and tolerance during the studies.

I would like to thank Prof. Kabele for acting as the second examiner for this thesis.

I am fortunate to have the opportunity to work with a group of energetic people in our department. I would like to thank all former and present members including Dipl.-Ing Matthias Schuss, Dr. Kristina Orehounig, Dipl.-Ing Sergio M. Camara, Dr. Bojana Spasojevic, Dr. Claus Pröglhöf and Josef Leichleitner for their support toward the accomplishment of the dissertation.

I would like to thank my very good friend, Ilir Koskija for his generous help toward the software programming related-issues of my work. I would like to thank him also for his constant encouragement and moral support throughout these years. I would like to specially thank Seda Kacel for loving and believing in me. I also would like to thank Taulant Gashi, Everist Limaj and all other friends who were near me in good and difficult moments.

Above all, I am indebted to my parents and my lovely sisters, Nora and Silva for making this effort worthwhile. This work is totally dedicated to them.

Dedicated to my parents and my lovely sisters, Nora and Silva

Table of Contents

Kurzfassung	i
Abstract.....	ii
Acknowledgements	iii
Table of Contents	v
List of Figures.....	viii
List of tables	xiii
1 Introduction	1
1.1 Objective.....	1
1.2 Motivation.....	2
1.3 Background.....	5
1.3.1 Overview	5
1.3.2 Sky models	6
1.3.3 Sky models for inclined surfaces.....	7
1.3.4 Luminous efficacy models.....	8
1.4 Thesis outline.....	9
2 Approach.....	10
2.1 Overview.....	10
2.2 Context model.....	12
2.2.1 General.....	12
2.2.2 Sky luminance mapping	12
2.2.3 Sky models for vertical surfaces.....	18
2.2.3.1 Overview.....	18
2.2.3.2 Methods selected.....	18
2.2.3.3 Measurements	24
2.2.3.4 Comparison.....	27
2.2.4 Luminous efficacy models.....	27
2.2.4.1 Overview.....	27
2.2.4.2 Model selection.....	28
2.2.4.3 Measurements	28
2.2.4.4 Models.....	29

2.2.4.5 Comparison.....	32
2.3 Implementation.....	32
2.3.1 Overview.....	32
2.3.2 Implementation in the testbed.....	34
2.3.2.1 General.....	34
2.3.2.2 Test space.....	34
2.3.2.3 Daylight availability.....	36
2.3.2.4 Control devices and control state space.....	38
2.3.2.5 Control objective.....	40
2.3.2.6 Control process.....	42
2.3.2.7 Validation.....	44
2.3.3 Implementation in the real office space.....	50
2.3.3.1 General.....	50
2.3.3.2 Test space.....	50
2.3.3.3 Daylight availability.....	52
2.3.3.4 Control devices and control state space.....	53
2.3.3.5 Control Objective.....	56
2.3.3.6 Control Process.....	58
3 Results.....	59
3.1 Overview.....	59
3.2 Comparison of sky models on vertical surface.....	59
3.3 Comparison of sky luminous models.....	66
3.4 Simulation Assisted Lighting and Shading Control.....	70
3.4.1 Implementation in the testbed.....	70
3.4.2 Implementation in a real office buildings.....	74
4 Discussion	79
4.1 Overview.....	79
4.2 Sky models for vertical surfaces.....	79
4.3 Luminous efficacy models.....	80
4.4 Simulation-assisted lighting systems control.....	81
5 Conclusion	89
5.1 Contribution.....	89
5.2 Future research.....	90
5.3 Publications.....	91

6	References.....	93
7	Appendix.....	103
7.1	Measurement Equipments.....	103
7.1.1	External.....	103
7.1.2	Internal.....	104
7.2	Reindl Algorithm	104
7.3	Comparison of the vertical irradiance data	106
7.4	Validation of the lighting system of the testbed.....	110
7.4.1	Validation due to the operation of Luminaires.....	110
7.4.2	Validation due to the operation of daylight emulator	112
7.5	Ten-day operation of simulation-assisted lighting control in the testbed (scenario 1).....	115
7.6	Example of sky radiance/luminance map	118

List of Figures

<i>Figure 1 Digital camera with a fisheye lens</i>	<i>15</i>
<i>Figure 2 Fisheye digital image of sky dome (together with the projection of twelve sky sectors as "seen" by illuminance sensors)</i>	<i>15</i>
<i>Figure 3 Comparison of measured external illuminance obtained by twelve sky sectors with the corresponding camera-based values (CIRCUMSOLAR REGION) (Mahdavi 2008).....</i>	<i>17</i>
<i>Figure 4 Comparison of measured external illuminance obtained by twelve sky sectors with the corresponding camera-based values (SUN PATCH) (Mahdavi 2008).....</i>	<i>17</i>
<i>Figure 5 Comparison of measured external illuminance obtained by twelve sky sectors with the corresponding camera-based values (SOLAR DISC) (Mahdavi 2008).....</i>	<i>18</i>
<i>Figure 6 Schematic representation of the DG-I option.....</i>	<i>20</i>
<i>Figure 7 Schematic representation of the DG-P option.....</i>	<i>21</i>
<i>Figure 8 Schematic representation of the G-I option.....</i>	<i>22</i>
<i>Figure 9 Schematic representation of the G-P option.....</i>	<i>22</i>
<i>Figure 10 Schematic representation of the C option</i>	<i>24</i>
<i>Figure 11 Instrumentation for the measurement of horizontal global and diffuse irradiance.....</i>	<i>25</i>
<i>Figure 12 Weather station of the Department of Building Physics and Building Ecology at the Vienna University of Technology, Vienna, Austria</i>	<i>25</i>
<i>Figure 13 Instrumentation for the measurement of the vertical irradiances</i>	<i>26</i>
<i>Figure 14 Digital camera with a fisheye lens (left) and an example of fisheye image of the sky with superimposed patch structure (right)</i>	<i>26</i>
<i>Figure 15 Data processing collected every fifteen minutes during the two-month observation period</i>	<i>26</i>
<i>Figure 16 Test bed's external view.....</i>	<i>35</i>
<i>Figure 17 Internal view of the test room showing the sensors which measure horizotnal illuminance for different dimming levels of the luminaires and the the daylight emulator</i>	<i>35</i>
<i>Figure 18 Schematic representation of the test room.....</i>	<i>36</i>

<i>Figure 19 Schematic section of the test room with daylight emulator</i>	<i>37</i>
<i>Figure 20 External Illuminance at the desk place as a function of lumen flux output</i>	<i>37</i>
<i>Figure 21 Control system scheme (L1, L2: Luminaires; B: Blind; C: Central control instance; E_m: mean workstation illuminance levels as per equation 15)</i>	<i>39</i>
<i>Figure 22 Discretized blind deployment steps</i>	<i>39</i>
<i>Figure 23 Snapshots of six blind positions</i>	<i>40</i>
<i>Figure 24 Preference function for task illuminance.....</i>	<i>41</i>
<i>Figure 25 Preference function for electrical power.....</i>	<i>41</i>
<i>Figure 26 Preference function for cooling.....</i>	<i>42</i>
<i>Figure 27 Schematic representation of the control algorithms.....</i>	<i>43</i>
<i>Figure 28 Instrumentation for the measurement of illuminance levels at 10 locations in the testroom.</i>	<i>45</i>
<i>Figure 29 Comparison of measured and simulated illuminance levels at 10 points in the test room due to the operation of luminaire 1 for light output level 100%.</i>	<i>45</i>
<i>Figure 30 Comparison of measured and simulated illuminance levels at 10 points in the test room due to the operation of luminaire 1 for light output level 100%.</i>	<i>46</i>
<i>Figure 31 Comparison of measured and simulated illuminance levels at 10 points in the test room (see Figure 2) due to the operation of daylight emulator for output level 100%.</i>	<i>46</i>
<i>Figure 32 Comparison of measured and simulated illuminance levels at 10 points in the test room (see Figure 2) due to the operation of daylight emulator for output level 50%</i>	<i>47</i>
<i>Figure 33 Comparison of measured and simulated luminance levels at various points in the test room (desks, walls) under the operation of luminaires L1 and L2.</i>	<i>47</i>
<i>Figure 34 Instrumentation for the measurement of the luminance levels at various levels in the test room (desk, walls)</i>	<i>48</i>
<i>Figure 35 internal view of the testbed showing the camera used to measure the luminance levels on the desk.</i>	<i>48</i>
<i>Figure 36 Operation of luminaire 1 for light output level 50% and daylight emulator for light output level 100%.</i>	<i>49</i>

<i>Figure 37 Operation of luminaire 1 for light output level 100% and daylight emulator for light output level 100%.</i>	<i>49</i>
<i>Figure 38 Operation of daylight emulator for light output level 50%.</i>	<i>49</i>
<i>Figure 39 Operation of daylight emulator for light output level 100%.</i>	<i>49</i>
<i>Figure 40 Operation of luminaire 1 for light output level 100%.</i>	<i>50</i>
<i>Figure 41 Operation of luminaire 1 for light output level 100%.</i>	<i>50</i>
<i>Figure 42 Exterior view of the building, Styria</i>	<i>51</i>
<i>Figure 43 Interior view of the office</i>	<i>51</i>
<i>Figure 44 Schematic illustration of the test space (L1, L2: luminaires; B: blind; E1 to E3: virtual illuminance sensors)</i>	<i>52</i>
<i>Figure 45 Schematic representation for the prediction of the lighting conditions inside the test room.....</i>	<i>53</i>
<i>Figure 46 Control system scheme (L1, L2: Luminaires; B: Blind; C: Central control instance; E_m: mean workstation illuminance levels as per equations 1) , UGR (Unified Glare Rating)</i>	<i>54</i>
<i>Figure 47 internal view of the blinds used as control devices</i>	<i>55</i>
<i>Figure 48 Discretized blind deployment steps</i>	<i>55</i>
<i>Figure 49 Luminaire 1 and Luminaire 2 used as control devices</i>	<i>56</i>
<i>Figure 50 Preference function for task illuminance</i>	<i>57</i>
<i>Figure 51 Preference function for electrical power.....</i>	<i>57</i>
<i>Figure 52 Preference function for unified glare rating (UGR)</i>	<i>57</i>
<i>Figure 53 Percentage of the results (predicted vertical irradiance values) with respective maximum Relative Error for the five options (orientation: North).....</i>	<i>60</i>
<i>Figure 54 Percentage of the results (predicted vertical irradiance values) with respective maximum Relative Error for the five options (orientation: East)</i>	<i>61</i>
<i>Figure 55 Percentage of the results (predicted vertical irradiance values) with respective maximum Relative Error for the five options (orientation: South)</i>	<i>61</i>
<i>Figure 56 Percentage of the results (predicted vertical irradiance values) with respective maximum Relative Error for the five options (orientation: West)</i>	<i>62</i>
<i>Figure 57 Percentage of the results (predicted vertical irradiance values) with respective maximum Relative Error for the five options (All orientations).....</i>	<i>62</i>

<i>Figure 58 Comparison of measured and simulated vertical irradiance values (option DG-I)</i>	<i>63</i>
<i>Figure 59 Comparison of measured and simulated vertical irradiance values (option DG-I)</i>	<i>63</i>
<i>Figure 60 Comparison of measured and simulated vertical irradiance values (option: G-I).....</i>	<i>64</i>
<i>Figure 61 Comparison of measured and simulated vertical irradiance values (option: G-P).....</i>	<i>64</i>
<i>Figure 62 Comparison of measured and simulated vertical irradiance values (option: C).....</i>	<i>65</i>
<i>Figure 63 Percentage of the results (pairs of measured and derived luminous efficacy values) with respective maximum Relative Error for the four models with the original coefficients</i>	<i>67</i>
<i>Figure 64 Percentage of the results (pairs of measured and derived luminous efficacy values) with respective maximum Relative Error (RE) for the four models with the adapted coefficients</i>	<i>67</i>
<i>Figure 65 MBD results for the adapted luminous efficacy models as a function of solar altitude</i>	<i>69</i>
<i>Figure 66 RMSD results for the adapted luminous efficacy models as a function of solar altitude</i>	<i>69</i>
<i>Figure 67 External Global Illuminance levels in the course of one day.....</i>	<i>71</i>
<i>Figure 68 Predicted values of the relevant control parameter (workstation illuminance level) together with the prevailing external global illuminance (Scenario 1).....</i>	<i>71</i>
<i>Figure 69 Recommended states of shading devices together with global horizontal illuminance values for a reference day (Scenario 1)</i>	<i>72</i>
<i>Figure 70 Recommended states of lighting and shading devices together with the resulting UF values for a reference day (Scenario 1)</i>	<i>72</i>
<i>Figure 71 Predicted values of the relevant control parameter (workstation illuminance level) together with the prevailing external global illuminance (Scenario 2).....</i>	<i>73</i>
<i>Figure 72 Recommended states of shading devices together with global horizontal illuminance values for a reference day (Scenario 2)</i>	<i>73</i>
<i>Figure 73 Recommended states of lighting and shading devices together with the resulting UF values for a reference day (Scenario 2)</i>	<i>74</i>

<i>Figure 74 Predicted workstation illuminance levels together with the prevailing external global illuminance for a reference day in February</i>	<i>75</i>
<i>Figure 75 Recommended states of lighting and shading devices together with the resulting UF values for a reference day in February.</i>	<i>75</i>
<i>Figure 76 Predicted workstation illuminance levels together with the prevailing external global illuminance for a reference day in May.</i>	<i>76</i>
<i>Figure 77 Recommended states of lighting and shading devices together with the resulting UF values for a reference day in May.</i>	<i>76</i>
<i>Figure 78 Predicted workstation illuminance levels together with the prevailing external global illuminance for a reference day in August.</i>	<i>77</i>
<i>Figure 79 Recommended states of lighting and shading devices together with the resulting UF values for a reference day in August.</i>	<i>77</i>
<i>Figure 80 Predicted workstation illuminance levels together with the prevailing external global illuminance for a reference day in November.</i>	<i>78</i>
<i>Figure 81 Recommended states of lighting and shading devices together with the resulting UF values for a reference day in November.</i>	<i>78</i>
<i>Figure 82 Ranking of the system's recommendation amongst all possible control options over the experiment period of 10 days, expressed in terms of relative frequency distribution.</i>	<i>82</i>
<i>Figure 83 Ranking of the scenarios in terms of energy consumption [%] over a year.</i>	<i>86</i>
<i>Figure 84 Ranking of the scenarios in terms of mean illuminance.</i>	<i>86</i>
<i>Figure 85 Ranking of the scenarios in terms of mean glare (UGR) indices</i>	<i>87</i>
<i>Figure 86 Ranking of the scenarios in terms of mean glare (UGR) indices</i>	<i>87</i>

List of tables

<i>Table 1 The three specification options for sky regions associated with the sun position (Mahdavi 2008).....</i>	<i>16</i>
<i>Table 2 Overview of the five options</i>	<i>20</i>
<i>Table 3 Coefficients of Perez et al. model (original version).....</i>	<i>31</i>
<i>Table 4 Coefficients of Perez et al. model (adapted for Vienna data).....</i>	<i>31</i>
<i>Table 5 Discretized device states (dimming steps) for luminaires 1 and 2</i>	<i>40</i>
<i>Table 6 Discretized dimming steps for luminaires 1 and 2</i>	<i>56</i>
<i>Table 7 Maximum relative errors (in %) for 80% of the results</i>	<i>65</i>
<i>Table 8 Percentage of results with a relative error of less than $\pm 20\%$</i>	<i>65</i>
<i>Table 9 Comparison of the options in terms of correlation coefficient and RMSD</i>	<i>66</i>
<i>Table 10 Percentage of results with corresponding maximum relative Error (RE) with original model coefficients.....</i>	<i>68</i>
<i>Table 11 Percentage of results with corresponding maximum relative Error (RE) with adapted model coefficients.....</i>	<i>68</i>
<i>Table 12 Comparison of luminous efficacy models based RMSD and MBD with original model coefficients.....</i>	<i>68</i>
<i>Table 13 Comparison of luminous efficacy models based RMSD and MBD with adapted model coefficients.....</i>	<i>68</i>
<i>Table 14 Mean RE (all options) as a function of incident irradiance range</i>	<i>80</i>
<i>Table 15 Shading deployment schedule</i>	<i>83</i>
<i>Table 16 Overview of the scenarios</i>	<i>84</i>
<i>Table 17 Overview of weight factors for the three cases of scenario five.....</i>	<i>84</i>
<i>Table 18 Overview of the scenarios and their respective energy consumption (for one year), mean task illuminance level, glare (unified glare rating) and utility function</i>	<i>85</i>

1 Introduction

1.1 Objective

The main objective of the work described in this thesis is the advances in the implementation and test of simulation-based building systems control methodology in the lighting and shading domain. A principal goal of this study is to understand the features, functionalities, technology and a prototypical implementation of the control strategy for the optimization of the overall building performance.

For reliable prediction of daylight availability inside the space toward the implementation of simulation-based control systems, the development of detailed and accurate sky luminance models are presented. Given this context, five methods for the derivation of sky model generation are presented. These methods can be used to compute illuminance and irradiance values on arbitrarily oriented surfaces. In the present contribution, computed irradiance values on four vertical surfaces with corresponding measurements were compared based on the availability of the monitoring data of the department of building physics and building ecology. However, for the prediction of the daylight inside the space the simulation tools need as input illuminance data. On the other side, measured external illuminance levels are not available for many locations. Given this fact, the work focuses on the comparison of four global luminous efficacy models for the translation of more widely available irradiance measurements to illuminance levels based on Vienna data.

The sky information data can be incorporated to advanced simulation program for the calculation of the sky luminance maps toward the implementation of simulation-assisted systems control in lighting and shading domain. Two test spaces are selected for the implementation of

the systems control: a testbed (in the laboratory of building physics and building ecology department) and an office space (a real office building in Styria, Austria). The control functionality and performance approach are shown. The concept shows how advanced simulation can be incorporated into building system control logic in the framework of sentient building technologies.

1.2 Motivation

Energy consumption in buildings is a large share of total end use energy. European Union is increasingly dependent on external energy sources and, on the other hand, greenhouse gas emissions are on the increase (European Commission 2009). According to IEA (2008), buildings are responsible for approximately 40% of energy consumption and 36 % CO₂ emissions of European Union. Artificial lighting is estimated to account for 25%–40% of this energy consumption. The potential savings of energy efficiency in the building sector would highly contribute to the reduction of energy consumption. Furthermore, energy performance of buildings is becoming a key to achieve the European Union Climate and Energy objectives, for the reduction of the greenhouse gases and energy saving till 20% by 2020 (European Commission 2009).

Over the past few years, daylighting has emerged as a new potential source toward energy savings. The European Commission merges to produce design guidelines wishing to incorporate daylight utilization principles within buildings for the displacement of the electrical power consumption associated with artificial lighting. As an alternative to artificial lighting, daylighting is a lighting source that most closely matches human visual response and provides more attractive and pleasant indoor environment (Webb 2006).

Many authors have studied the positive effect of daylight on visual comfort, energy efficiency as well as human health, productivity and

work ability. People highly prefer windows in their office and associate daylighting with healthy buildings and indoor quality of the environment. They demand natural light for their performance improvement and well-being and value the view provision of the window (Leslie 2003). View gives the occupant visual information about the changing weather during the time of the day and surrounding environment. Occupants prefer to be near windows, where the natural light is better and they like to have activities in bright spaces.

Besides the visual aspect, daylight is concerned with biological effect, such as its relationship with human productivity and performance. Gwinner et al. (1997) has proved that exposure of the light levels influence the suppression of melatonin. This hormone is responsible for regulating the circadian rhythm. As the magnitude of the daylighting levels is above normal electric lighting levels in buildings the influence for the suppression of melatonin is higher. Rea et.al (2001) has shown that the melatonin suppression is more efficient with natural light sources which have higher energy levels in the shorter wavelengths. The quantity and quality of light for the control of the circadian system can be provided with the use of daylight. Besides, daylight light levels with darkness exposure at night make possible to synchronize human sleep/wake cycle. In addition, it can avoid other disorders such as mood shifts (seasonal effective disorder), fatigue or reduced performance. These disorders can result during the light intensity disruption, duration or time exposure to light.

Holick (2010) gives an in-depth research of the positive effect of sunlight for calcium regulation and bone metabolism. Sun exposure can generate vitamin D. This vitamin is vital for the regulating calcium and bone metabolism and for a variety of other non-calcemic actions which are related to decreasing risk of common cancers, autoimmune diseases, infectious diseases and heart disease. Overall, people value the variety of daylight, naturally adapt and enjoy the presence of sunlight inside a building.

However, on the other hand, buildings with integrated daylighting strategies are rare. The complexity of the daylight may explain this situation. Daylighting is dynamic in nature, non uniform, composed of the diffuse skylight, direct sunlight, which varies during the time and weather change. For instance, for commercial buildings in USA only 10% have some daylighting schemes while almost 50% of the buildings are equipped with energy efficient lamps and ballasts (Roisin 2008).

The integration of daylight with electrical light is an important and useful strategy toward energy-efficient building environment and for the provision of the desired light levels throughout the day of the year. Different lighting control systems have been developed for achieving the combination of daylighting with artificial light. The combinations can use simple daylight coefficients, advanced calculation algorithms or accurate simulation tools mainly for photosensor-based lighting control systems. These studies have researched on the implementation of lighting control systems, but made no link with the daylight modeling. The advanced algorithm systems are mainly used for various photoelectric and manual controls for the simulation of photosensor-based lighting control toward the improvement of photosensors (Littlerfair 1998). The simulation mainly involves the comparison between the systems, their selection, placement and commissioning (Choi et al 2005). However, these control systems are limited for different reasons. Firstly, the photosensors require significant effort to properly place and calibrate the photosensor system. In additions, there is a wide range of variety of the photosensor selection which brings difficulties for the prediction and comparison among them (Ehrlich et al. 2002). In addition, physical sensors can typically monitor only limited kinds of performance indicators (e.g., illuminance in case of lighting controls) (Mahdavi 2008).

Reliable and real-time information of the daylight availability is enhanced by different techniques, using digital imaging or detailed sky luminance models. The sky information data can be incorporated to advanced simulation program for the calculation of the sky luminance maps.

The use of simulation techniques offers a number of advantages. In comparison to physical sensors (e.g., illuminance in case of lighting controls), virtual sensors consider more performance indicators (such as illuminance distribution, uniformity factors and various glare indices). In addition, changes in the test space can be reflected digitally in the building model which can reduce the use of physical sensors. Moreover, accurate simulation tools can support proactive control processes (Mahdavi 2008). In this case building simulation programs can produce a multi-aspect virtual model of the building that runs parallel to the building actual operator (Mahdavi 1997, 2001a, 2003a).

1.3 Background

1.3.1 Overview

For the generation of sky luminance mapping via simulation toward the implementation of simulation-assisted lighting and shading systems control appropriate sky models are needed. In the past, various sky luminance distribution models have been developed. Given this context, an in-depth background of different sky models for the derivation of sky luminance maps is presented. Concerning the estimation of illuminance and irradiance on building surfaces, different methods proposed by various authors are investigated.

Simulation tools need illuminance data as an input for the generation of sky luminance maps for daylight prediction inside the space. As measured external illuminance levels are not available for many locations, the more widely available irradiance measurements can be translated, using proper luminance efficacy functions, into illuminance values. This section presents an overview of different luminous efficacy models developed in various locations.

1.3.2 Sky models

Several authors have suggested different of sky luminance distribution for the evaluation of the daylight environment.

Moon and Spencer (1942) suggested the first empirical equation for the luminance distribution on the overcast sky which was adopted by the International Commission on Illuminance (CIE) as the standard for the luminance overcast-sky. A trigonometric relation was used to describe the changes of luminance from the horizon to zenith. The CIE Standard Overcast sky resembles a considerably dark sky covered with thick clouds and it is the first CIE standard sky with non-uniform luminance distribution (CIE 1955).

Kittler (1967) proposed the luminance distribution on the clear model as standard which was adopted as the CIE standard clear sky (1973). The CIE Standard Clear Sky shows very close luminance distribution of the completely clear up sky with variance over both, altitude and azimuth. It is brighter around the sun and dimmer opposite it.

Both CIE standard skies show extreme sky conditions from completely cloudy to clear sky. The luminance distribution frequency of occurrence for both CIE standard skies was small since most of real skies lie between these skies. A need for a more detailed representation of the real skies was necessary. The CIE standard overcast skies and CIE standard clear skies were developed in a series of publications between 1955 and 1994. Intermediate standard sky was developed by Nakamura et al (1985) to define the distribution of the intermediate sky luminance, by classifying sky conditions into overcast, clear and intermediate. An equation concerning the zenith luminance of the Intermediate sky was proposed at the same time. This model is a kind of the average sky models of each solar altitude of all the skies except for the ones similar to the two CIE Standard Skies (Igawa et al. 1997, 1999).

Different sky luminance models were proposed after by other authors in the past decades. (Igawa et al. 1999, Mardaljevic 1999)

- i. ASRC-CIE model: described as is a linear combination of four skies – the CIE Clear Sky, the Gusev turbid clear sky, the intermediate sky and the CIE Overcast Sky. Depending on the prevailing sky clearness, values of two of the above mentioned skies are selected and combined according to sky clearness and sky brightness (Littlefair 1994).
- ii. The “Matsuura intermediate sky” model. This formulation is based on a model that was proposed by Matsuura to describe sky conditions that have a higher turbidity than the CIE clear sky model. (Mardaljevic 1999)
- iii. Brunger’s model: Parameterising isolation conditions as functions of global to extraterrestrial irradiance ratio is used to describe the sky luminance distribution (Lam et al. 1997).
- iv. Kittler’s model: Illuminance turbidity coefficient, derived from direct illuminance data, of Kittler Homogeneous Sky is used as an input for the Kittler homogeneous sky (Roy et al. 1995).
- v. Perraudau (1988) model: Basic equations for sky luminance distribution with adjustable coefficients were expressed. This model is classified into five categories, that is, the overcast sky, the intermediate overcast sky, the intermediate sky, the intermediate clear sky, and the clear sky. (Littlefair 1994).

Advanced sky models show detailed sky luminance distribution. These models account for other functions such as sky clearness and sky brightness, diffuse and direct components of the solar radiation, sun position and zenith luminance. Such models are Perez all weather sky model (Perez et.al 1993), CIE general sky standard (Darula and Kittler 2002), All Sky Model (Igawa et. Al 1999).

1.3.3 Sky models for inclined surfaces

Over the years, there are a number of models available to estimate global irradiance or illuminance on inclined surfaces from irradiance or

illuminance on a horizontal surface. These models require information of the global and the direct or the diffuse irradiance or illuminance on a horizontal surface and are tested with data obtained for vertical surfaces (Lie et al. 2002).

Temps and Coulson (1977) used an algorithm for calculating the diffuse and direct components on tilted surfaces. Klucher (1978) added a cloudiness function (F) to Temps and Coulson algorithm. The diffuse sky term described by Hay and Davies (1980) includes the circumsolar radiation. Kittler et al. (1997) proposed a new range of 15 standard skies based on more than a hundred selected cases scanned in Berkeley, CA, Tokyo and Sydney. Perez's model (1993) developed five critical coefficients that can be adjusted to account for the luminance distributions under all-weather conditions ranging from totally overcast to very clear. Li et al. (2002) developed an approach to estimate the vertical global irradiance based on direct beam and ground-reflected components. Chirarattananon et al. (2007) investigated various mathematical models for computing global vertical irradiance on building surfaces.

1.3.4 Luminous efficacy models

Several authors have suggested models to derive luminous efficacy for different sky conditions. Littlefair (1988), Aydinli and Krockman (1990), and Chung (1992) presented polynomial relations of different degrees using solar altitude as the only independent input variable for beam luminous efficacy. Another model, which also uses solar altitude as independent variable, was proposed by Robledo and Soler (2000). Littlefair (1988) establishes diffuse luminous efficacy as an interpolation between overcast and clear sky using sky clearness as an indicator. Using Littlefair's model, Chung (1992) and Robledo et al. (2000) developed local luminous efficacy models (based on data from Hong Kong and Madrid respectively) for overcast and intermediate skies. Perez et al.

(1990) developed a luminous efficacy model for all sky types as a function of the solar zenith angle (z), atmospheric precipitable water content (W) and the sky brightness index (Δ). The coefficients of these variables were specified as a function of sky clearness ranges. Munner and Kinghorn (1997) derive global luminous efficacy as a polynomial model for all sky types in which the clearness index (k_t) is the only independent variable. Clearness index is defined as the ratio of global horizontal irradiance (I_g) to extraterrestrial irradiance (I_e). Ruiz et al. (2001) developed a different model for global luminous efficacy for all sky types using clearness index (k_t), and the sun altitude (α) as independent variables.

1.4 Thesis outline

The dissertation is structured in terms of five chapters. Chapter two explains the approach underlying the dissertation. Chapter three shows the main results of the work, including: i) comparison of different methods to computationally derive irradiance (or illuminance) data on vertical surfaces, ii) comparison of the global luminous efficacy models, iii) the implementation results of the simulation-assisted lighting and shading control systems in a test-bed and real office buildings. Chapter four entails the discussion of the results and the section five includes the conclusions.

2 Approach

2.1 Overview

A prototypically implementation of daylight-responsive lighting and shading systems control in buildings is presented. Using real-time sensing and numeric lighting simulation, this system can dynamically control the position of window blinds and the status (on/off, dimming level) of the luminaires. The control system possesses an internal digital representation consisting of room, sky and occupancy models. The room model entails information about geometry, furniture, location and size of windows, reflectance and transmittance properties of surfaces, as well as the position of virtual sensors that monitor pertinent performance parameters such as illuminance levels, light distribution uniformity, or glare indices. (Dervishi and Mahdavi 2010).

Simulation-based systems control requires detailed and accurate sky luminance models for the prediction of daylight availability in indoor environments. Specifically, assumptions regarding sky luminance distribution can significantly affect the outcome of simulations (Mahdavi 2008). Given this context, five methods for the derivation of sky model generation are presented. These methods can be used to compute illuminance and irradiance values on any oriented surfaces. However, in the present contribution the methods are used to compare computed irradiance values on four vertical surfaces with corresponding measurements based on the availability of the monitoring data.

One approach makes use of digital imaging for the provision of sky luminance mapping. The past research efforts (Roy et al. 1998; Spasojević and Mahdavi 2007; Mahdavi et al. 2006) have demonstrated that sky luminance mapping with digital photography can provide an alternative to high-end research-level sky scanners. This approach

requires, a calibration procedure, as the camera is not a photometric device. Besides, alternative methods for sky model generation were based on typically available monitored data of measured global and diffuse horizontal irradiance data.

For the simulation-based lighting and shading systems control, RADIANCE lighting simulation program (Ward 1994, Ward Larson and Shakespeare 2003) is used to construct the sky luminance distribution pattern. RADIANCE is a powerful ray tracing program that enables accurate and physically valid simulations. It supports both daylight and artificial lighting simulation. During the past decade, RADIANCE was validated intensively. Different authors (e.g. Mardaljevic 1999, 2004) have shown that the lighting simulation program possesses high accuracy. However, for the prediction of daylight availability inside the space, RADIANCE lighting simulation program needs illuminance as an input for sky model generation. As measured external illuminance levels are not available for many locations, the more widely available irradiance measurements can be translated, using proper luminance efficacy functions, into illuminance values. This chapter compares four global luminous efficacy models based on a database of measured illuminance and irradiance data from Vienna, Austria. These models typically involve mathematical formulations with multiple coefficients, whose values are derived for a specific location (Dervishi and Mahdavi 2010).

To address the research and development of the implementation of the daylight-responsive lighting and shading systems control, two test spaces were selected (a testbed in the building physics laboratory of the Department and a room in an office building in Styria, Austria). Approaches to dynamically provide the context model (sky luminance distribution map) to the simulation engine of the lighting control system are shown.

2.2 Context model

2.2.1 General

This section illustrates advances in accurate sky model generation and luminous efficacy models for the provision of accurate daylight simulation toward the implementation of lighting systems control in building. The first part illustrates the procedure to provide sky luminance maps of various real occurring skies using a digital camera with a fish-eye converter. The past research efforts (Roy et al. 1998; Spasojević and Mahdavi 2007; Mahdavi et al. 2006, 2008) have demonstrated that sky luminance mapping with digital photography can provide an alternative to high-end research-level sky scanners. The second part shows alternative methods for sky model generation applied to derive vertical irradiance data based on typically available monitored data. Please note that the methods can be used to compute illuminance and irradiance values on arbitrarily oriented surfaces. In the present scenario irradiance values on four vertical surfaces were used for comparison based on the availability of the monitoring data. The third part shows alternative methods for luminous efficacy models based on Vienna data.

2.2.2 Sky luminance mapping

High-resolution sky radiance and luminance distribution still requires complex and high-cost sensing technologies (Mahdavi 2009). Past research efforts (Roy et al. 1998, Mahdavi et al. 2006) have shown that sky luminance mapping with digital photography can provide an alternative to high-cost sky scanners.

“In a recent research effort, the use of a digital camera with a fish-eye converter (figure 1) is further explored toward provision of sky luminance maps of various real occurring skies. Toward this end, an original calibration method is developed. This method involves

simultaneous generation of digital images of the sky hemisphere and measurement of global external horizontal illuminance. A digital camera equipped with a fisheye lens makes it possible to capture images of the entire sky dome. Such a camera is used for the present research, mounted on top of the tower of the Vienna University of Technology. Synchronous measurements of outdoor daylight levels are performed using a precision illuminance meter (with an error range of maximum $\pm 10\%$) integral to the Department's weather station. For each image, the initial estimate of the illuminance resulting from all sky patches on a horizontal surface can be compared to the measured global illuminance. The digitally derived luminance values of the sky patches can be corrected to account for the difference between measured and digitally estimated horizontal illuminance levels. For overcast and intermediate sky conditions (without direct sun), this correction may be applied uniformly to all sky patches. The presence of direct sun, however, necessitates the application of a differential (non-uniform) correction to sky patches. Based on a set of iterations, a simple method is devised for the distribution of this difference across the sky model. Thereby, the difference between measured and calculated global illuminance can be assigned to a sky area associated with the sun position" (Mahdavi 2008). RADIANCE lighting simulation program is used to construct the sky model for the sky luminance distribution pattern.

An algorithm proposed by Roy et al. (1998) allows deriving the luminance values of the particular portions of the sky dome using the RGB values of the image's pixels and the camera metadata such as shutter speed, f-stop number, and ISO number. This algorithm is used as the basis of the initial calculation of sky patch luminance values. A pattern of 256 patches is used to map sky luminance distributions. As mentioned before, the difference between the global horizontal illuminance derived from this initial sky patch luminance distribution and the measured global illuminance provides a means for calibration of

digital sky images. A correction factor, defined as a ratio of the measured global illuminance to the horizontal illuminance obtained from initially calculated sky patch luminance values, can be uniformly applied toward calibration of the sky luminance maps of cloudy skies without visible sun (Spasojević and Mahdavi 2007). While experimental results suggest that the uniform correction factor corresponding to the cloudy skies without visible sun does not exceed 1.1, it may be much larger in case of sunny skies. Thus, for sky conditions involving visible sun, the application of a uniform correction factor is not appropriate. In order to arrive at a generally applicable calibration procedure to derive sky luminance maps from digital images, the aforementioned illuminance difference is assigned to a sky region associated with the sun position (Mahdavi 2008).

Three alternatives are compared to identify experimentally the extent of the region of the sky. Table 2 shows the respective sky areas of the three alternatives.

To empirically test the performance of calibrated digital sky luminance distribution mapping, a sky monitoring device equipped with twelve illuminance sensors was used. The sensors measured the horizontal illuminance resulting from twelve different sky sectors. Figure 2 shows the projection of the twelve sky sectors “viewed” by the sky-monitoring device onto the fish-eye images obtained from the digital camera. The error range of the sensors is maximum $\pm 10\%$. A precision illuminance meter is used to obtain the global horizontal illuminance levels. The illuminance predictions resulting from calibrated sky luminance maps are compared to the respective photometric measurements (Mahdavi 2008). The figures 3 to 5 illustrate comparisons of the measured illuminance values resulting from the twelve sky sectors with the corresponding illuminance levels derived from digital imaging.



Figure 1 Digital camera with a fisheye lens

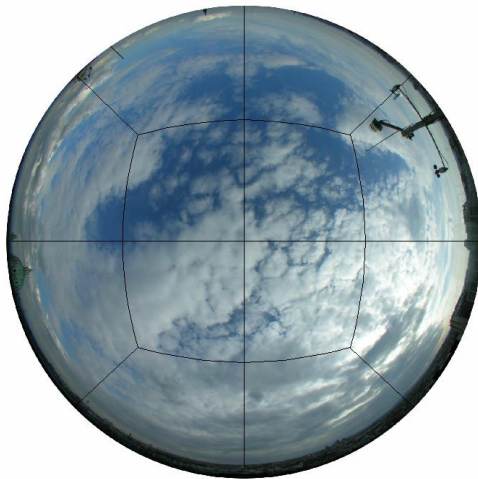


Figure 2 Fisheye digital image of sky dome (together with the projection of twelve sky sectors as "seen" by illuminance sensors)

Table 1 The three specification options for sky regions associated with the sun position (Mahdavi 2008)

Solar region	Description
i. CIRCUMSOLAR REGION	This method includes five patches, one corresponding to the sun position and the four adjacent patches represent sun and its circumsolar region. The initial luminance values of the other 251 patches remain unaltered.
ii. SUN PATCH	This method includes only one patch, where the sun position has been detected. The sun is modeled as a source of direct illumination. The initial luminance values of the other 255 patches remain unaltered.
iii. SOLAR DISC	A small solid angle with an opening cone subtending 0.533 degrees (Duffie and Beckman 1991) is modeled as a source of direct illumination. Solar disc is separately modeled and added to the sky luminance map. The luminance of all 256 sky patches within the initial sky luminance map remains unaltered.

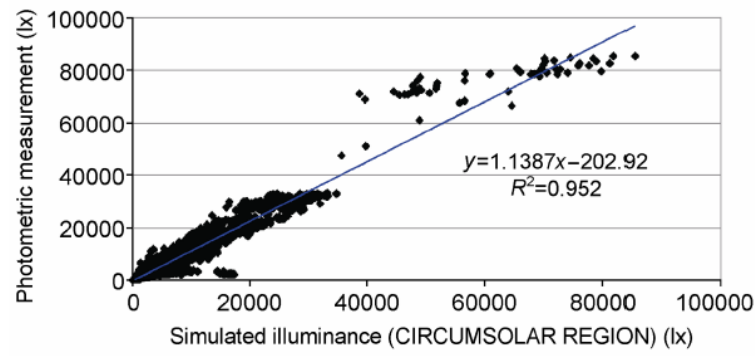


Figure 3 Comparison of measured external illuminance obtained by twelve sky sectors with the corresponding camera-based values (CIRCUMSOLAR REGION) (Mahdavi 2008)

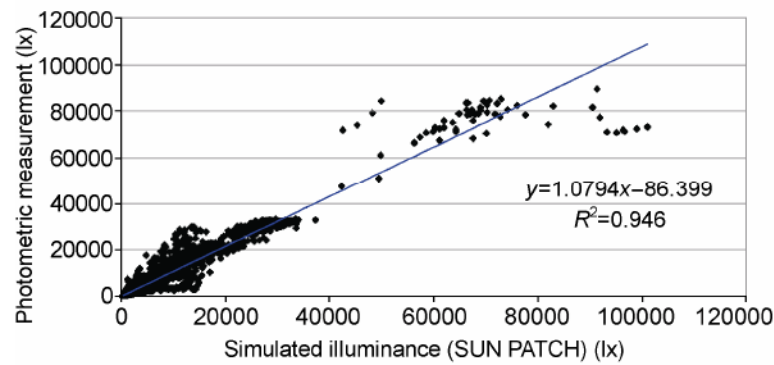


Figure 4 Comparison of measured external illuminance obtained by twelve sky sectors with the corresponding camera-based values (SUN PATCH) (Mahdavi 2008)

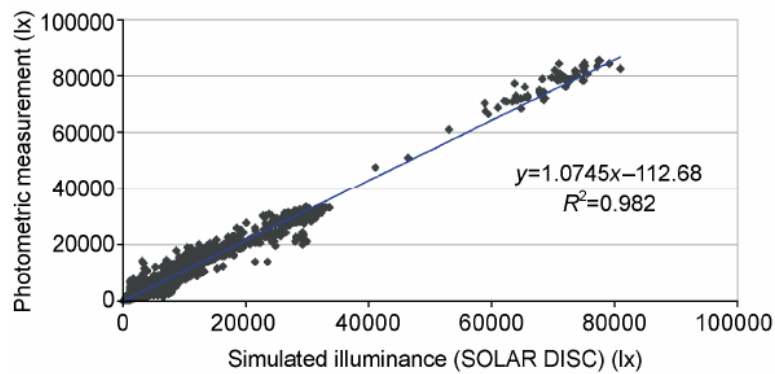


Figure 5 Comparison of measured external illuminance obtained by twelve sky sectors with the corresponding camera-based values (SOLAR DISC) (Mahdavi 2008)

The results suggest that calibrated sky luminance maps derived based on digital photography can provide a reliable basis for locally representative sky descriptions in daylight simulation tools. Thus, the effectiveness of daylight simulation can be enhanced both to support design decision-making and model based lighting control applications. (Spasojevic and Mahdavi 2007, Mahdavi 2008, 2009)

2.2.3 Sky models for vertical surfaces

2.2.3.1 Overview

Five methods for the generation of the sky radiance distribution maps are compared. These methods can be used to compute illuminance and irradiance values on arbitrarily oriented surfaces. However, in present contribution, these maps were used to predict vertical irradiance values based on typically available monitored data of measured global and diffuse horizontal irradiance data.

2.2.3.2 Methods selected

To computationally derive vertical irradiance values, five options were considered (see Table 2). Note that, the options can be used to predict

the illuminance levels as well, given the fact that solar irradiance and outdoor illuminance have characteristics similar in nature (Danny et al 2005). However, in this research, the prediction of the illuminance levels on vertical surfaces was limited on the availability of the monitory instruments of the department.

The first option (DG-I) involves the use of the measured horizontal diffuse and global irradiance values. Using this information, the horizontal direct irradiance can be derived. With the values of horizontal direct and diffuse irradiance as input, the Intermediate sky model (Darula and Kittler 2002, CIE 2003) was applied to generate detailed sky radiance distribution maps. From these maps, vertical irradiance values were derived using the simulation application RADIANCE (Ward Larson and Shakespeare 2003). Figure 6 shows the schematic representation of the DG-I option.

The second option (DG-P) is similar to the first option. However, in this case, the Perez sky model (Perez et al. 1993) was used to generate the sky radiance distribution maps. Perez model requires, as input, the direct normal and the horizontal diffuse irradiance. We calculated the former based on measured values of the direct horizontal irradiance using standard trigonometric functions. Figure 6 shows the schematic representation of the DG-I option. Figure 7 shows the schematic representation of the DG-P option.

Table 2 Overview of the five options

Option	Utilized measured values	Derived values for sky model input	Applied sky model
DG-I	Horizontal diffuse and global irradiance	Horizontal diffuse and direct irradiance	Intermediate
DG -P	Horizontal diffuse and global irradiance	Horizontal diffuse and direct normal irradiance	Perez
G-I	Horizontal global irradiance	Horizontal diffuse and direct irradiance	Intermediate
G-P	Horizontal global irradiance	Horizontal diffuse and direct normal irradiance	Perez
C	Horizontal global irradiance and illuminance, sky luminance map (via calibrated digital photography)	Sky patch radiance values	NA

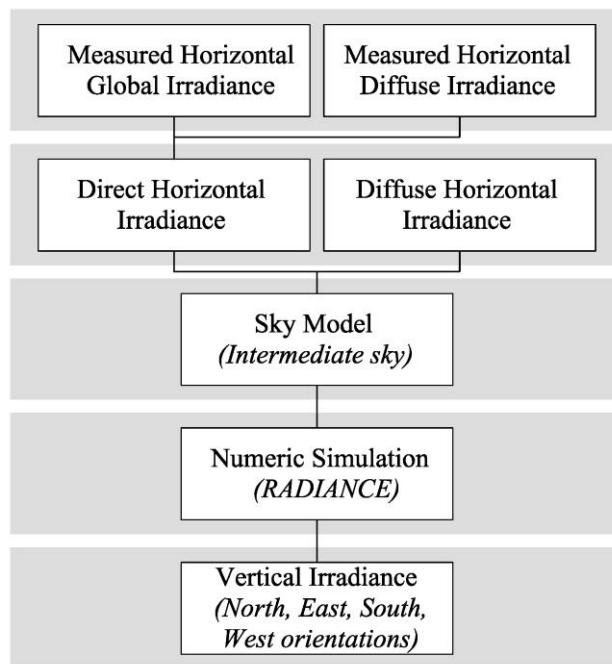


Figure 6 Schematic representation of the DG-I option

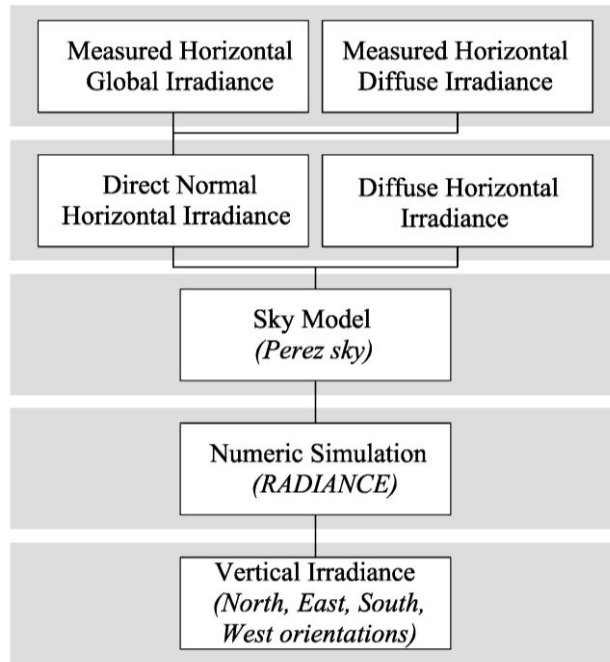


Figure 7 Schematic representation of the DG-P option

The third option (G-I) uses only the measured horizontal global irradiance values as the starting point. From this information, the corresponding diffuse radiation components are derived (Mahdavi et al. 2006) using an algorithm by Reindl et al. (1990). The following parameters are considered for this algorithm: clearness index (k_t), sun altitude (α), outdoor air temperature (T_a) and the relative humidity (RH). The measurements of global horizontal irradiance, outdoor air temperature and the relative humidity were obtained from the weather station of the Department of Building Physics and Building Ecology of Vienna University of Technology. A detailed description of the Reindl algorithm is explained in the Appendix 7.2. For the generation of sky radiance distribution maps, intermediate sky model is used. Sky radiance distribution maps are then generated based on the Intermediate sky model. Figure 8 shows the schematic representation of the G-I option.

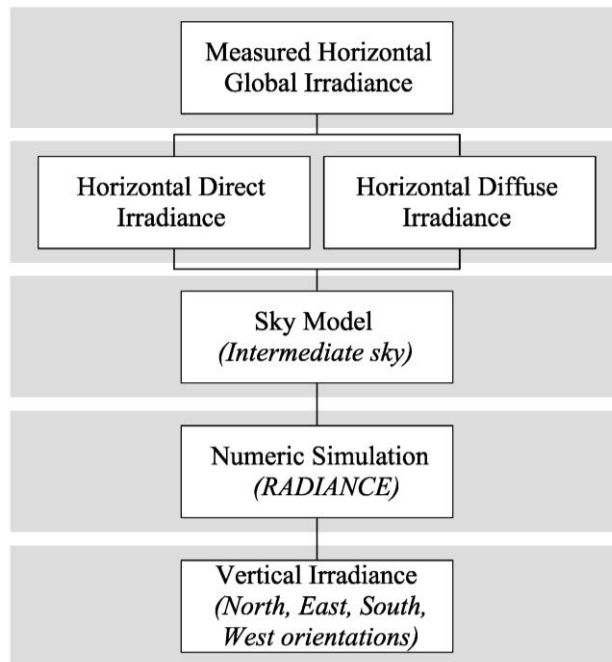


Figure 8 Schematic representation of the G-I option

The fourth option (G-P) is similar to the third option, other than in this case; the sky radiance maps are generated based on the Perez sky model. Figure 9 shows the schematic representation of the G-P option.

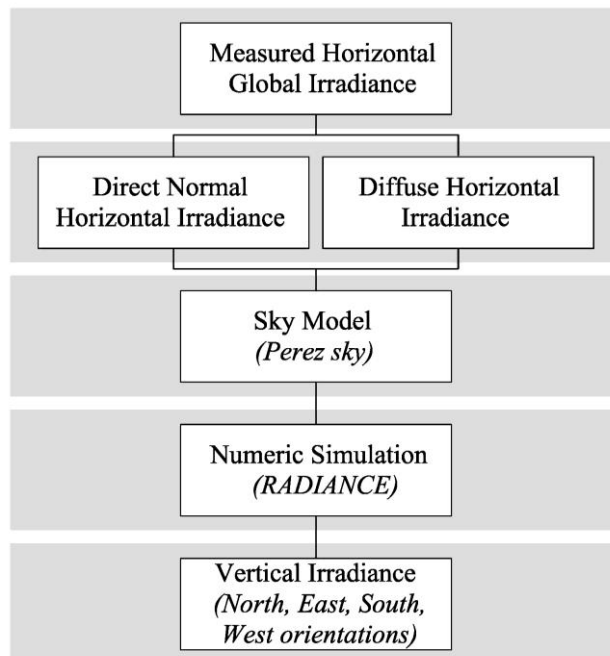


Figure 9 Schematic representation of the G-P option

The fifth option (C) involves the generation of sky radiance distribution maps based on a low-cost sky scanning technique. Thereby, sky images are taken using a digital camera with a fisheye converter. The process of calibrating such digital images to yield photometrically reliable information (sky luminance distribution) has been described in section 2.2.2. The resulting sky patch luminance values were converted into corresponding sky patch radiance values based on the comparison of simultaneously measured global horizontal irradiance and global horizontal illuminance. As with the previous options, the vertical irradiance values are then generated via the RADIANCE simulation application. Figure 10 shows the schematic representation of the C option (Mahdavi and Dervishi 2010).

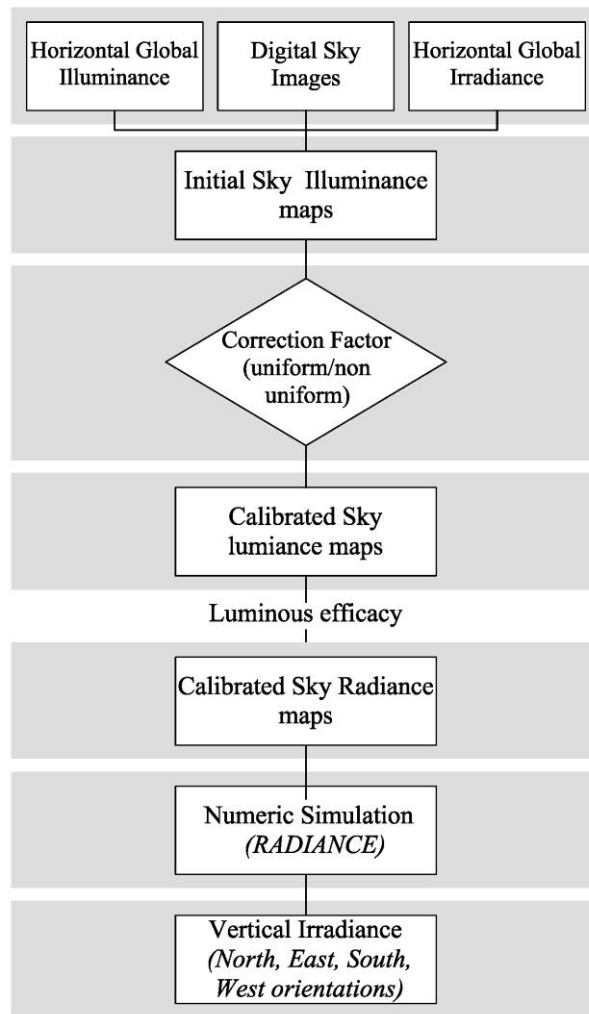


Figure 10 Schematic representation of the C option

2.2.3.3 Measurements

A microclimatic monitoring station of the Department of Building Physics and Building Ecology at the Vienna University of Technology, Vienna, Austria was used to obtain the input data needed for the application of the alternative options. The data was collected on both global and diffuse horizontal irradiance (see figure 11) as well as global horizontal illuminance (figure 12) over a period of 66 days. Moreover, to allow for an empirically based comparison of the options, parallel measurements of vertical irradiance were conducted at the same location for four surfaces facing south, west, north, and east (see Figure 13). Operating in

the same period, the previously mentioned calibrated digital camera took regularly fish eye images of the sky (see Figure 14). The measurements were organized in terms of a data base containing information collected every 15 min during the 2-month observation period (from 25 May 2008 to 29 July 2008), resulting in measured values for 2240 discrete intervals. Only intervals with daylight were taken into account. The measurement period included a variety of sky conditions, from sunny, to partly cloudy, to overcast (Mahdavi and Dervishi 2010). Figure 15 shows a sample of the data processing gathered from the microclimatic monitoring station collected during the two-month observation period. For further information regarding the accuracy of the sensors, see Appendix 7.1

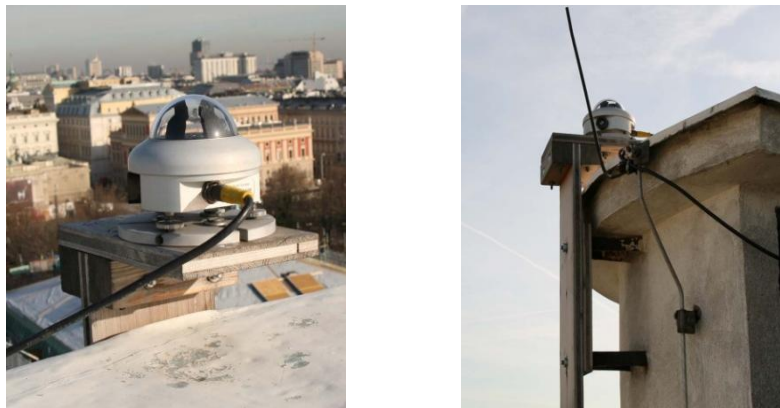


Figure 11 Instrumentation for the measurement of horizontal global and diffuse irradiance



Figure 12 Weather station of the Department of Building Physics and Building Ecology at the Vienna University of Technology, Vienna, Austria

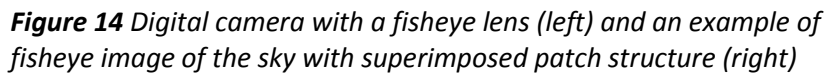
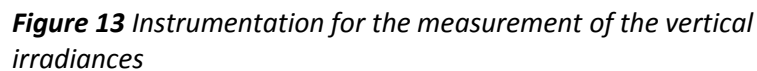


Figure 15 Data processing collected every fifteen minutes during the two-month observation period

2.2.3.4 Comparison

To compare the measurement and simulation results statistically, correlation coefficient (r^2) for the respective linear regressions that describe the relationship between computed and measured vertical irradiance values was considered. In addition, the Root Mean Square Difference (RMSD) as per equation 1, and the Relative Error (RE) as per equation 2 was computed.

$$\text{RMSD} = \sqrt{\frac{\sum_{i=1}^n (M_i - C_i)^2}{n}} \quad \text{Eq. 1}$$

$$\text{RE}_i = \frac{(M_i - C_i)}{M_i} \cdot 100 \quad [\%] \quad \text{Eq. 2}$$

In the above equations:

- n The number of observations
- M Measured value
- C Simulated value

2.2.4 Luminous efficacy models

2.2.4.1 Overview

To perform detailed daylight prediction inside the space via simulation for the implementation of the lighting and shading systems control, appropriate sky models are needed. Such models, however, require illuminance data for the relevant location. As measured external illuminance levels are not available for many locations, the more widely available irradiance measurements can be translated, using proper luminance efficacy functions, into illuminance values. This section focuses on the comparison of four global luminous efficacy models

based on measured photometric and radiometric data obtained in Vienna, Austria (Mahdavi and Dervishi 2010).

2.2.4.2 Model selection

Four models were selected, namely three global luminous efficacy models (Ruiz et al. 2001, Munner and Kinghorn 1997, and Perez et al. 1990) together with a polynomial model proposed by the authors (Mahdavi and Dervishi 2010) based on data obtained in Vienna, Austria. Thereby, two versions of these models were considered: the first with the respective authors' original coefficients, the second with modified coefficients based on Vienna data. Note that the two versions are identical in the case of Mahdavi and Dervishi (2010) model.

2.2.4.3 Measurements

A first database containing measured irradiance and illuminance values over a 2-year period (from January 2005 to December 2006) was established to derive the local version of the models. To compare the selected models in terms of their accuracy, a second database of measured irradiance and illuminance values was used, covering a 30-month period (from January 2007 to 31 of July 2009). Measurements of global irradiance and illuminance were performed every 5 minutes during the daylight hours, covering a variety of sky conditions, from sunny, to partly cloudy, to overcast. A comprehensive data check was performed including 68395 pairs of measured irradiance and illuminance values in the first database and 77244 pairs in the second database. Given the position of the measurement station, time intervals involving very low sun altitudes (less than 5 degrees) were excluded. Likewise, very low global horizontal irradiance values (less than 50 W.m^{-2}) were excluded, given the uncertainty in the sensor accuracy for this radiation intensity range (Mahdavi and Dervishi 2010).

A weather station at the same location monitored other external environmental parameter such as air temperature and air relative humidity parallel to radiometric and photometric measurements.

2.2.4.4 Models

i) Ruiz, Soler, and Robledo model

Ruiz et al. (2001) derive the global luminous efficacy (K_g) as a function of solar altitude (α) and clearness index (k_t) (equation 3).

$$K_g = 104.83 (\sin\alpha)^{0.026} k_t^{-0.108} \quad \text{Eq. 3}$$

Using Vienna data (first data set), a locally adjusted version of this formulation was derived as per equation 4.

$$K_g = 124.84(\sin\alpha)^{0.1176} k_t^{-0.064} \quad \text{Eq. 4}$$

ii) Munner and Kinghorn Model

Munner and Kinghorn (1997) used measurement data from five locations in UK in the 1990s for their model (equation 5).

$$K_g = 136.6 - 74.541 k_t + 57.342 k_t^2 \quad \text{Eq. 5}$$

The locally adjusted version of this formulation (for Vienna data) is expressed in equation 6.

$$K_g = 143.9 - 96.27k_t + 86.22k_t^2 \quad \text{Eq. 6}$$

iii) Perez et al. Model

Perez et al. (1990) express global luminous efficacy as a function of clearness of the sky (ϵ), atmospheric precipitable water content (W), solar zenith angle (z), and the sky brightness index (Δ), by the following equation:

$$K_g = a_i + b_i W + c_i \cos(z) + d_i \ln(\Delta) \quad \text{Eq. 7}$$

Here, a_i , b_i , c_i and d_i are coefficients corresponding to various ranges of the clearness of the sky (ϵ) (see table 1 and 2 for original and adapted coefficients respectively). The clearness of the sky (ϵ) is given by

$$\epsilon = \left[\frac{I_d + I_n}{I_d} + 1.041 z^3 \right] / [1 + 1.041 z^3] \quad \text{Eq.8}$$

where I_d is the diffuse horizontal irradiance, and I_n is the normal incidence direct irradiance. As diffuse irradiance is not measured for most locations, I_d must be calculated. In the present study, an algorithm proposed by Reindl et al. (1990) was used to derive the diffuse component from measured global horizontal irradiance values.

The sky brightness index (Δ) is calculated using equation 9.

$$\Delta = I_d \cdot \frac{m}{I_e} \quad \text{Eq.9}$$

where I_e is the extraterrestrial irradiance and m the optical mass obtained based on Kastens (1993).

The atmospheric precipitable water content (W in units of cm) is given by Wright et al. (1989) as a function of surface dew-point temperature T_d in ($^{\circ}\text{C}$):

$$W = \exp (0.07 T_d - 0.075) \quad \text{Eq.10}$$

Table 3 Coefficients of Perez et al. model (original version)

Range	ε'		Global coefficients			
	Lower bound	Upper bound	a_i	b_i	c_i	d_i
1	1	1.065	96.63	-0.47	-11.50	-9.16
2	1.065	1.230	107.54	0.79	1.79	-1.19
3	1.230	1.500	98.73	0.70	4.40	-6.95
4	1.500	1.950	92.72	0.56	8.36	-8.31
5	1.950	2.800	86.73	0.98	7.10	-10.94
6	2.800	4.500	88.34	1.39	6.06	-7.60
7	4.500	6.200	78.63	1.47	4.93	-11.37
8	6.200	-	99.65	1.86	-4.46	-3.15

Table 4 Coefficients of Perez et al. model (adapted for Vienna data)

Range	ε'		Modified coefficients (for Vienna)			
	Lower bound	Upper bound	a_i	b_i	c_i	d_i
1	1	1.065	103.61	3.60	11.06	-7.78
2	1.065	1.230	94.97	4.06	14.84	-11.84
3	1.230	1.500	97.17	4.33	18.48	-6.80
4	1.500	1.950	111.07	5.40	25.30	11.46
5	1.950	2.800	97.17	4.44	31.34	2.83
6	2.800	4.500	81.34	4.41	28.44	-8.18
7	4.500	6.200	79.20	4.77	28.82	-8.19
8	6.200	-	95.39	4.83	26.52	-0.09

iv) *Mahdavi and Dervishi model*

Using a polynomial formulation (see equation 9), global luminous efficacy (for Vienna) is derived from the clearness index (k_t) and the outdoor air temperature ($^{\circ}\text{C}$):

$$K_g = 140.9 + 0.273 t - 102 k_t + 0.60 t \cdot k_t - 0.001 t^2 + 77.28 k_t^2 \quad \text{Eq.11}$$

2.2.4.5 Comparison

Both the original model versions (with the respective authors' coefficients) and the modified versions (derived by the authors of this paper for the first Vienna data set) were compared using the second Vienna data set. Three common statistical indicators were used for the comparison: the relative mean bias difference MBD (equation 12), the relative error RE (equation 13), and the relative root mean square difference RMSD (equation 14).

$$MBD = \frac{\sum_{i=1}^n (M_i - C_i)}{n} \quad [\%] \quad \text{Eq. 12}$$

$$RE_i = \frac{(M_i - C_i)}{M_i} \cdot 100 \quad [\%] \quad \text{Eq. 13}$$

$$RMSD = \sqrt{\frac{\sum_{i=1}^n [(M_i - C_i) / M_i]^2}{n}} \cdot 100 \quad [\%] \quad \text{Eq. 14}$$

In these equations, M_i is the measured luminous efficacy, C_i is the computed luminous efficacy, and n the total number of pairs of irradiance and illuminance values.

2.3 Implementation

2.3.1 Overview

This section presents a prototypical implementation of an energy-efficient, daylight-responsive lighting systems control in buildings that makes use of real-time sensing and lighting simulation. The simulated-based and proactive system control technology has been formulated in various publications (e.g Mahdavi 2001b, Mahdavi 2008, Mahdavi et al. 2005). The core of this concept is to base the decision of the system of

its future states on virtual experiments with its own digital representation. The virtual model of the building takes information real-time about the properties and states of the components and systems of the building, about the surrounding environment and internal processes (Mahdavi 2009).

The control system possesses an internal digital representation consisting of room and context (external conditions). The room model entails information about geometry, furniture, location and size of windows, reflectance and transmittance properties of surfaces, as well as the position of virtual sensors that monitor pertinent performance parameters such as illuminance levels and glare indices. The room model provides the basis of system's internal representation and is intended to be dynamically updated (Içoğlu, O. & Mahdavi 2007, Mahdavi et al. 2007). The context model (weather and sky conditions) is generated on a real-time basis using different sky model generation (explained in detailed in section 2.2) To provide and maintain the desired performance under dynamically changing internal and external conditions, the proposed simulation-based predictive control system operates as follows: i) At regular time intervals, the system considers a set of candidate control states (i.e., a set of alternative combinations of the states of control devices, namely the position of blinds and the dimming levels of luminaires) for the subsequent time step; ii) These alternatives are then virtually enacted via numeric lighting simulation. Thereby, the simulation application uses the aforementioned digital representation toward the prediction of the implications of these alternative control actions, resulting in values for corresponding performance indicators (e.g. task illuminance levels); iii) These results are compared and ranked according to the preferences (objective function) specified by the occupants and/or facility manager to identify the candidate control state with the most desirable performance; iv) The system either autonomously instructs the pertinent control device-actuator(s) or informs the user to adjust the control state. In the

following sections of this work, we present the implementation of such a control system in two test spaces (a test bed in the building physics laboratory of the Department and a room in an office building in Styria, Austria). (Dervishi and Mahdavi 2010, Mahdavi and Dervishi 2009).

2.3.2 Implementation in the testbed

2.3.2.1 General

In the following sections, firstly the test bed components and configuration, including the installed devices are described. Then, the external data monitoring solution concerning daylight availability is shown. In the end, an illustration of the implementation and validation of simulation-powered building systems control approach in lighting and shading domain is presented.

2.3.2.2 Test space

A realistic office space, located within a larger, general use laboratory space at the Department of Building Physics and Building Ecology of the Vienna University of Technology was used as testbed to demonstrate the simulation-assisted lighting system control strategy. The structure of the testbed is modular and is divided into two rooms. The lighting system consists of two ceiling mounted luminaries and motorized window with blind. A mobile special flat luminaire placed outside the window of the test room is used to emulate the daylight. The daylight emulator can be programmed to provide variable quantities of light of the spaces. Figure 16 shows the external view of the physical test bed layout. Figure 17 shows the internal view of the test room together with

the sensors which measure horizontal illuminance levels. Figure 18 illustrates a schematic section of the test space.



Figure 16 *Test bed's external view*



Figure 17 *Internal view of the test room showing the sensors which measure horizontal illuminance for different dimming levels of the luminaires and the daylight emulator*

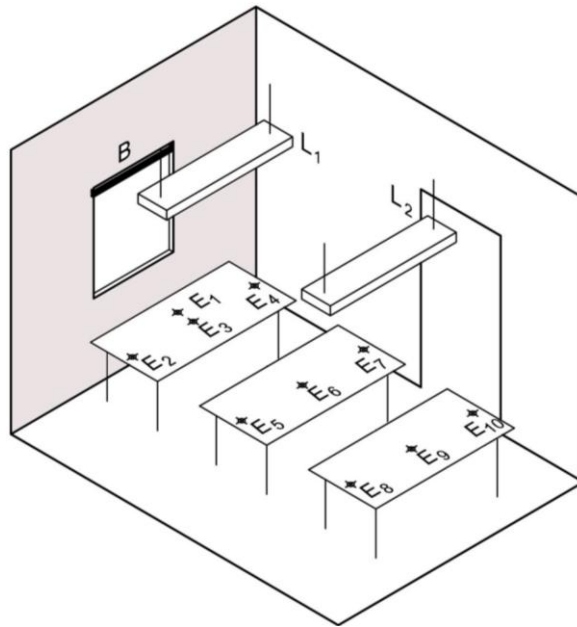


Figure 18 Schematic representation of the test room

2.3.2.3 Daylight availability

For the implementation of simulation assisted lighting and shading control in buildings, two approaches were considered.

In the first scenario, daylight is emulated using a special flat luminaire (STRATO 2008) placed outside the window of the test room (see the schematic illustration in Figure 19). The luminous flux of this source is controlled dynamically according to available external global horizontal illuminance measured via a weather station installed on top of a close-by university building. This daylight emulator is modeled in the lighting simulation application as a light source with a variable luminous flux output that is dynamically determined as a function the of prevailing outdoor global horizontal illuminance. Figure 20 shows the relation between the global horizontal illuminance at the deskplace and lumen flux output concluded based on a set of experiments.

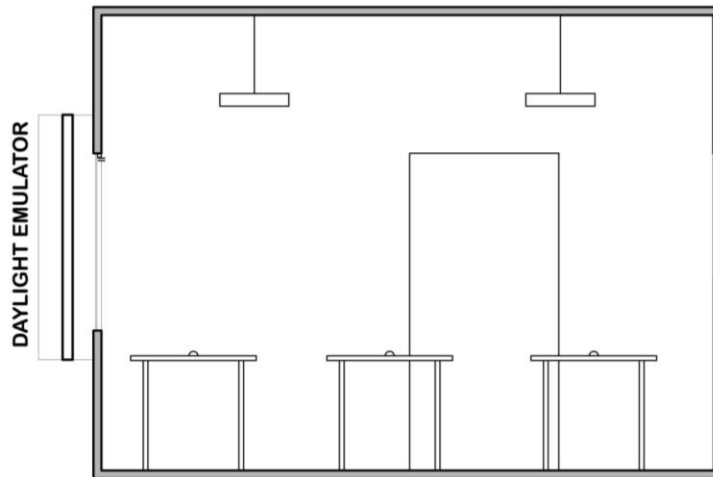


Figure 19 Schematic section of the test room with daylight emulator

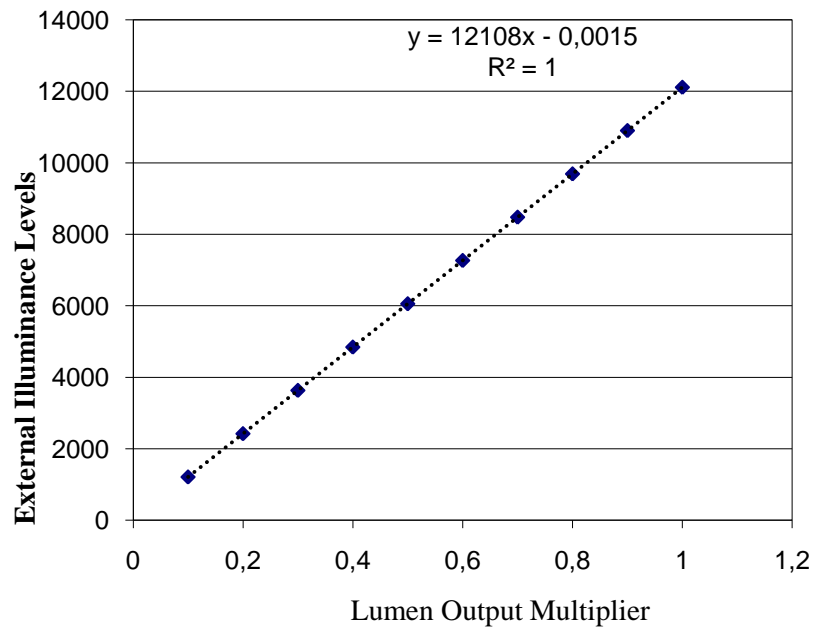


Figure 20 External Illuminance at the desk place as a function of lumen flux output

In the second scenario, the digital camera with a fish-eye converter (figure 14) is used toward provision of sky luminance maps of various real occurring skies (Mahdavi 2008, Mahdavi et al. 2006).

The resulting luminance maps are used as input to the lighting simulation application toward prediction of light distribution inside the test room. Note that, in the latter case, a validation of system's predictions is not possible, as the test room is currently inside a larger laboratory space and does not receive direct daylight (Mahdavi and Dervishi 2009).

Daylight simulations were performed using *RADIANCE* lighting simulation system. *RADIANCE* is a powerful ray tracing program that enables accurate and physically valid lighting and daylighting simulation (Ward 1994, Ward Larson and Shakespeare 2003). For both scenarios, the lighting simulation program, besides the surface properties and geometry of the model, provides detailed information on characteristics of the light source (Mardaljevic 1999, 2004).

2.3.2.4 Control devices and control state space

The lighting system which integrates the daylight and artificial light consists of three control devices. For the amount of the daylight control motorized blind placed inside the windows facing south-west is considered. The artificial light is provided by two suspended dimmable luminaires *Zumtobel Opalis* ($L1$, $L2$) and the window blind (B). In the control scenarios considered, the blinds can be moved up and down, and the slats can be set into horizontal and vertical positions. As a primary indicator of lighting performance, we considered the mean illuminance levels E_m as per equation 15.

$$E_m = (E_1 + E_2 + E_3)/3 \quad (\text{Eq. 15})$$

For the provision of sufficient illuminance on the working places, a central control instance C is required to coordinate the three devices

(two dimmable luminaires, L_1 , L_2 and the window blind B). Figure 21 illustrates the control system, as relevant to the present test scenario. To each device, a discrete number of possible states is allocated. These options include six different positions of the blind (see Figures 22-24) and six discrete dimming positions for each of the two luminaires (see Table 5).

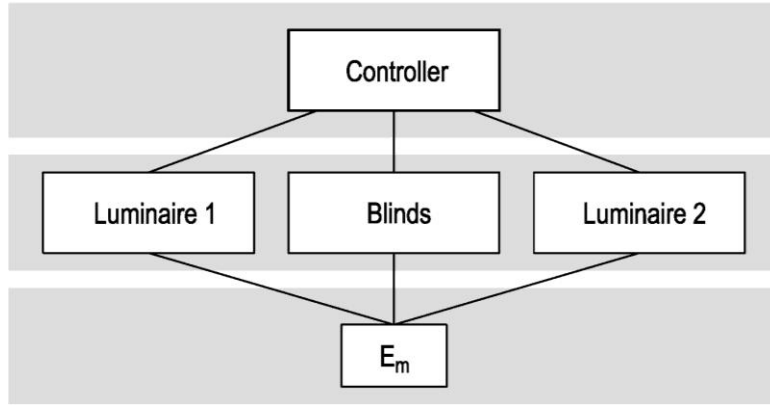


Figure 21 Control system scheme (L_1 , L_2 : Luminaires; B : Blind; C : Central control instance; E_m : mean workstation illuminance levels as per equation 15)

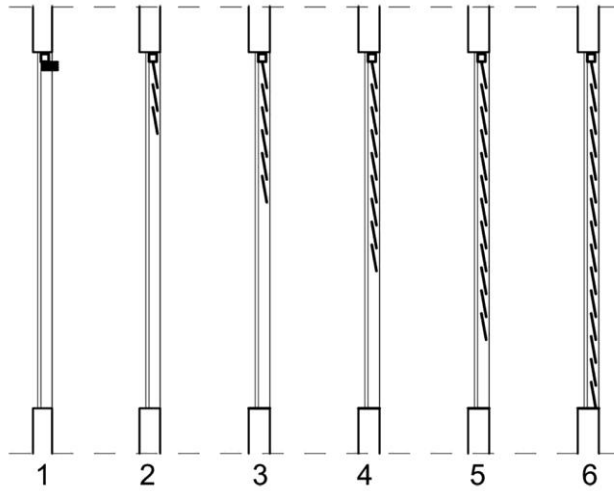


Figure 22 Discretized blind deployment steps



Figure 23 Snapshots of six blind positions

Table 5 Discretized device states (dimming steps) for luminaires 1 and 2

Dimming state	1	2	3	4	5	6
Power output [%]	0	20	40	60	80	100

2.3.2.5 Control objective

A simple control scenario is used to demonstrate the control system. It involves three objectives:

- i) Minimize the deviation of the average illuminance (E_m) on the working planes. The concept of “useful daylight illuminance” (Nabil and Mardaljevic 2005) provided, in this case, the basis for corresponding preference function PE (see Figure 24);
- ii) Minimize electrical energy use. A possible formulation of the corresponding preference function P_L is shown in Figure 25. It is obtained by "inverting" the luminaires' dimming curve (luminous flux as a function of electrical energy input);
- iii) Minimize cooling load. A possible corresponding preference function (PC) for the latter objective is shown in Figure 26. The reason is to avoid unnecessary high illuminance levels as they typically involve heat gain, which introduces additional cooling loads.

The overall behavior of the control system is determined through a utility function (UF). The objective of the control process is to maximize

UF. Equation (16) provides an example for such a utility function (Mahdavi 2006 et al., 2008, 2009).

$$UF = w_E \cdot P_E + w_c \cdot P_c + w_L \cdot P_L \quad (\text{Eq.16})$$

In this equation P_E , P_c and P_L are the preferences for illuminance levels (E_m), cooling load, and electrical energy consumption. The corresponding weights are represented by w_E , w_c and w_L . Related illustrative preference functions are shown in Figs. 24 – 26.

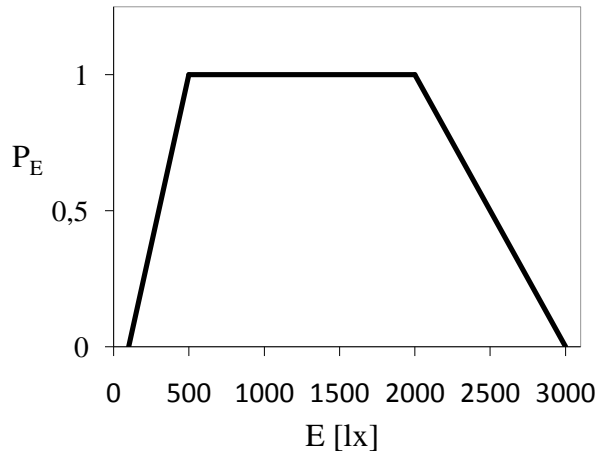


Figure 24 Preference function for task illuminance

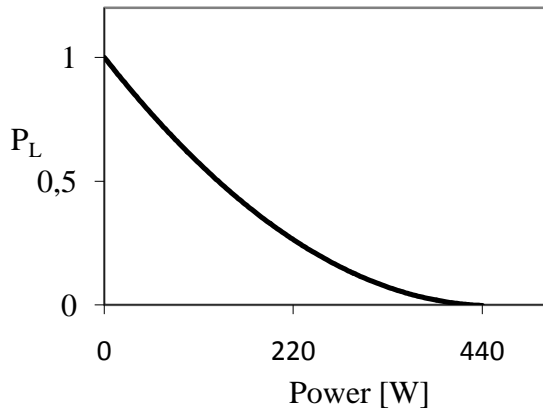


Figure 25 Preference function for electrical power

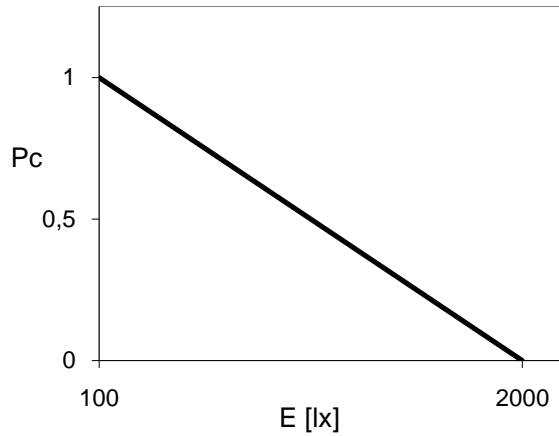


Figure 26 Preference function for cooling

2.3.2.6 Control process

A control scenario is involved through a control cycle repeated regularly every 15 minutes steps. The set interval is not fixed and it can be changed at any time with a condition not to be shorter than the time needed for the simulation-based assessment of the control state space (less than 15 minutes in the present scenario) (Mahdavi 2008).

The controller application C, at time step t_i , considers a list of candidates for each device (two luminaires, L_1 and L_2 and the blinds, B) for the time step t_{i+1} . In the present case, four alternative options are considered for each device. These options are the device's current position, the two neighboring states, and a fourth—randomly chosen—option from the rest of the device's control state space. Thus, the resulting overall option space encompasses a maximum of 64 distinctive control states. Thus, values of multiple building performance indicators (e.g. horizontal illuminance at various locations in the space, illuminance distribution uniformity, different glare indicators, electrical energy use for lighting) are computed for a future time step t_{i+1} . In the present case, the options were compared in view of the corresponding resulting workstation illuminance E (arithmetical average of illuminance levels computed for positions E_1 to E_3 as per equation 15) and electrical power demand of

the artificial lighting. For this purpose, the lighting simulation program RADIANCE (Ward Larson & Shakespeare 2003) is adopted.

Given the obtained values of E_m as well as electrical energy use (derived based on the identified dimming state of the luminaires), UF values can be derived using Equation 16. Thus, at each time step, the control state with the maximum utility function can be identified for the subsequent time step. For the purpose of the following illustrative system operation experiments, the values of these weights were assigned to be 0.4, 0.35, and 0.25 respectively. Illustrative preference functions are shown in Figures 24-26 (P=1 indicates highest, P=0 lowest preference). Note that these preference functions and weights merely serve toward demonstration of the overall system operation. In real use situations, more sophisticated functional relationships between user preferences and ranges of measurable indoor environmental parameters must be formalized and implemented. Moreover, such preference functions need not be static, but can be dynamically manipulated by users to facilitate transient changes in operational requirements (Mahdavi and Dervishi 2009). Figure 27 shows a schematic representation of the control system.

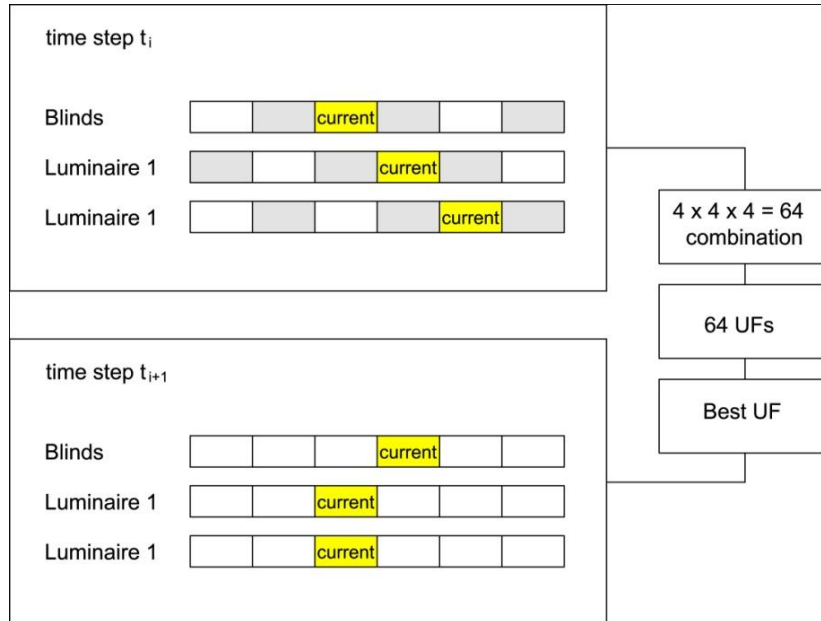


Figure 27 Schematic representation of the control algorithms

2.3.2.7 Validation

The system demonstrates the working of the feed forward lighting and shading control mechanism. However, the performance of the system is dependent on the accuracy of the predictions of the system's simulator. As mentioned previously, it was possible to validate the predictions of the control system's embedded lighting simulator. Toward this end, simulated illuminance and luminance values with corresponding measurements were compared.

A Luxmeter cell instrumentation (C. A 808 Chauvin Arnoux) (figure 28) was used to measure the illuminance levels at 10 locations in the test room (figure 18 and 19) due to the operation of the luminaires and the daylighting emulator. The detailed description of the sensor is in the appendix 7.1.

Figure 29 and 30 show a comparison of measured and simulated horizontal illuminance levels at 10 locations in the test room due to the operation of Luminaire 1. Thereby, two dimming states (100% and 60%) are considered. Likewise, Figure 31 and 32 show a comparison of measured and simulated horizontal illuminance levels at the same 10 locations due to the daylight emulator operation (at two output levels, namely 100% and 50%).

Figure 33 contains the comparison of simulated and measured luminance values at 24 points in the test space (9 on the desks and 15 on the walls). A luminance meter instrumentation (figure 34) was used to measure the luminance levels at various levels in the test room (desk, walls). The detailed description of the instrumentation is referred in the appendix 7.1. Measurements (and corresponding simulations) were conducted for different dimming levels of the luminaires (L1 and L2) (figure 35) and the daylight emulator, resulting in 49 data pairs shown in Figure 33. Figure 36 to figure 41 illustrate the operation of the luminaire and the daylight emulator for different output levels.

As Figures 29-33 illustrate, there is a high degree of agreement between measured and simulated results. This documents the reliability of the simulation kernel of the predictive control unit and, consequently, the validity of the recommended control actions. (Mahdavi and Dervishi 2009)



Figure 28 Instrumentation for the measurement of illuminance levels at 10 locations in the testroom.

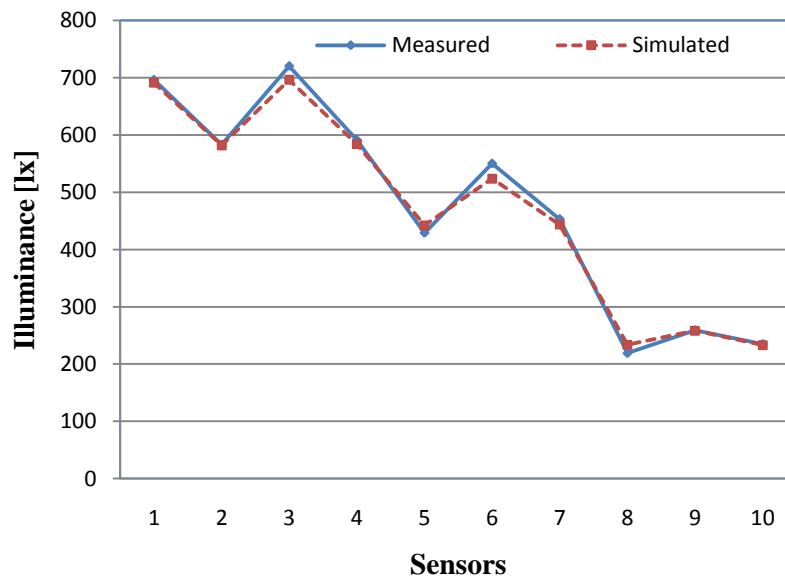


Figure 29 Comparison of measured and simulated illuminance levels at 10 points in the test room due to the operation of luminaire 1 for light output level 100%.

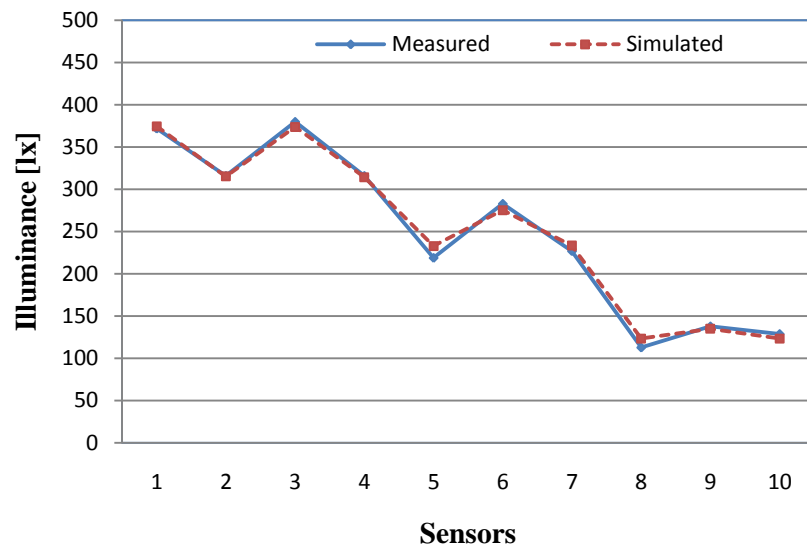


Figure 30 Comparison of measured and simulated illuminance levels at 10 points in the test room due to the operation of luminaire 1 for light output level 60%.

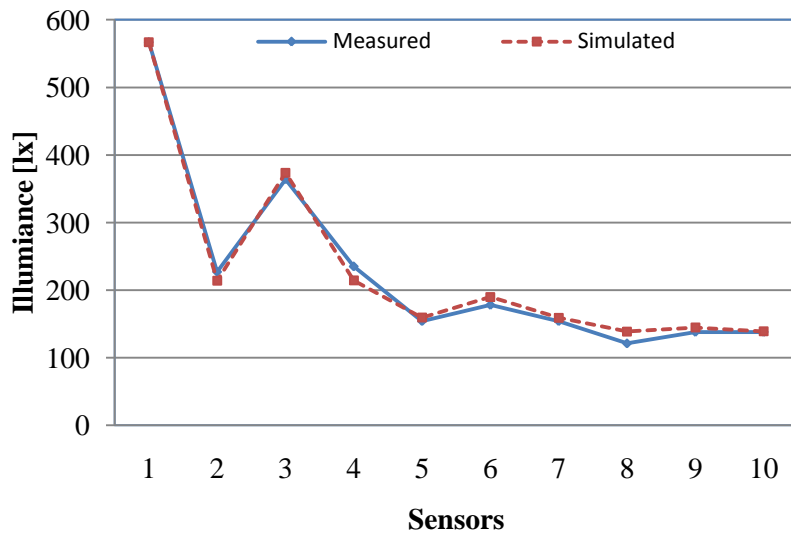


Figure 31 Comparison of measured and simulated illuminance levels at 10 points in the test room (see Figure 2) due to the operation of daylight emulator for output level 100%.

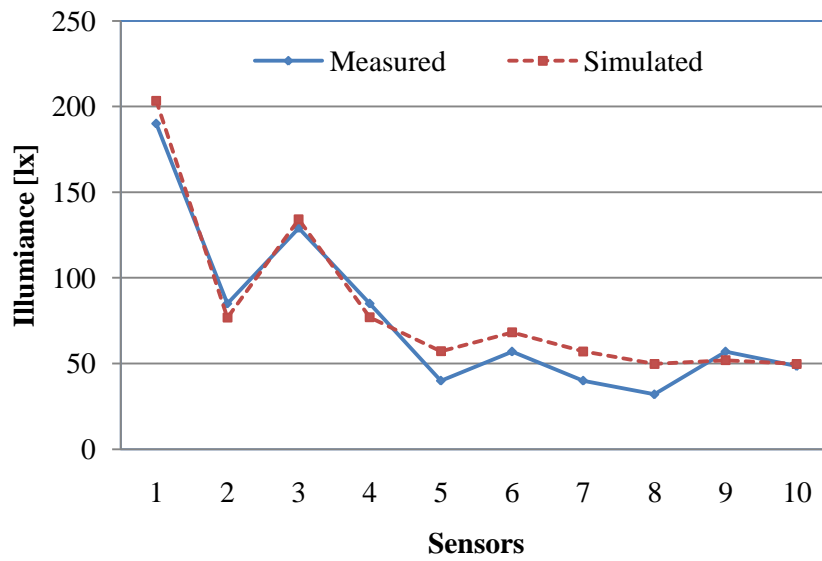


Figure 32 Comparison of measured and simulated illuminance levels at 10 points in the test room (see Figure 2) due to the operation of daylight emulator for output level 50%

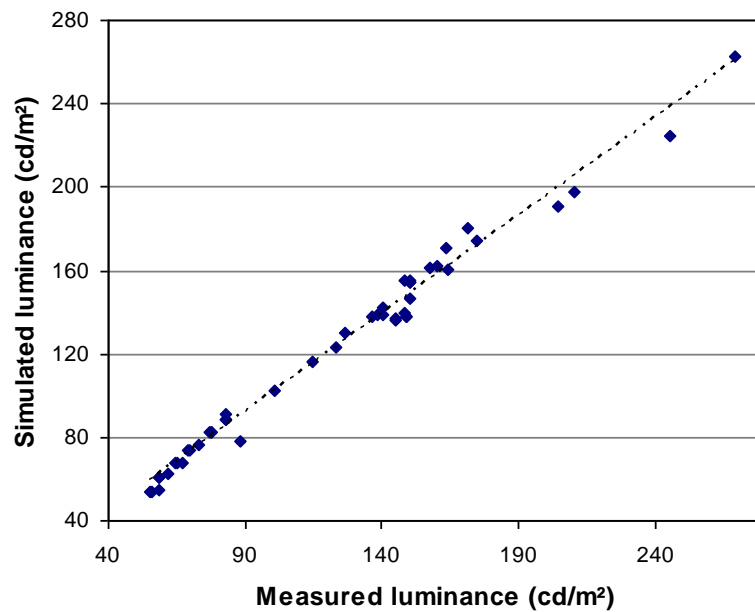


Figure 33 Comparison of measured and simulated luminance levels at various points in the test room (desks, walls) under the operation of luminaires L1 and L2.



Figure 34 Instrumentation for the measurement of the luminance levels at various levels in the test room (desk, walls)



Figure 35 internal view of the testbed showing the camera used to measure the luminance levels on the desk.



Figure 36 Operation of luminaire 1 for light output level 50% and daylight emulator for light output level 100%.



Figure 37 Operation of luminaire 1 for light output level 100% and daylight emulator for light output level 100%.



Figure 38 Operation of daylight emulator for light output level 50%.



Figure 39 Operation of daylight emulator for light output level 100%.



Figure 40 Operation of luminaire 1 for light output level 100%.

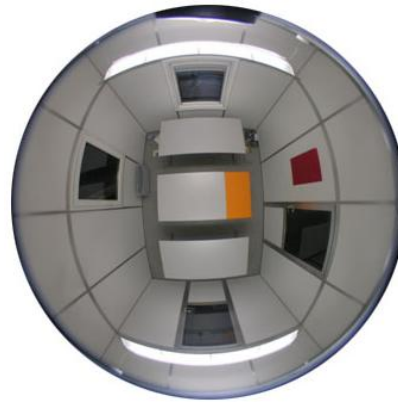


Figure 41 Operation of luminaire 1 for light output level 100%.

2.3.3 Implementation in the real office space

2.3.3.1 General

In the following sections, firstly the test space components and configuration, of a real office building in Styria, Austria is described. Then briefly the external data monitoring solution concerning daylight availability is described. In the end, an illustration of the virtual implementation and validation of simulation-powered building systems control approach in lighting and shading domain is presented.

2.3.3.2 Test space

As the test space, a room in an office building in Styria, Austria was selected. The office's control devices are, in this case, two suspended dimmable luminaires (L_1 , L_2) and a window blind (B). Figure 42, shows the exterior view of the building. Figure 43 show the interior view of the office selected as the test space while figure 44 illustrates a schematic section of the test room with the control devices (two luminaires L_1 , L_2 and Blind, B).



Figure 42 *Exterior view of the building, Styria*



Figure 43 *Interior view of the office*

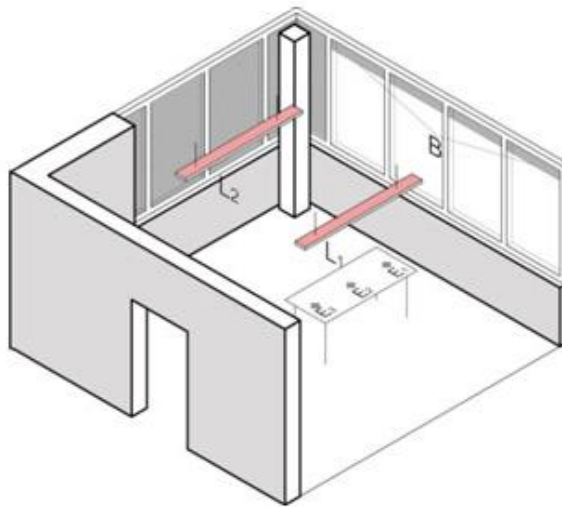


Figure 44 Schematic illustration of the test space (L1, L2: luminaries; B: blind; E1 to E3: virtual illuminance sensors)

2.3.3.3 Daylight availability

The simulation application for the prediction of daylight availability inside the office relies on sky luminance distribution information. To generate such sky luminance models, a number of steps are necessary. First, from measured global horizontal irradiance values corresponding diffuse and direct irradiance components are computationally derived based on the Reindl algorithm (Reindl et al. 1990) (see appendix 7.2 for further details). To transform irradiance values into corresponding illuminance values, luminous efficacy functions were applied. These functions were derived based on long-term observations of the relationship between incident irradiance and illuminance conducted in our micro-climatic monitoring station. Given the calculated horizontal direct and diffuse illuminance values and using the intermediate sky model (Darula, S. Kittler R. 2002, CIE 2003), the sky luminance distribution maps for use in the simulation application RADIANCE (Ward Larson & Shakespeare 2003) were generated toward predicting the lighting conditions inside the test room. Figure 45 illustrates the steps for the prediction of the lighting conditions inside the test room. Note that,

for the purpose of illustrative test runs included in this paper, the global horizontal irradiance data were taken from a reference file for the test space location (Stallhofen, Styria, Austria) using the application Meteonorm (2008) (Dervishi and Mahdavi 2010).

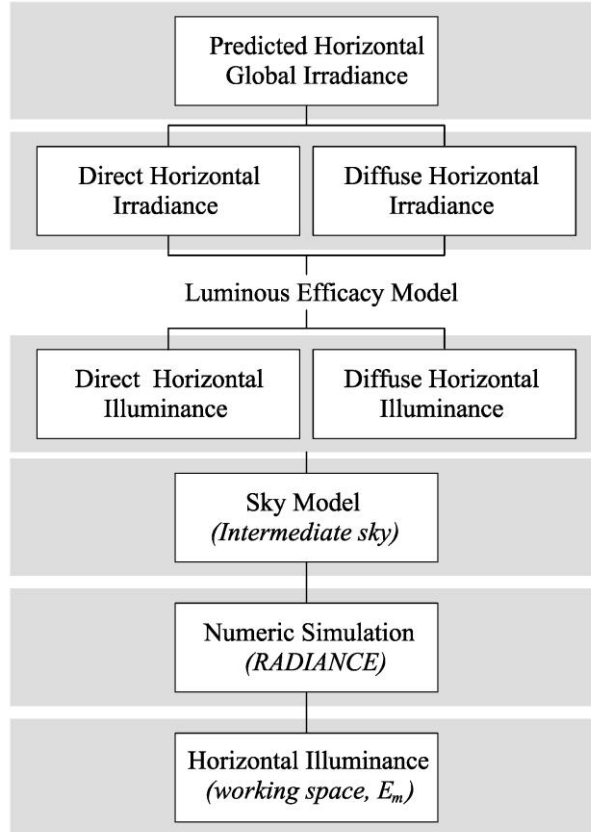


Figure 45 Schematic representation for the prediction of the lighting conditions inside the test room

2.3.3.4 Control devices and control state space

For the second scenario, the lighting system consists of three control devices. For the amount of the daylight control motorized (give the name) blind placed inside the windows facing south is considered. The artificial light is provided by two suspended dimmable luminaires *Zumtobel Opalis* (L_1 , L_2) and the window blind (B). In the control scenarios considered, the blinds can be moved up and down. As a

primary indicator of lighting performance, the mean illuminance levels E_m as per equation 17 and UGR (unified glare rating) was considered.

$$E_m = (E_1 + E_2 + E_3)/3 \quad (\text{Eq. 15})$$

For the provision of sufficient illuminance on the working places, a central control instance C is required to coordinate the three devices (two dimmable luminaires, L_1 , L_2 and the window blind B). Figure 46 illustrates the control system scheme, as relevant to the present test scenario.

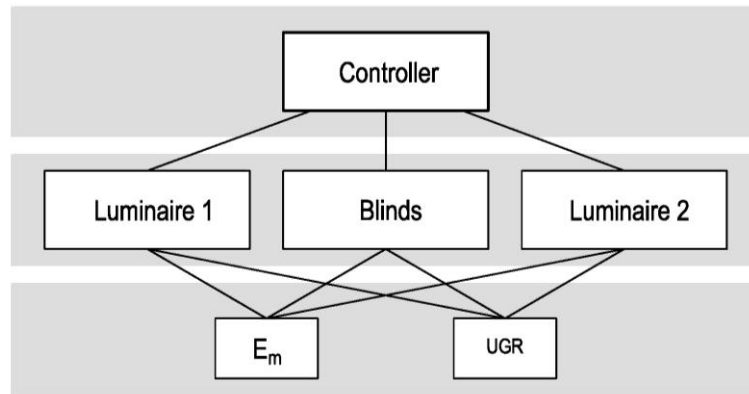


Figure 46 Control system scheme (L1, L2: Luminaires; B: Blind; C: Central control instance; E_m : mean workstation illuminance levels as per equations 1), UGR (Unified Glare Rating)

To each device, a discrete number of possible states is allocated. These options include five different positions of the blind (see Figures 47 and 48) and ten discrete dimming positions for each of the two luminaires (see figure 49 and Table 6).



Figure 47 internal view of the blinds used as control devices

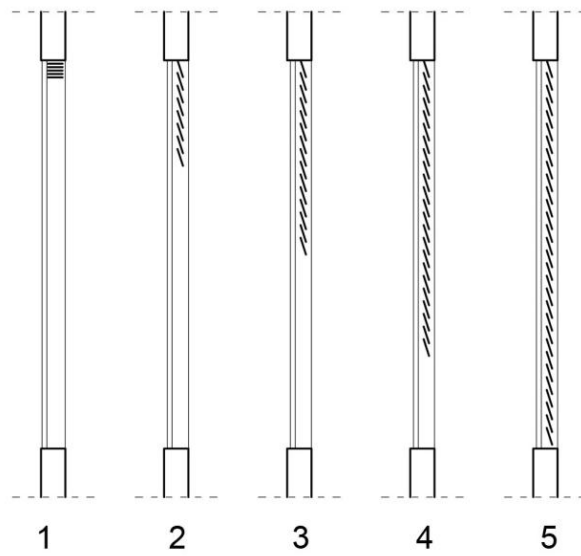


Figure 48 Discretized blind deployment steps



Figure 49 Luminaire 1 and Luminaire 2 used as control devices

Table 6 Discretized dimming steps for luminaires 1 and 2

Dimming state	1	2	3	4	5	6	7	8	9	10
Power output [%]	0	20	30	40	50	60	70	80	90	100

2.3.3.5 Control Objective

The control scenario involves three objectives:

- i) Minimize the deviation of the average illuminance (E_m) on the working planes (see figure 50).
- ii) Minimize electrical energy use. The formulation of the corresponding preference function P_L is shown in Figure 51.
- iii) Minimize glare. Unified glare rating is used as performance indicator (see figure 52)

The overall behavior of the control system is determined, in this case, through a utility function (UF) as shown in equation 16.

$$UF = w_E \cdot P_E + w_L \cdot P_L + w_G \cdot P_G \quad (\text{Eq.16})$$

In this equation P_E , P_L and P_G are the preferences for illuminance levels (E_m), electrical energy consumption and glare rating (UGR). The corresponding weights are represented by w_E , w_L and w_G . Related illustrative preference functions are shown in Figs. 49 – 51.

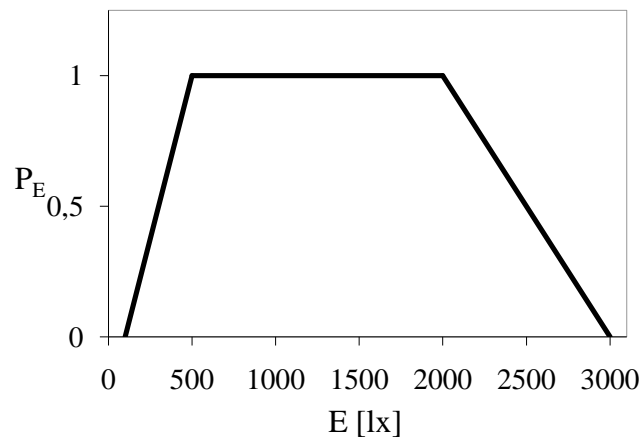


Figure 50 Preference function for task illuminance

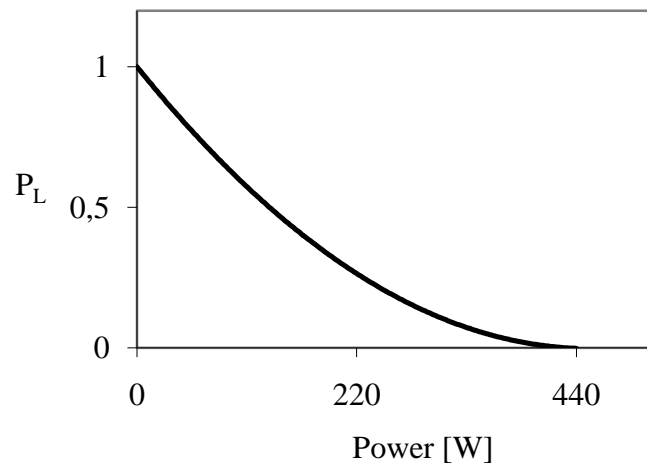


Figure 51 Preference function for electrical power

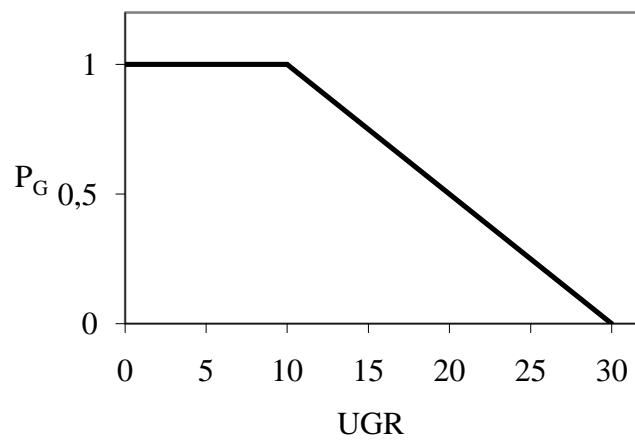


Figure 52 Preference function for unified glare rating (UGR)

2.3.3.6 Control Process

As mentioned above, the controller application C , at time step t_i , considers a list of candidates for each device (two luminaires, L_1 and L_2 and the blinds, B) for the time step t_{i+1} . Four alternative options are considered for each device. These options are the device's current position, the two neighboring states, and a fourth—randomly chosen—option from the rest of the device's control state space. Thus, the resulting overall option space encompasses a maximum of 64 distinctive control states. For this purpose, the lighting simulation program RADIANCE (Ward Larson & Shakespeare 2003) is adopted.

In the present case, the options were compared in view of the corresponding resulting workstation illuminance E (arithmetical average of illuminance levels computed for positions E_1 to E_3 as per equation 15), glare rating (UGR) and electrical power demand of the artificial lighting.

Given the obtained values of E_m , glare rating (UGR) as well as electrical energy use, UF values can be derived using Equation 16. Thus, at each time step, the control state with the maximum utility function can be identified for the subsequent time step. The relative importance of the applicable performance indicators can in turn be weighted via corresponding weights w_E , w_L and w_G . In the following illustrative virtual test runs of the systems, these values were assumed to be as follows: $w_E = 0.5$; $w_L = 0.3$; $w_G = 0.2$. (Mahdavi and Dervishi 2010).

3 Results

3.1 Overview

This chapter summarizes the main results. It is divided in three main sections. The first section illustrates the comparison of the alternative methods for sky model generation applied here to derive vertical irradiance data based on typically available monitored data. The second section compares the performance of the four luminous efficacy models based on a database of measured illuminance and irradiance data. The last section illustrates the functionality and performance of the simulation-assisted lighting and shading systems control applied in a testbed (department of building physics and building ecology) and a real office building in Styria, Austria.

3.2 Comparison of sky models on vertical surface

A total of about 2240 pairs of measured-predicted vertical irradiance values were used to determine the relative error (RE), the correlation (r^2) and root mean square difference (RMSD) between the measurements and predicted derived of each model for North, East, South, West and All-Orientation.

Figures 53–57 show the percentage of the results (measurement versus simulation comparisons) with associated maximum REs for the five aforementioned options (see Table 2). Thereby, Figures 53–56 pertain to the results for north, east, south, and west directions, respectively, whereas Figure 57 entails the results for all directions combined. Note that these figures do not include REs above 150%, given the very small numbers of results with errors beyond this value.

Figures 58–62 illustrate the relationship between the computed (vertical axis) and the measured (horizontal axis) for all orientations. Their correlation coefficient of their linear regression is defined. The graphs illustrating the

comparison for North, East, South and West orientation are shown in the appendix 7.3.

To further facilitate the comparison of options, Table 7 shows the maximum RE for 80% of the comparisons. Table 8 shows the percentage of the comparisons, whose RE was less than $\pm 20\%$. Table 9 compares the five options in terms of correlation coefficient (r^2) and RMSD.

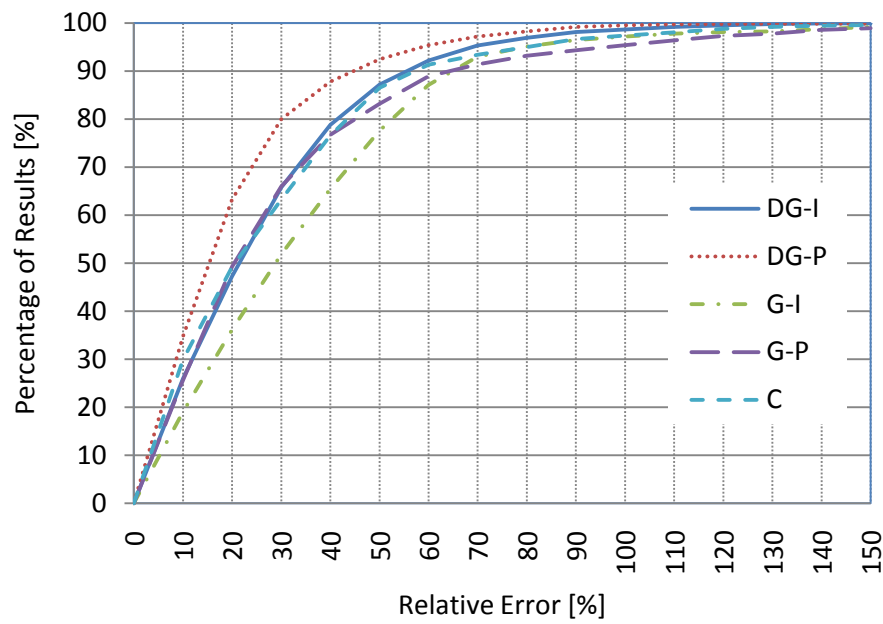


Figure 53 Percentage of the results (predicted vertical irradiance values) with respective maximum Relative Error for the five options (orientation: North)

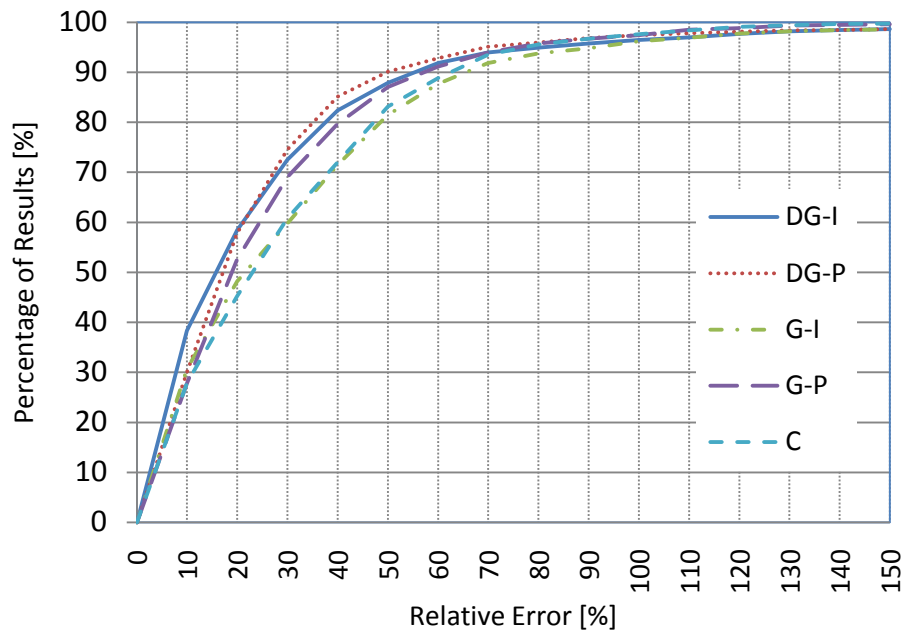


Figure 54 Percentage of the results (predicted vertical irradiance values) with respective maximum Relative Error for the five options (orientation: East)

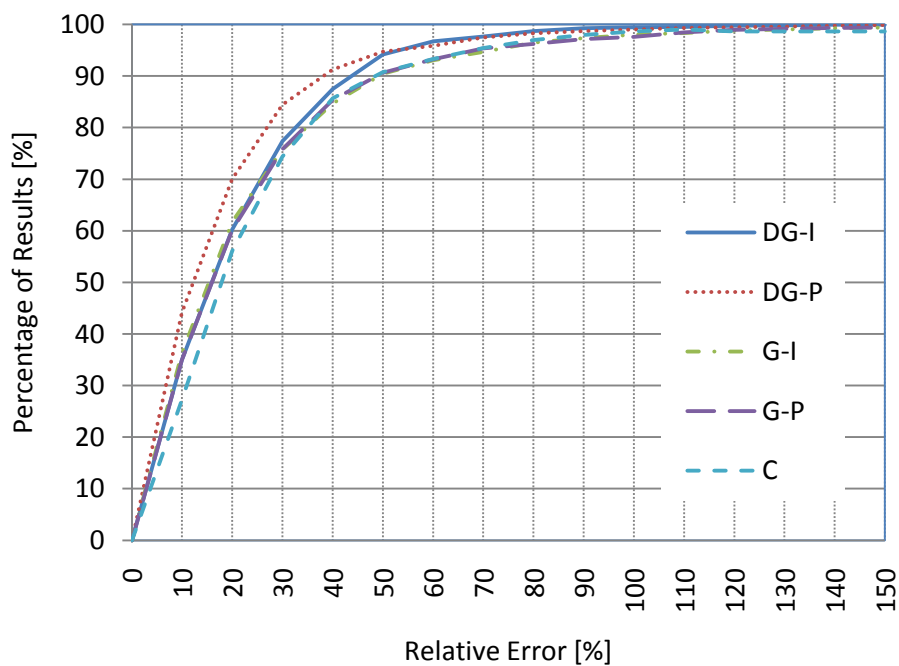


Figure 55 Percentage of the results (predicted vertical irradiance values) with respective maximum Relative Error for the five options (orientation: South)

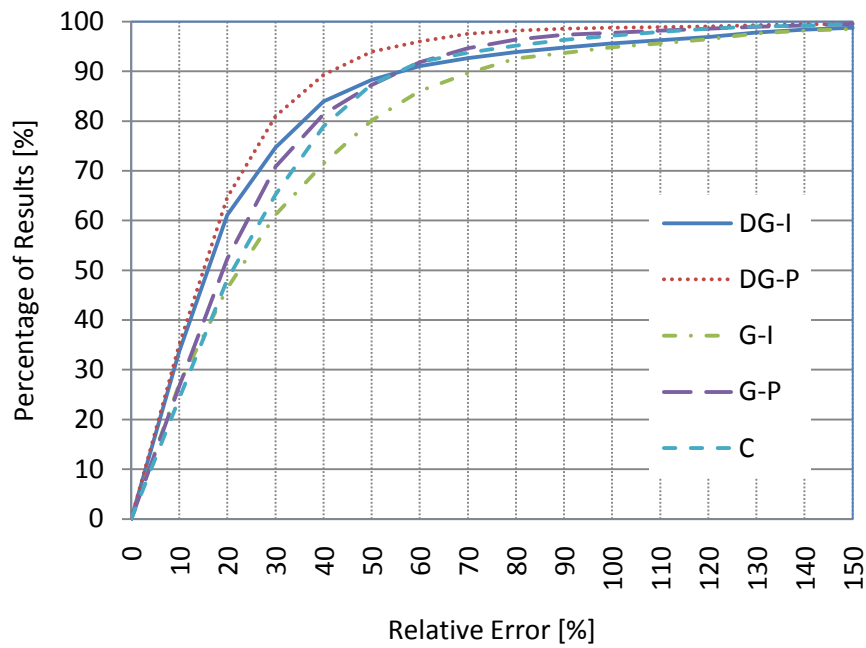


Figure 56 Percentage of the results (predicted vertical irradiance values) with respective maximum Relative Error for the five options (orientation: West)

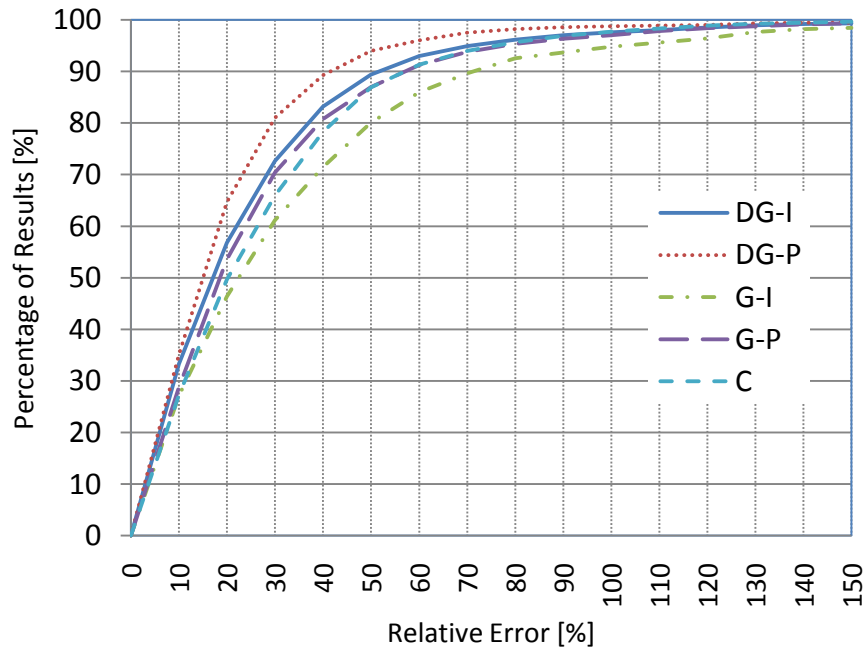


Figure 57 Percentage of the results (predicted vertical irradiance values) with respective maximum Relative Error for the five options (All orientations)

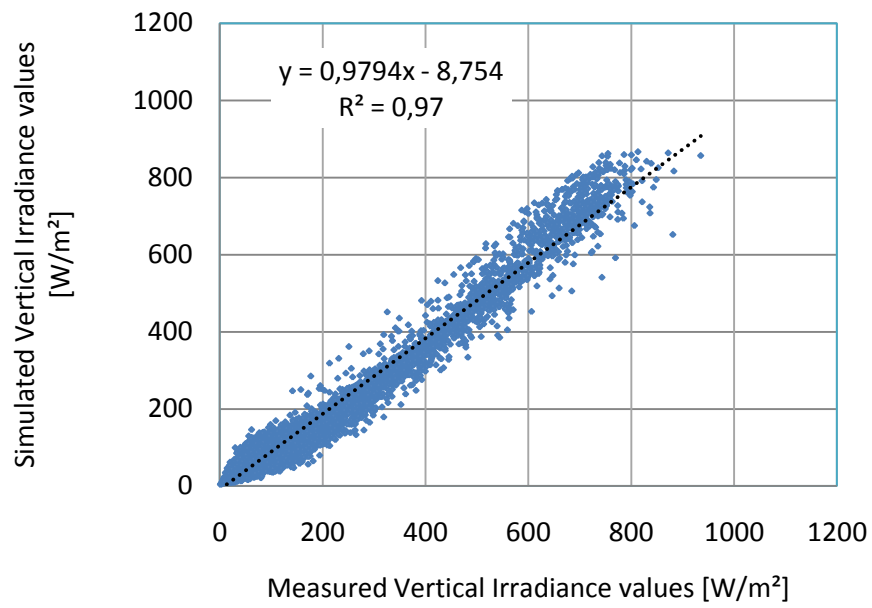


Figure 58 Comparison of measured and simulated vertical irradiance values (option DG-I)

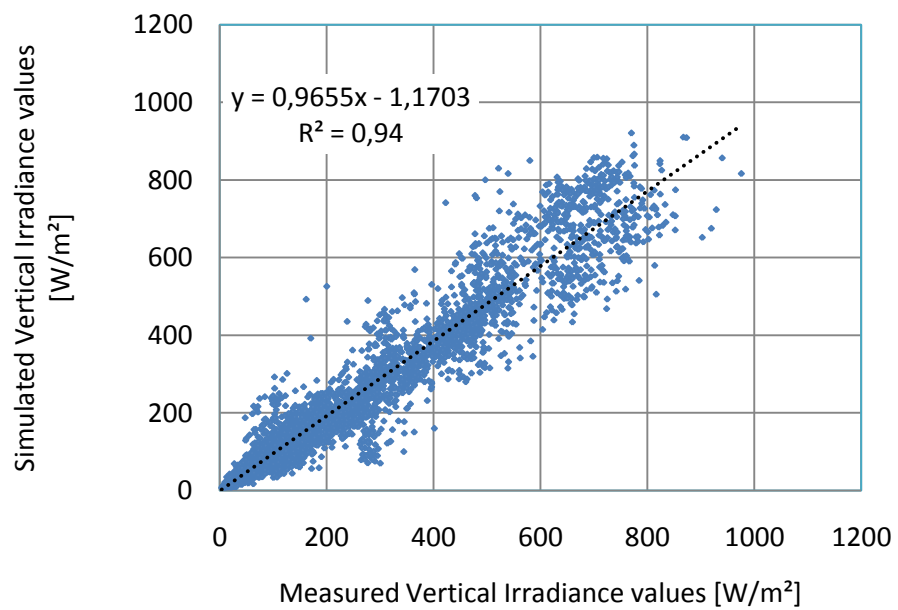


Figure 59 Comparison of measured and simulated vertical irradiance values (option DG-P)

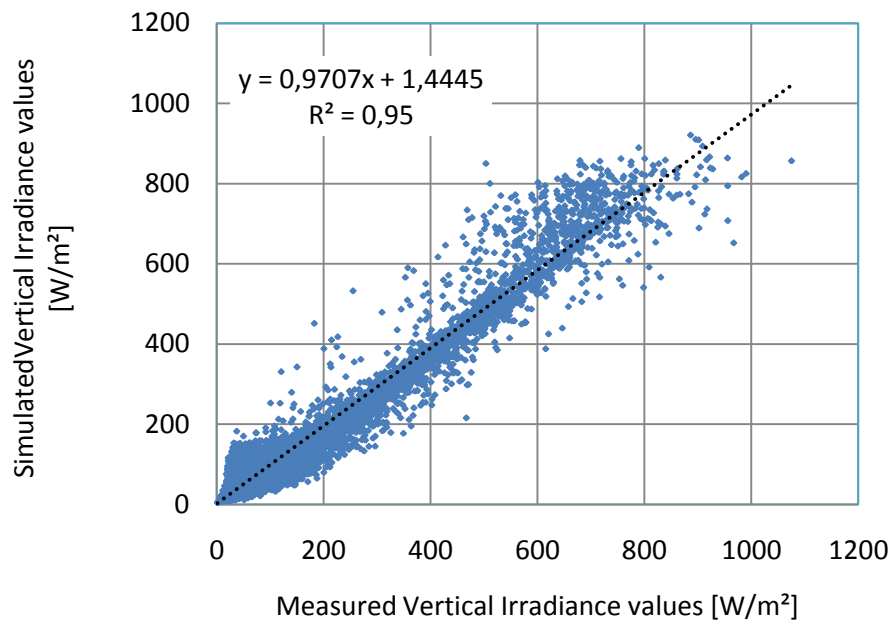


Figure 60 Comparison of measured and simulated vertical irradiance values (option: G-I)

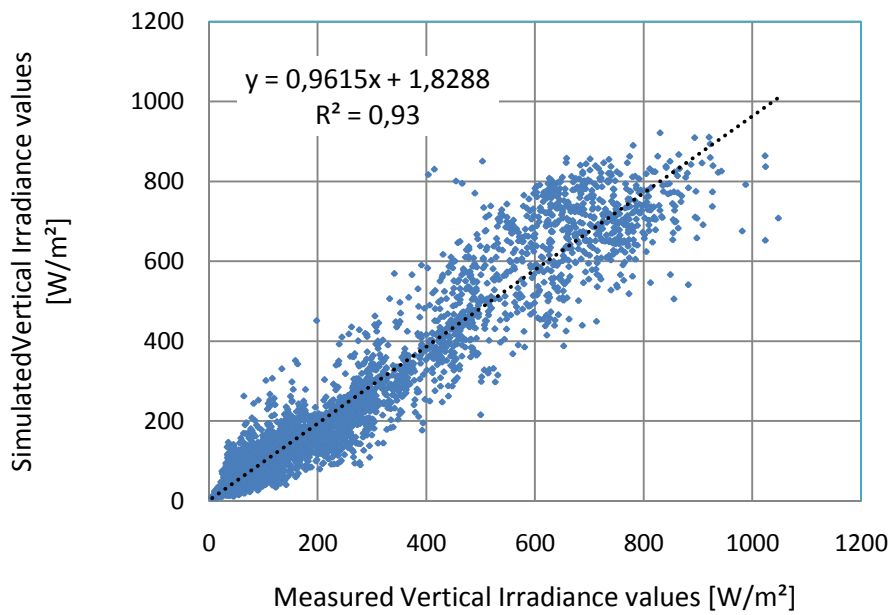


Figure 61 Comparison of measured and simulated vertical irradiance values (option: G-P)

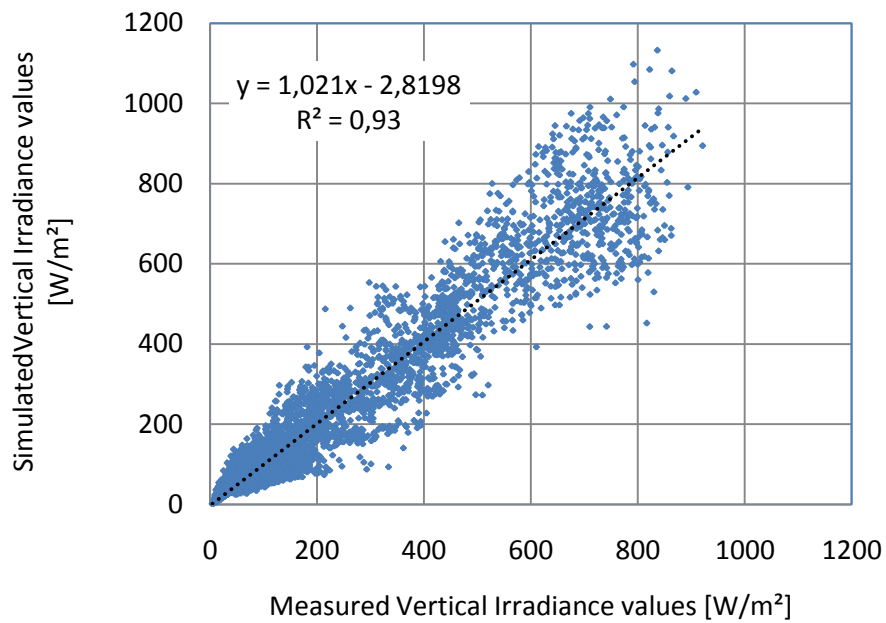


Figure 62 Comparison of measured and simulated vertical irradiance values (option: C)

Table 7 Maximum relative errors (in %) for 80% of the results

Option	North	East	South	West	All orientations
DG -I	41,6	37,0	32,2	35,9	36,4
DG-P	29,9	35,1	26,3	29,0	29,0
G-I	52,2	48,6	34,4	49,8	49,9
G-P	44,5	40,4	34,1	38,6	39,1
C	43,4	46,7	34,5	41,4	41,8

Table 8 Percentage of results with a relative error of less than $\pm 20\%$

Option	North	East	South	West	All orientations
DG -I	47,3	58,5	60,2	61,1	56,8
DG -P	63,3	57,9	70,1	64,7	64,7
G-I	36,2	48,2	61,7	46,4	46,4
G-P	49,3	52,6	60,1	52,3	53,6
C	49,2	45,3	56,1	48,1	49,7

Table 9 Comparison of the options in terms of correlation coefficient and RMSD

Option	Indicator	North	East	South	West	All orientations
DG -I	r^2	0,7	0,98	0,98	0,98	0,97
	RMSD	21,2	35,3	36,8	41,2	34,5
DG -P	r^2	0,8	0,96	0,96	0,97	0,94
	RMSD	15,9	60,9	35,3	55,6	45,6
G-I	r^2	0,49	0,96	0,97	0,96	0,95
	RMSD	27,6	50,1	32,5	52,4	43,4
G-P	r^2	0,52	0,95	0,94	0,96	0,93
	RMSD	28,4	66,6	32,7	59,9	59,7
C	r^2	0,46	0,96	0,88	0,96	0,93
	RMSD	27,6	73,2	52,8	49,4	54,7

3.3 Comparison of sky luminous models

To compare the performance of the four luminous efficacy models (using the second data set of measurements), Figure 63 and 64 show the percentage of the results (pairs of measured and computed luminous efficacy levels) with associated maximum relative errors using the versions with the original (Figure 63) and adapted coefficients (Figure 64). Table 10 and 11 shows the same information numerically for discrete values of relative error ($\pm 5\%$, $\pm 10\%$, $\pm 15\%$, $\pm 20\%$).

Table 12 and 13 compares the four models in terms of RMSD and MBD for original and adapted coefficients respectively. Note that RMSD results are expressed both in percentage and in absolute ($\text{lm}\cdot\text{W}^{-1}$) terms. Figure 65 and 66 show MBD and RMSD results of the adapted luminous efficacy models as a function of different solar altitude. For this illustration, the solar altitude was divided into discrete bins (5-10°, 10-20°, 20-30°, 30-40°, 40-50°, 50-60°).

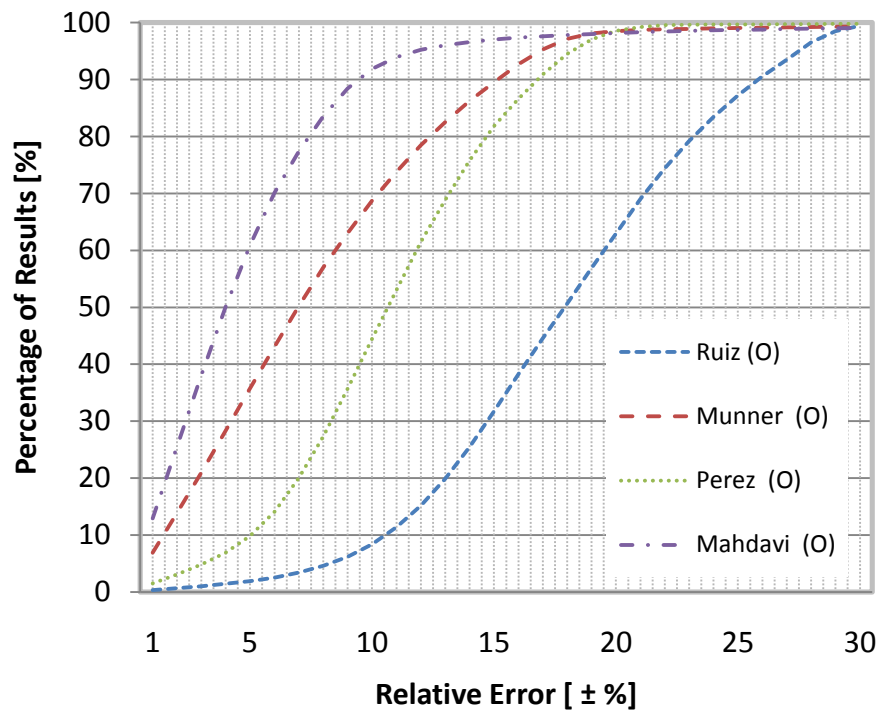


Figure 63 Percentage of the results (pairs of measured and derived luminous efficacy values) with respective maximum Relative Error for the four models with the original coefficients

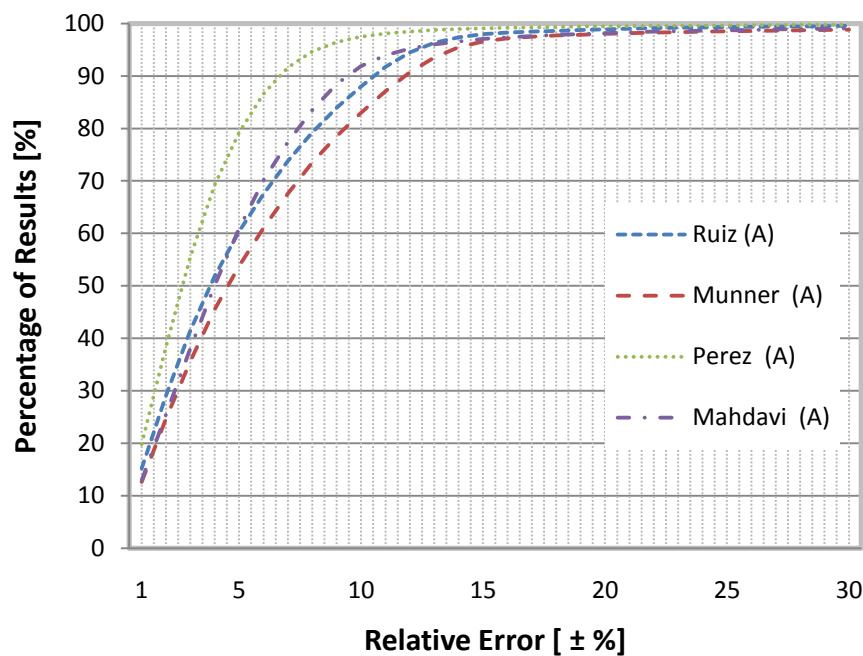


Figure 64 Percentage of the results (pairs of measured and derived luminous efficacy values) with respective maximum Relative Error (RE) for the four models with the adapted coefficients

Table 10 Percentage of results with corresponding maximum relative Error (RE) with original model coefficients

Model	Original coefficients			
	± 5 %	± 10 %	± 15 %	± 20 %
Ruiz	1.9	8.4	31.7	62.9
Munner	35.8	68.7	89.5	98.5
Perez	9.8	44.4	81.8	98.5
Mahdavi	60.9	91.9	97.0	98.2

Table 11 Percentage of results with corresponding maximum relative Error (RE) with adapted model coefficients

Model	Adapted coefficients			
	± 5 %	± 5 %	± 5 %	± 5 %
Ruiz	60.3	60.3	60.3	60.3
Munner	53.7	53.7	53.7	53.7
Perez	79.2	79.2	79.2	79.2
Mahdavi	60.9	60.9	60.9	60.9

Table 12 Comparison of luminous efficacy models based RMSD and MBD with original model coefficients.

Model	Original coefficients		
	RMSD (lm.W ⁻¹)	RMSD (%)	MBD (%)
Ruiz	24.5	18.9	22.4
Munner	12.5	10.1	7.7
Perez	15.0	11.8	13.1
Mahdavi	9.5	8.5	1.7

Table 13 Comparison of luminous efficacy models based RMSD and MBD with adapted model coefficients.

Model	Adapted coefficients		
	RMSD (lm.W ⁻¹)	RMSD (%)	MBD (%)
Ruiz	8.1	7.1	2.6
Munner	11.7	10.2	2.4
Perez	5.5	5.0	1.5
Mahdavi	9.5	8.5	1.7

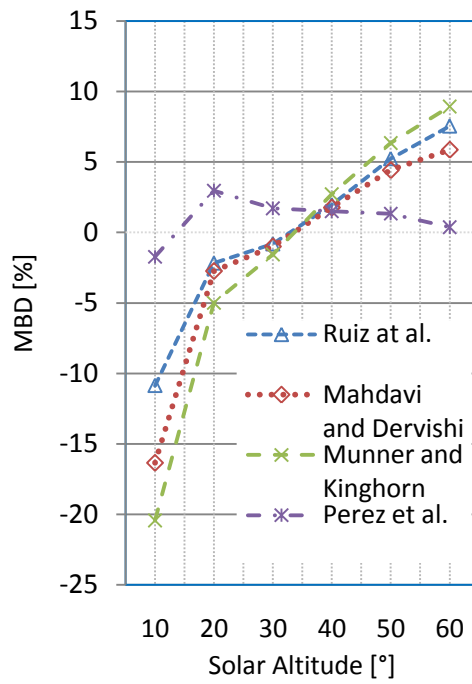


Figure 65 MBD results for the adapted luminous efficacy models as a function of solar altitude

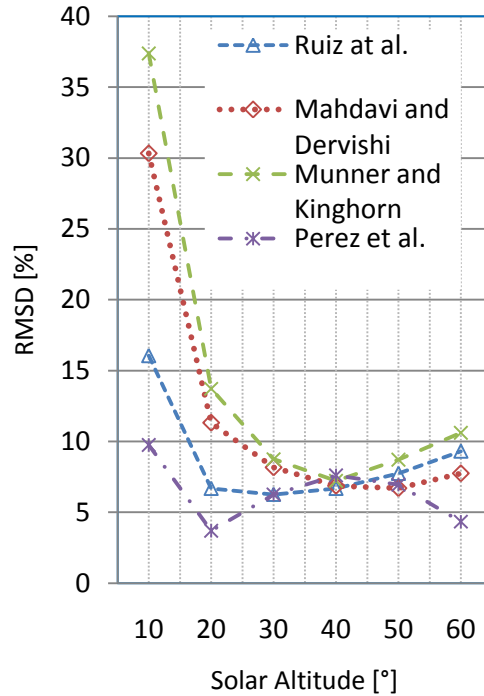


Figure 66 RMSD results for the adapted luminous efficacy models as a function of solar altitude

3.4 Simulation Assisted Lighting and Shading Control

3.4.1 Implementation in the testbed

The controller application was regularly evaluating the possible control actions range and identifying the candidate control state with the most desirable performance in approximately fifteen minutes interval, during the office hours (8:00-18:00) and over ten days (June-July).

To illustrate the control functionality, the operation of the system for one day (in 7 June 2008) is shown. The documentation of the lighting system performance of all 10 days (scenario 1) is given in the Appendix 7.2

Figures 67 – 73 illustrate the results of the test operation for scenario 1 (daylight emulated via flat luminaire) and scenario 2 (sky luminance maps dynamically obtained via calibrated digital sky scanning) in terms of system's recommendations and its performance (based on data for a day in June 2008).

Figure 67 illustrates the measured global horizontal illuminance of the referred day. Figures 68 and 71 show the corresponding values of the external global illuminance and the values of the relevant control parameter (i.e., mean workstation illuminance level, derived as the arithmetical average of the illuminance at points E2, E3, and E4) over the course of the reference day for the two scenarios. Figures 69 and 72 show the corresponding values of the external global illuminance and the deployment position of the blinds. Figures 70 and 73 show the system's recommendations (the dimming position of the two luminaries and the deployment position of the blind) together with the resulting UF values over the course of the reference day (office hours) for the two scenarios.

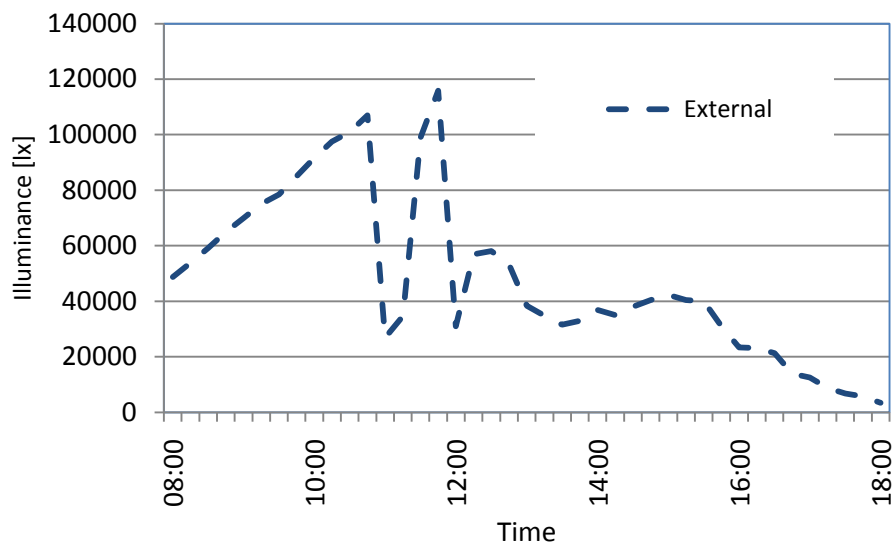


Figure 67 External Global Illuminance levels in the course of one day

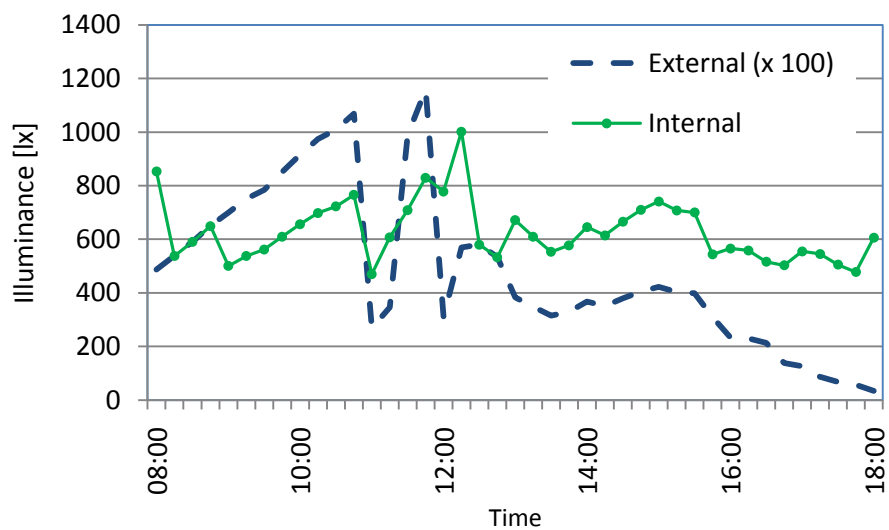


Figure 68 Predicted values of the relevant control parameter (workstation illuminance level) together with the prevailing external global illuminance (Scenario 1)

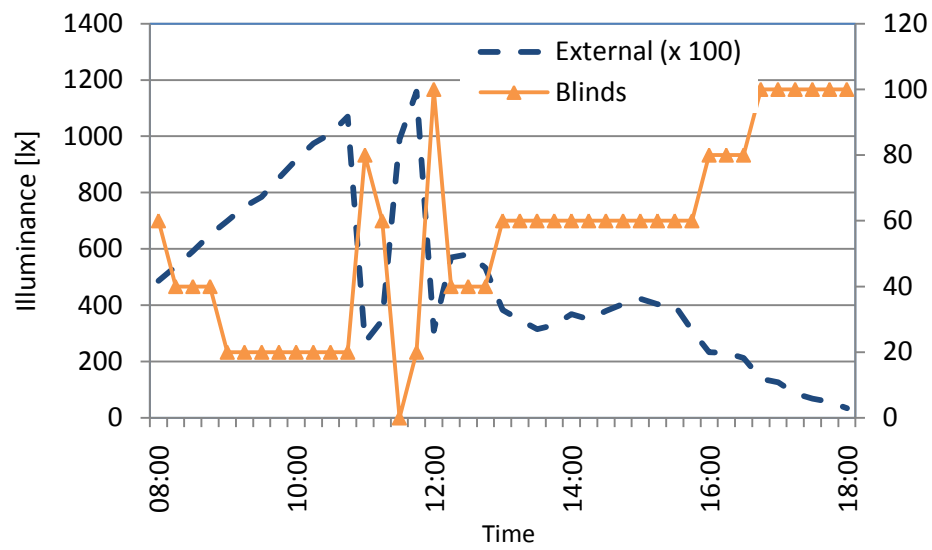


Figure 69 Recommended states of shading devices together with global horizontal illuminance values for a reference day (Scenario 1)

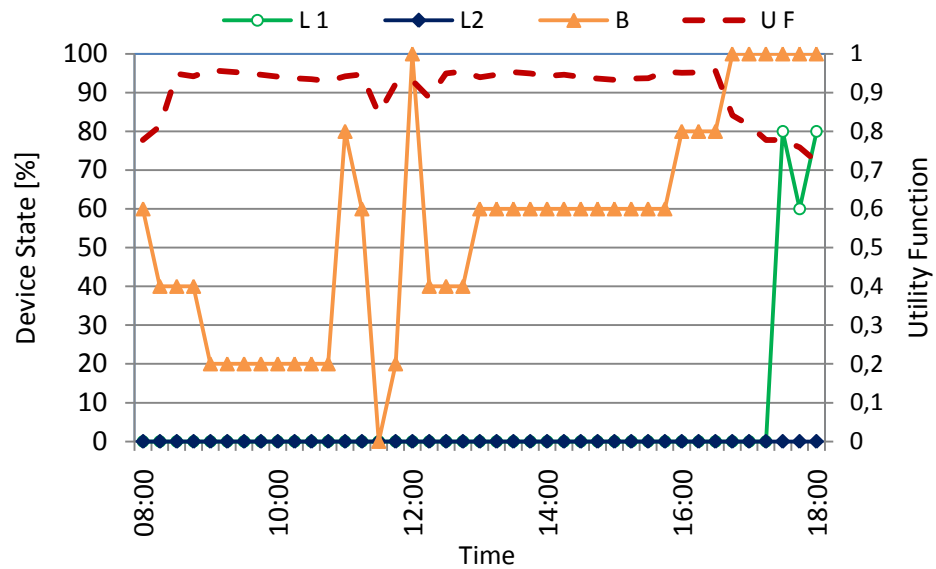


Figure 70 Recommended states of lighting and shading devices together with the resulting UF values for a reference day (Scenario 1)

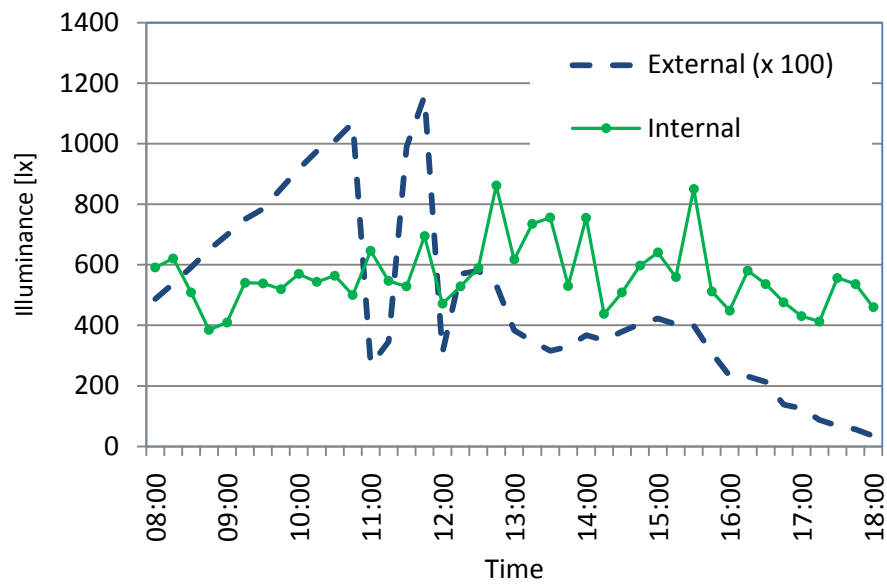


Figure 71 Predicted values of the relevant control parameter (workstation illuminance level) together with the prevailing external global illuminance (Scenario 2)

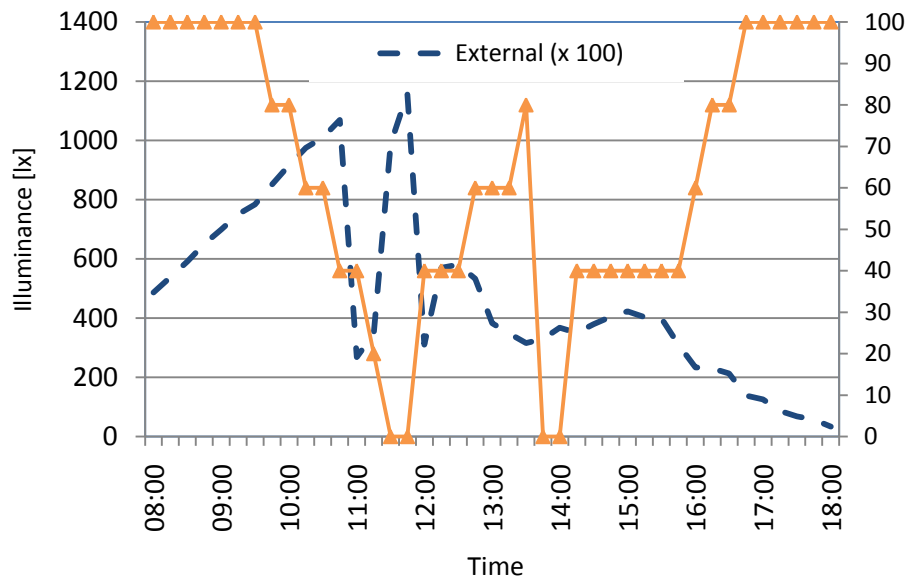


Figure 72 Recommended states of shading devices together with global horizontal illuminance values for a reference day (Scenario 2)

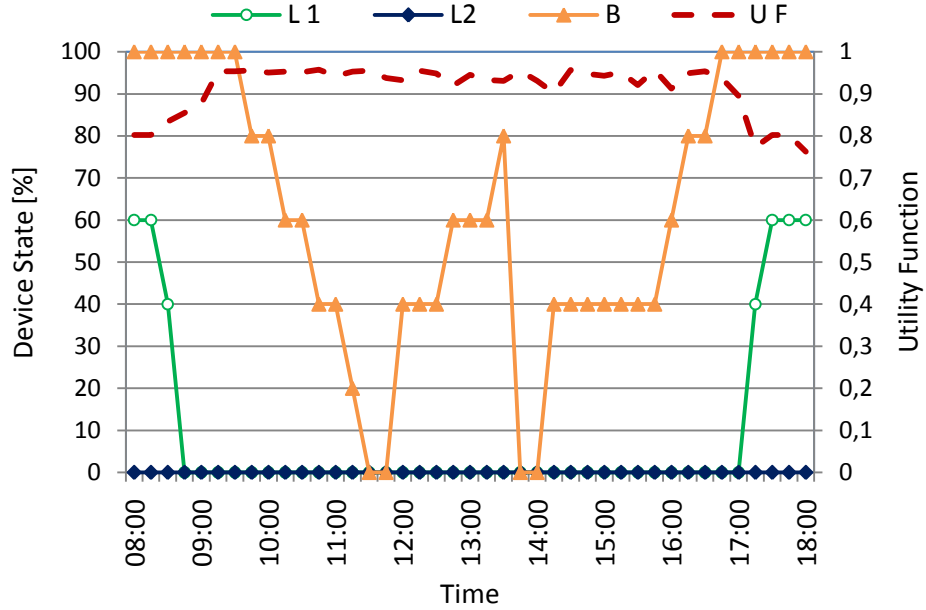


Figure 73 Recommended states of lighting and shading devices together with the resulting UF values for a reference day (Scenario 2)

3.4.2 Implementation in a real office buildings

To illustrate the working of the above-described control method functionality, the operation of the system over the course of 24 days (one week for each season) was documented. In the present scenario, the control system's reassessment of the desirable control state occurs regularly every 15 minutes. The following figures illustrate the results of the simulation-based predictive system's operation in terms of the system's recommendations (for the blind position and the dimming state of the luminaires) and its performance (maintained illuminance levels, UF value).

Thereby, to provide a compact overview, results are shown only for four days (one day for each season, namely 8. February, 11. May, 11. August, 8. November, office working hours). Figures 74, 76, 78, and 80 show the maintained illuminance level E_m (See Eq. 15 and Figure 44) as well the prevailing outdoor illuminance levels throughout the course of the four above-mentioned reference days. Figures 75, 77, 79, and 81 show the system's recommendations (the dimming position of the two luminaires and the

deployment position of the blind) together with the resulting UF values over the course of the four reference days.

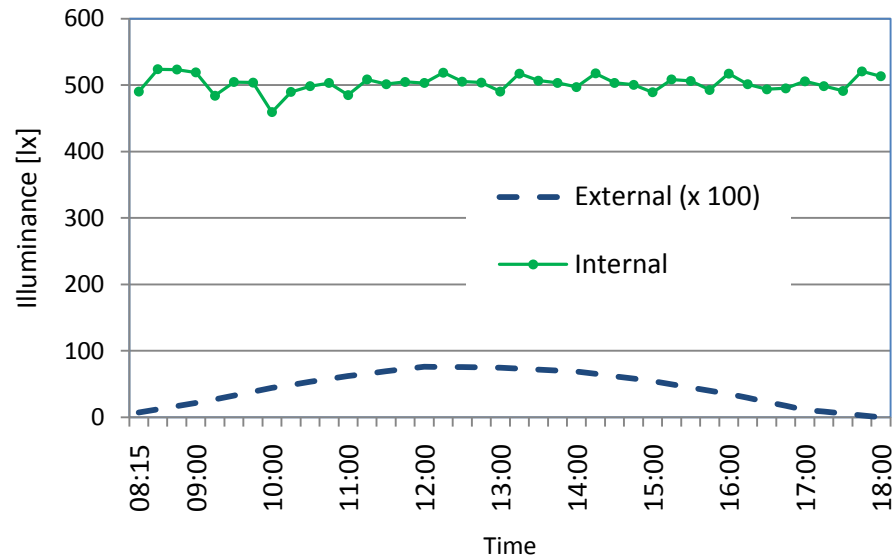


Figure 74 Predicted workstation illuminance levels together with the prevailing external global illuminance for a reference day in February

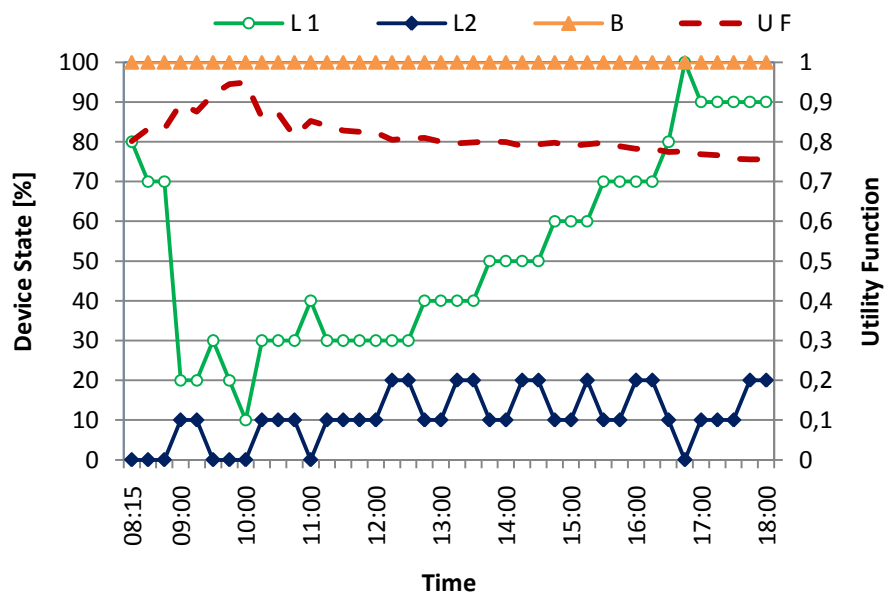


Figure 75 Recommended states of lighting and shading devices together with the resulting UF values for a reference day in February.

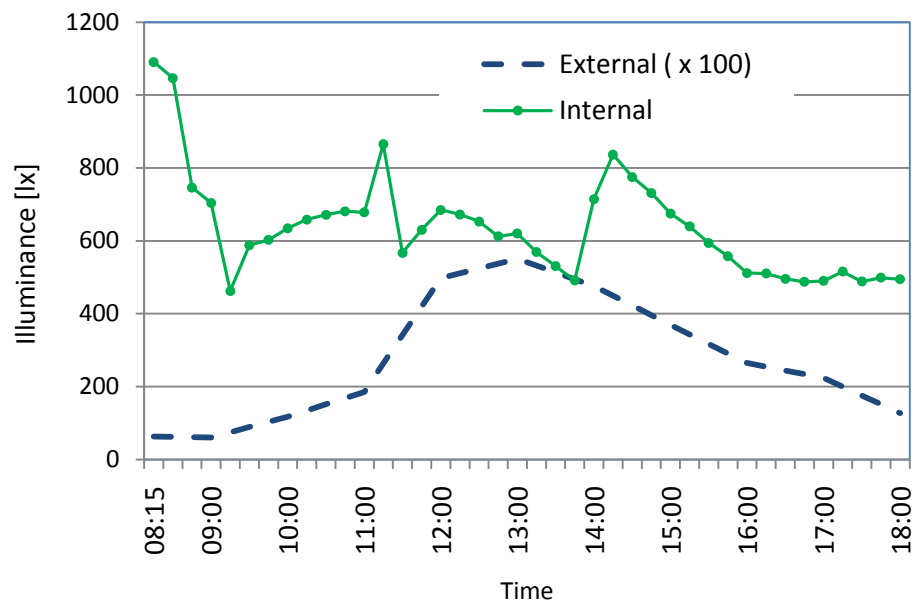


Figure 76 Predicted workstation illuminance levels together with the prevailing external global illuminance for a reference day in May.

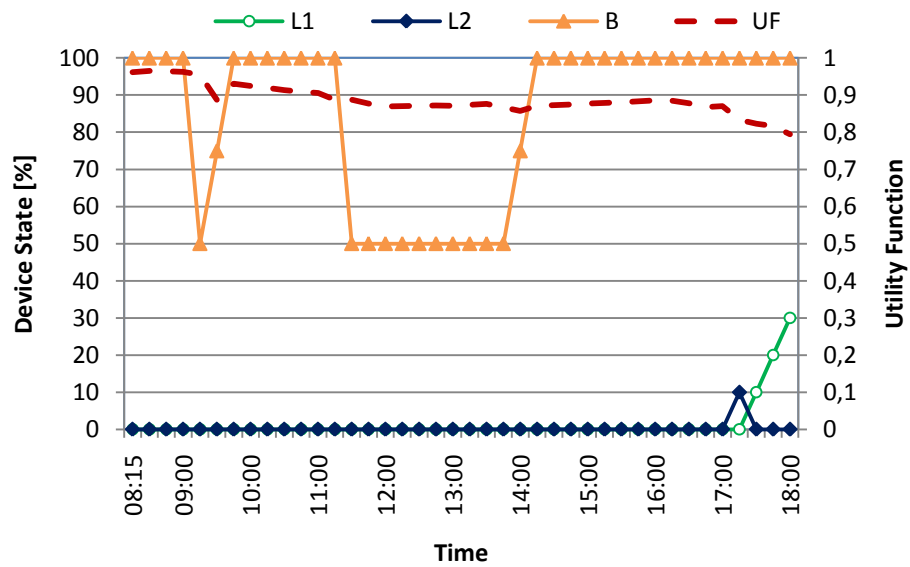


Figure 77 Recommended states of lighting and shading devices together with the resulting UF values for a reference day in May.

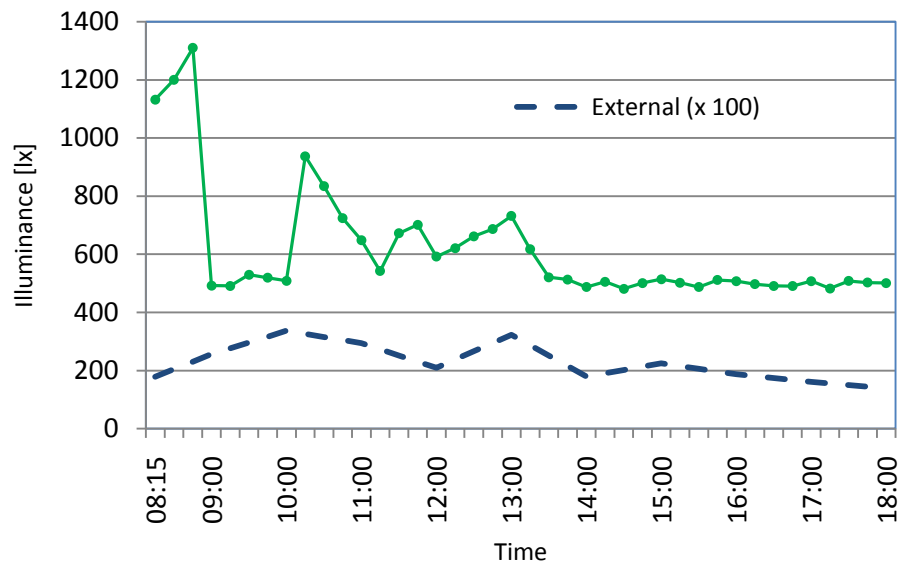


Figure 78 Predicted workstation illuminance levels together with the prevailing external global illuminance for a reference day in August.

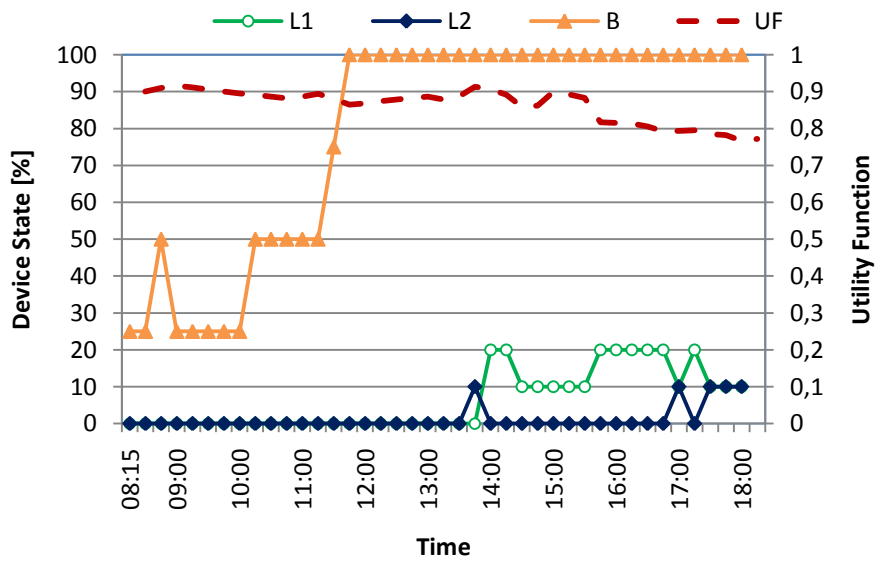


Figure 79 Recommended states of lighting and shading devices together with the resulting UF values for a reference day in August.

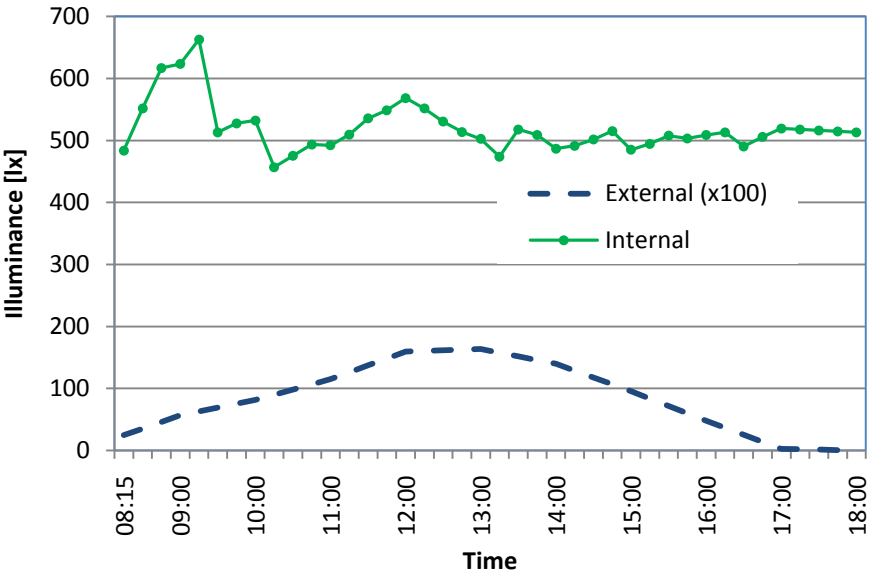


Figure 80 Predicted workstation illuminance levels together with the prevailing external global illuminance for a reference day in November.

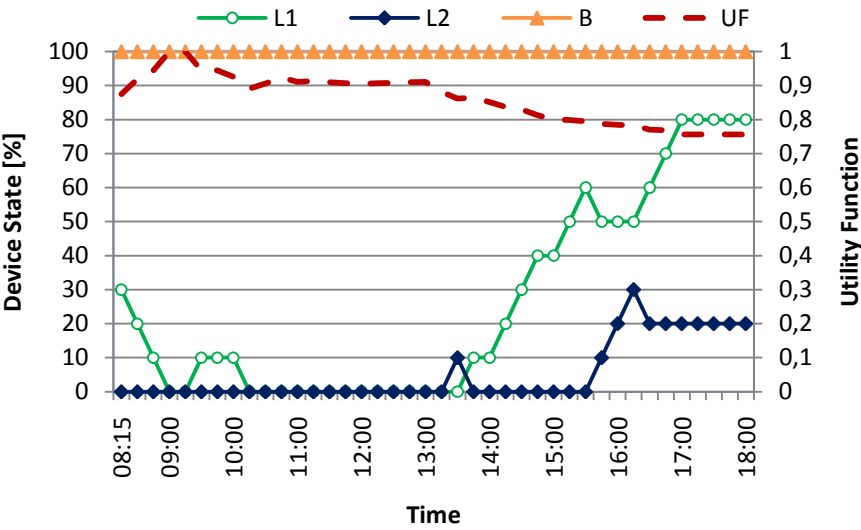


Figure 81 Recommended states of lighting and shading devices together with the resulting UF values for a reference day in November.

4 Discussion

4.1 Overview

This chapter provides a summary discussion of the main results of the dissertation. It is divided into sections dealing with: i) approaches for the generation of the sky models (here irradiance) on building surfaces. ii) comparison of the global luminous efficacy models. iii) implementation of simulation-assisted lighting system control. The systems control

4.2 Sky models for vertical surfaces

A visual inspection of the cumulative REs shown in Figures 53–57 imply that the option DG-P provides for somewhat better reproduction of measured vertical irradiance values, followed by the option DG-I. A visual comparison of Figures 58–62 suggests option DG-I to be the better performing one. Table 8 clearly identifies DG-P and DG-I as the options with lower REs (both for individual orientations and all orientations combined). Likewise, Table 9 suggests (with a few exceptions pertaining to North and South orientations) that DG-P and DG-I options perform better. Overall, the differences between the options in view of correlation coefficient and RMSD are not highly pronounced (see Table 10). Option DG-I does, however, possess the highest r^2 and the lowest RMSD, whereas option DG-P shows the third highest r^2 and third lowest RMSD.

Moreover, data displayed in Figures 53-57, as well as Table 7 suggest that errors are smaller in case of the south orientation, independent of the option applied. This could be explained if it could be shown, that errors are smaller in case of higher irradiance values: incident irradiance values are typically higher for the south orientation. To test this conjecture, we considered the mean REs (for all options) as a function of the incident irradiance range (see Table 14).

These results appear to confirm the conjecture. Altogether, the slightly better performance of DG-I and – to some extent – DG-P is consistent with the circumstance, that they involve the use of measured values of both global and diffuse horizontal irradiance. Option C displays a rather mediocre performance, even though in this case detailed sky radiance maps are generated. A contributing factor thereby may be the previously mentioned circumstance that the camera was originally calibrated for sky luminance mapping: sky patch radiances were derived based on measure luminous efficacy, introducing potential errors in the results (Mahdavi and Dervishi 2010).

Table 14 Mean RE (all options) as a function of incident irradiance range

Incident irradiance range (W m^{-2})	Mean relative error range (%)
< 300	26...29
Between 300 and 400	18
> 400	10...12

4.3 Luminous efficacy models

A visual inspection of the results warrants a number of conclusions:

The global luminous efficacy models examined do not "transport" well. As data shown in Figure 63 and Tables 10 and 13 suggest, Mahdavi and Dervishi model, whose coefficients were explicitly derived for Vienna, performs significantly better than the other models, whose original coefficients were obtained for other locations. The Perez model in the version with its original coefficients, even though intended to function as general model of global luminous efficacy, does not perform satisfactorily for Vienna data.

As it could be expected, all models perform better, when their coefficients are modified based on local data (see Figure 64 as well as Tables 11 and 14). For all models, a large fraction of the relevant results (more than 96%) show a relative error less than $\pm 15\%$. Comparison of model versions with adapted coefficients

further suggests that Perez et al. model performs best for Vienna data, followed by the Mahdavi and Dervishi model.

A systematic relationship between model errors and the intensity of global horizontal irradiance could not be founded. However, model errors are noticeably higher for lower solar altitudes (see Figure 65 and Figure 66) (Dervishi and Mahdavi 2010)

4.4 Simulation-assisted lighting systems control

The demonstration of the overall systems control functionality shows the effective use of advanced lighting simulation toward the building control system in the lighting and shading domain. This control system illustrated in the two test spaces (see figure 18 and figure 44) optimizes the lighting system by: i) minimizing the deviation of the values of E_m (see equation 15) from the preferred illuminance levels specified by the user (e.g. see figure 68) ii) minimizing the electrical energy use (e.g. see figure 70). iii) minimizing the glare effect (see equation 16). In addition, simulation-based systems control offers the use of virtual sensors which can consider more performance indicators (such as illuminance distribution, uniformity factors and various glare indices) in comparison to physical sensors. In this case, the use of physical sensors can be reduced as the changes in the test space can be digitally reflected. Moreover, the proposed system can support proactive control processes (Mahdavi 2008).

However, the evaluation of the performance of the systems control over the entire duration of the simulation requires an in-depth analysis of the respective data. As mentioned before, at each time interval (i.e., every 15 minutes) the controller application considers 64 combinations of the control device states. For instance, for the implementation of the simulation-assisted lighting control in the testspace at the laboratory of building physics and building ecology) 216 options (6 possible blinds positions and 2 luminaires with 6 dimming positions each) were considered. Since simulated illuminance levels (E_m) are obtained for every interval and every possible blind position over the simulation period, the

performance of all 216 configurations at each time interval can be objectively ranked based on corresponding utility function values. This availability of simulation data for the entire search space at each time interval allows for an objective evaluation of the performance of the control method (Mahdavi 2008). The question rises, what was, then, the objective rank of the control system's recommended control state amongst all 216 possible control states? Figure 82 illustrates the results in terms of a relative frequency graph (for 820 intervals over the test period for both scenarios). It suggests that for approximately 97% of all intervals, the control state recommended by the controller is amongst the top 5% of all possible options. Only less than 0,24 % of the controller's recommendations fall outside the top 25% control options. This level of performance appears quite promising, given the large list of potential sources of error in the processes involved (e.g., sky luminance mapping, lighting simulation).

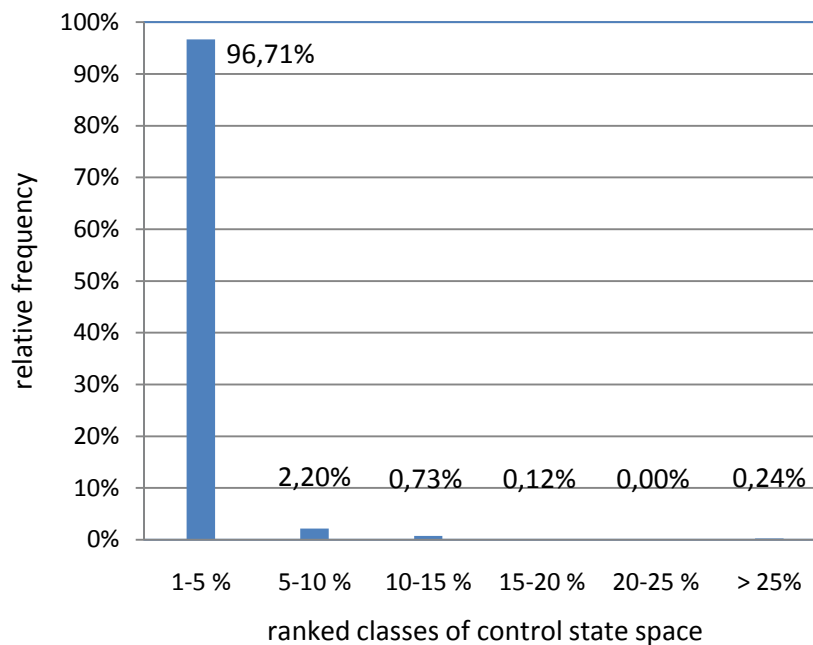


Figure 82 Ranking of the system's recommendation amongst all possible control options over the experiment period of 10 days, expressed in terms of relative frequency distribution.

To further identify the impact of simulation-assisted lighting systems control on lighting energy savings five different control systems are considered and virtually implemented in an office building in Styria, Austria (see figure 44). The main goal is to evaluate the reduction of the electrical energy use while maintaining a level of visual comfort. The scenarios considered are as follows:

- i) Scenario 1 considers the use of luminaires during the office hours to achieve task illuminance levels of at least 500 lx, independent of daylight. The electrical lights are on during the working hours and no shading is deployed.
- ii) Scenario 2 considers the use of luminaires during the office hours to achieve task illuminance levels at least 500 lx. The electrical lights are on during the working hours and shades are deployed according to the following schedule:

Table 15 Shading deployment schedule

Time	Shading deployment
8:00-12:00	close
12:00-18:00	open

- iii) Scenario 3 considers the use of luminaires in a dimming mode during the office hours to achieve task illuminance levels at least 500 lx including daylight availability. This means that electrical lights are used to maintain together with the daylight the aforementioned 500 lx.
- iv) Scenario 4 considers the use of luminaires in a dimming mode during the office hours to achieve task illuminance levels at least 500 lx including daylight availability. The shades are deployed according to the aforementioned schedule (see table 15).
- v) Scenario 5 uses simulation-assisted lighting and shading systems control. Table 16 illustrates the overview of the scenarios. As explained above, the overall behavior of the control system is determined through a utility function (UF) taking into consideration the preferences for task illuminance levels (E_m), electrical energy use and glare index (UGR) within their corresponding weights. Such

preference functions and their respective weights need not to be static, but can be dynamically changed by users to facilitate transient changes in operational requirements (Mahdavi 2008). What would be, then, the impact of changes of weight factors on energy consumption as well as other indicators (e.g. inside illuminance, glare, utility function)? In this context, scenario 5 considers three cases with different weight factors for task illuminance, electrical energy consumption and glare (URG) rating respectively. Table 17 illustrates the three cases.

Table 16 Overview of the scenarios

Scenarios	Luminaires	Shading
1	On	NO (fully open)
2	On	Deployment Schedule (See table 15)
3	Dimming mode (illuminance ≥ 500 lx including daylight)	NO (fully open)
4	Dimming mode (illuminance ≥ 500 lx including daylight)	Deployment Schedule (See table 15)
5	Simulation-assisted systems control	

Table 17 Overview of weight factors for the three cases of scenario five

case	w_E	w_L	w_G
5a	0.5	0.3	0.2
5b	0.4	0.6	0
5c	0.5	0	0.5

Table 18 summarizes the results for each scenario. Scenario 1 and 2 show the highest energy consumption for a period of one year. This is due to the fact that the two luminaires were on independent of daylight availability. However,

as expected, the mean illuminance levels and glare indices are higher for the first scenario with no shading application. Scenario 3 shows low energy consumption as the luminaires were in dimming mode with no shading application. As explained above, scenario 5 considered three cases with different weight factors for each preference function. The results clearly show the difference in energy consumption and the associated illuminance levels, glare indices and utility function respectively. Specifically, in the scenario 5b, the energy consumption is very low ($w_L=0.6$) and in scenario 5c the energy consumption is very high ($w_L=0$). Figure 83 summarizes the energy consumption in percentage for all the scenarios. Figures 84-86 illustrate the mean and standard deviation of inside illuminance, glare (UGR) and utility function for all the scenarios.

Table 18 Overview of the scenarios and their respective energy consumption (for one year), mean task illuminance level, glare (unified glare rating) and utility function

Senarios	P (kWh)	E (lx)		G (ugr)		UF	
		mean	Stdev	mean	Stdev	mean	stdev
1	1068.79	1652.16	1178.19	18.74	6.21	0.48	0.13
2	1068.79	1051.76	274.26	13.18	7.30	0.56	0.04
3	164.04	978.47	1111.89	18.74	6.21	0.72	0.09
4	410.66	575.25	141.62	13.18	7.30	0.69	0.06
5a	171.02	677.84	352.54	16.10	5.78	0.85	0.06
5b	44.23	600.46	528.48	17.50	5.98	0.87	0.15
5c	711.49	545.59	141.18	7.20	5.50	0.97	0.06

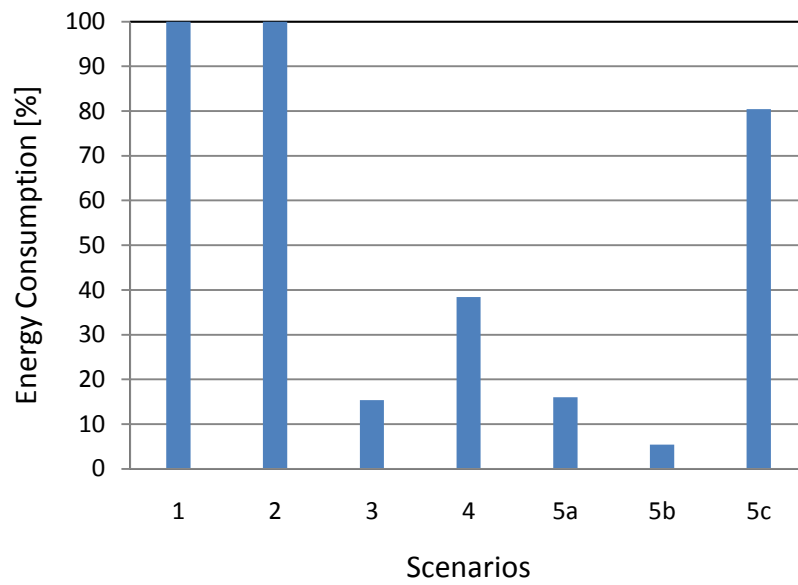


Figure 83 Ranking of the scenarios in terms of energy consumption [%] over a year.

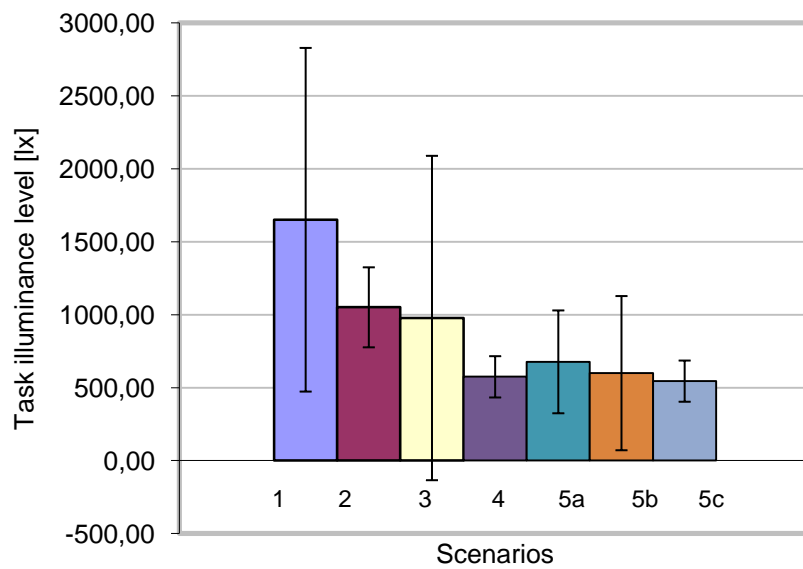


Figure 84 Ranking of the scenarios in terms of mean illuminance

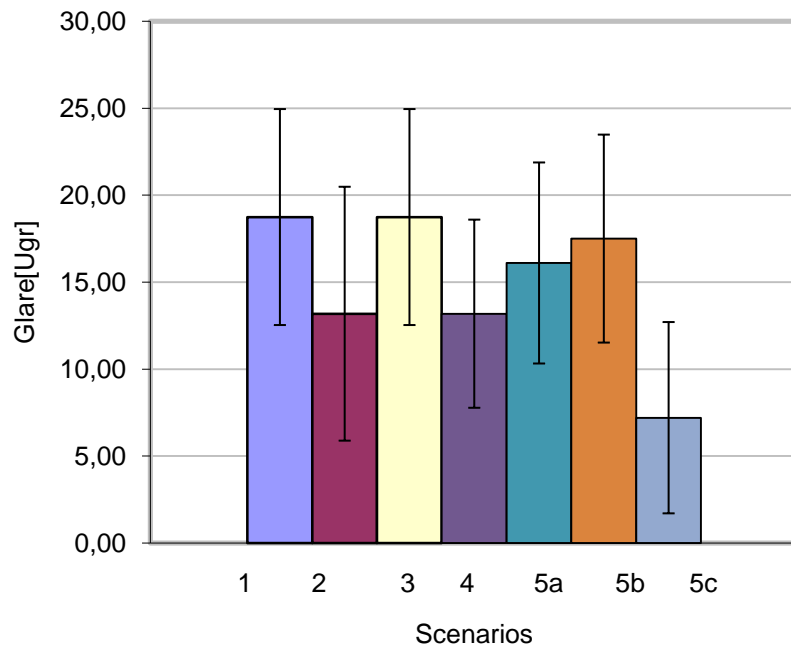


Figure 85 Ranking of the scenarios in terms of mean glare (UGR) indices

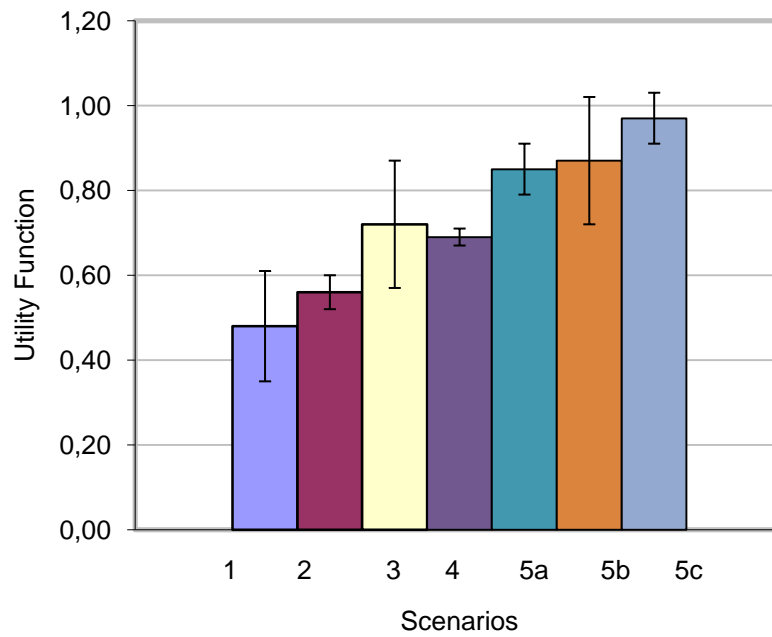


Figure 86 Ranking of the scenarios in terms of mean glare (UGR) indices

Simulation-assisted systems control compared to the other control scenarios (see table 16) show a number of advantages:

- i) The study shows the potential for energy use reduction using simulation-assisted lighting systems control. The savings vary based on the occupant's weight factor preferences. As figure 83 illustrates, the three cases with different weight factors show a variation in the energy use reduction.
- ii) The implementation of the simulation-assisted control strategies to achieve the objective functions, besides the energetic consideration, takes into account the provision of visual comfort. As figure 84 and 85 illustrate, the simulation-based control scenario minimizes the deviation of the average illuminance (E_m) on the working planes while reducing the glare index (see figure 85)
- iii) Simulation-assisted control systems show flexibility in dynamic determination of the weights (importance) of multiple performance indicators. The determination of the weights can be implemented by the users to facilitate transient changes in operational requirements.

5 Conclusion

5.1 Contribution

In the present work, the architecture and prototypical implementation of a simulation-assisted lighting and shading systems control in buildings is presented. To dynamically provide the context model to the simulation engine of the lighting control system, different methods were tested. The results warrant a number of conclusions (Dervishi and Mahdavi 2010a, 2010b, Mahdavi and Dervishi 2009, 2010):

For the generation of the sky luminance models, the present contribution compared computed irradiance values on four vertical surfaces with corresponding measurements based on the availability of the monitoring data. As the range of errors was rather high for all options simulation specialists must thus consider such order of magnitude in potential errors while making practically relevant inferences (e.g. design decisions) based on predicted values of incident solar radiation on building surfaces.

For the derivation of the illuminance data from more available irradiance data, four luminous efficacy models were tested for Vienna location. The results suggest that models the original versions of the models do not perform well for Vienna data, including the one, which has been proposed to function as a globally applicable model. However, once adapted to local context via modified sets of coefficients, all models show improved performance. In addition, luminous efficacy models showed noticeably higher for lower solar altitudes

The effectiveness of daylight simulation can be enhanced to support model-based lighting control applications. The prototypical implementation of such a model-based control approach was developed and tested in two test spaces, in a testbed of the building physics and building ecology laboratory and in room of a real office building in Styria, Austria. Developed to its full potential, the proposed system could offer a number of advantages: i) The use of virtual sensors can reduce the reliance on the physical sensors for performance

monitoring. ii) Physical sensors measure limited performance indicators (e.g., illuminance in case of lighting controls). On the other side, using virtual sensors more indicators can be considered (such as illuminance distribution, uniformity factors and various glare indices). iii) In a model-based control system, changes in rooms (e.g., remodeling, retrofit) can be digitally reflected in the building model. In this case, the need for extensive reconfigurations of physical sensory components is reduced. iv) integration of multiple systems (heating, cooling, ventilation, lighting, etc.) into a model-based control strategy can be achieved.

5.2 Future research

Further efforts and developments need to be involved to extend the methodology of the simulation-assisted lighting and shading systems control. (Mahdavi and Dervishi 2009, 2010, Dervishi and Mahdavi 2010a, 2010 b).

Additional experimental studies need to be carried out to further explore the statistical validity and significance of the results concerning the sky model generation. Moreover, the potential for alternative and locally calibrated sky model generation schemes are being explored. The improvement potential in the case of photographic sky scanning is likewise currently under investigation. Further study for the possibility of (and the necessary conditions for) developing more robust (globally applicable) luminance efficacy models need to be performed. Moreover, the validity of global luminous efficacy models for vertical (or any tilted) surfaces toward reliable derivation of incident illuminance levels is further being explored.

Future research and development challenges involve the integrated operation of multiple building systems, which requires full interoperability of control device communication protocols, high-resolution and seamless sensor and actuator networks, substantial computational power, and advanced search and optimization algorithms and methods. Consequently, ongoing work attempts to extend the methodology towards the integrated control of buildings lighting and thermal systems. Moreover, the scalability of the system and its self-

updating capability is to be improved via further implementation efforts involving longer operation runs with multiple environmental systems.

5.3 Publications

As of this writing, different portions and reports on the early stages of the work have been published in the following articles:

Mahdavi A, Dervishi S. 2010. Approaches to computing irradiance on building surfaces. *Journal of Building Performance Simulation*, Vol. 3 (2); pp. 129 - 134.

Dervishi S, Mahdavi A. 2010. Recent implementation efforts in simulation-powered lighting and shading systems controls in buildings"; 10th REHVA World Congress, Antalya; 09.05.2010 - 12.05.2010; in: "clima 2010 - 10th REHVA World Congress", 8 S.

Dervishi S, Mahdavi A. 2010. A simple Method for the Derivation of Illuminance Values from Radiance Data"; *BauSim2010 - Building Performance Simulation in a Changing Environment*, Technische Universität Wien; 22.09.2010-24.09.2010; in: "BauSim 2010 - Building Performance Simulation in a Changing Environment", A, ISBN: 978-3-85437-317-9; S. 495 - 498.

Mahdavi A, Dervishi S. 2009. A new model-based approach to lighting systems control in buildings. 4th International Building Physics Conference, Istanbul; 15.06.2009 - 18.06.2009; in: "Energy Efficiency and New Approaches", ISBN: 9789755613505; S. 719 - 723.

Mahdavi A, Dervishi S, Orehounig K. 2008. A feed forward scheme for building systems control"; *ECPPM - eWork and eBusiness in architecture, Engineering and Construction*, Sophia Antipolis, Frankreich; 10.09.2008 - 12.09.2008; in: "ECPPM 2008 eWork and eBusiness in Architecture, Engineering and Construction", (2008), ISBN: 978-0-415-48245-5; S. 381 - 387.

Mahdavi A, Dervishi S, Spasojevic B: "Computational Derivation of incident irradiance on building facades based on measured global horizontal irradiance data"; in: "BauSIM2006 (IBPSA) "Energieeffizienz von Gebäuden und Behaglichkeit in Räumen"", R. Koenigsdorff, C. van Treeck (Hrg.); Eigenverlag TU München, München, 2006, ISBN: 3-00-019823-7, S. 123 - 125.

Mahdavi, K. Orehounig, C. Pröglhöf, S. Dervishi. 2009. A new approach to passive cooling via natural ventilation"; Vortrag: Healthy Buildings 2009, Syracuse, USA; 13.09.2009 - 17.09.2009; in: "Healthy Buildings 2009", E.A. Bogucz et al. (Hrg.); Eigenverlag, - Paper-Nr. 37, 4 S.

Mahdavi A, Schuss M, Suter G, Metzger A.S., Camara S., Dervishi S. 2009. Recent advances in simulation-powered building systems control, Vortrag: Building Simulation 2009, University of Strathclyde, Glasgow; 27.07.2009 - 30.07.2009; in: "Building Simulation 2009", L.B. McElroy, J.S. Turley (Hrg.); 7 S.

6 References

Aydinli S, Krochman J. 1983. Data on daylight and solar radiation. Draft for CIE TC, Vol. 4 pp. 22.

Chang S, Mahdavi A. 2002. A hybrid system for daylight responsive lighting control. Journal of the Illuminating Engineering Society, Vol. 31, pp. 147 – 157.

Chirarattananon S. et al. 2007. Evaluation of vertical illuminance and irradiance models against data from north Bangkok. Building and Environment, Vol. 42, pp. 3894–3904.

Choi A S, Song K D, Kim Y.-S. 2005. The characteristics of photosensors and electronic dimming ballasts in daylight responsive dimming systems. Building and Environment, Vol. 40, pp. 39–50.

Chung T.M. 1992. A study of luminous efficacy of daylight in Hong Kong. Energy and Buildings, Vol. 19, pp. 45–50.

CIE Natural daylight, Official recommendation. 1955. Compte Rendu CIE 13th Session 1955, Committee E-3.2, vol. 2 (3), pp. 35–37.

CIE Standardization of Luminance Distribution on Clear Skies. 1973. Pub. CIE 22-1973 (TC-4.2).

CIE Spatial distribution of daylight. 1994. Luminance distributions of various reference skies. Pub. CIE No. 110. ISBN 3 900 734 52 6.

CIE, 2003. ISO 15469:2004/CIE S011/E-2003 Spatial distribution of daylight-CIE standard general sky.

Danny H.W. Li, Chris C.S. Lau, Joseph C. Lam. 2005. Predicting daylight illuminance on inclined surfaces using sky luminance data. *Energy and buildings*, Vol. 30, pp. 1649–1665

Darula S. and Kittler R. 2002. CIE Sky Standard defining luminance distributions. *Proceedings of eSim*, September 2002.

Dervishi S, Mahdavi A.: "A simple Method for the Derivation of Illuminance Values from Radiance Data"; Vortrag: BauSim2010 - Building Performance Simulation in a Changing Environment, Technische Universität Wien; 22.09.2010 - 24.09.2010; in: "BauSim 2010 - Building Performance Simulation in a Changing Environment", A. Mahdavi, B. Martens (Hrg.); Eigenverlag, Wien (2010), ISBN: 978-3-85437-317-9; S. 495 - 498.

Dervishi S, Mahdavi A. 2010. Recent implementation efforts in simulation-powered lighting and shading systems controls in buildings"; 10th REHVA World Congress, Antalya; 09.05.2010 - 12.05.2010; in: "clima 2010 - 10th REHVA World Congress", 8 S.

Duffie JA, Beckman WA. 1991. *Solar Engineering of Thermal Processes*, 2nd edn. New York: Wiley. Igawa N, Nakamura H, Matsuura K (1999). Sky Luminance Distribution Model for Simulation of Daylit Environment. In: *Proceedings of Sixth International IBPSA Conference*, Kyoto, Japan, Vol. 2, pp. 969 – 975.

Ehrlich C, Papamichael K, Lai J, Revzan K. 2002 A method for simulating the performance of photosensor-based lighting controls *Energy and buildings*, Vol. 34, pp. 883-889

European Commission. 2009. *Low energy buildings in Europe: current state of play, definitions and best practice*, Brussels.
http://ec.europa.eu/energy/efficiency/doc/buildings/info_note.pdf

Gwinner E A, Hau.M, Heigl. S. 1997. Melatonin: next term Generation and Modulation of Avian Circadian Rhythms Brain Research Bulletin, Vol. 44 (4), pp. 439-444

Hay JE, Davies JA. 1980. Calculation of the solar radiation incident on an inclined surface. In: Hay JE, Won TK, editors. Proceedings of the first Canadian solar radiation data workshop. Toronto, pp. 59–72.

Holick. M. F. 2010. Vitamin D: Extraskkeletal Health Endocrinology & Metabolism Clinics of North America, Vol. 39 (2), pp. 381-400

İçoğlu O. & Mahdavi A. 2007. VIOLAS: A vision-based sensing system for sentient building models. Automation in Construction. Volume 16 (5), pp.685 – 712.

Igawa N, Nakamura H, Matsuura K. 1999. Sky luminance distribution model for simulation of daylight environment, Proceedings of Building Simulation, Vol. 99, pp. 969–75.

Igawa N, Nakamura H, Koga Y, Kojo S. 1997. Relation between the indexes of sky conditions and luminance distribution — A study on classification method of sky luminance distribution, Part 2. Journal of Architectural and Environmental Engineering, AIJ, Vol. 496, pp: 23–28.

International Energy Agency (IEA). 2008. Energy efficiency requirements in building codes, energy efficiency policies for new buildings. France.

http://www.iea.org/g8/2008/Building_Codes.pdf

Kasten F. 1993. Discussion on the relative air mass. Light Res Technology, Vol. 25, pp. 129.

Kittler R. 1967. Standardization of the outdoor conditions for the calculation of the daylight factor with clear skies. In: Proceedings of the CIE international conference on sunlight in buildings, Bouwcentrum, Rotterdam, pp. 273–286.

Kittler R. 1985. Luminance distribution characteristics of homogeneous skies: a measurement and prediction strategy. *Lighting Research and Technology*, Vol. 17(4), pp.183–8.

Kittler R, Perez R, Darula S.1997. A new generation of sky standards. In: Proceedings of the LUX Europa conference, Amsterdam, pp. 359–73.

Klucher T.M. 1979. Evaluation of models to predict insolation on tilted surfaces. *Solar Energy*, Vol. 23 (2), pp. 111–114.

Leslie R.P. 2003. Capturing the daylight dividend in buildings: why and how? *Building and Environment*, Vol. 38, pp. 381 – 385.

Littlefair P.J. 1998. Measurements of the luminous efficacy of daylight. *Lighting Research and Technology* 1988, Vol. 20, pp. 177–188.

Li D.H.W, Lam J.C. and Lau C.C.S. 2002. A new approach for predicting vertical global solar irradiance. *Renewable Energy*, Vol. 25, pp. 591–606.

Li DHW, Lam JC. 2000. Measurements of solar radiation and illuminance on vertical surfaces and daylighting implications. *Renewable Energy*, Vol. 20 (4), pp. 389–404.

Littlefair P J. 1998. Predicting lighting energy use under daylight linked lighting controls, *Building Research & Information*, Vol. 26 (4), pp. 208–222.

Littlefair J. 1994. A comparison of sky luminance models with measured data from Garston, United Kingdom. *Solar Energy*, Vol. 53, pp. 315–322.

Littlefair PJ. 1981. The luminance distribution of an Average sky. *Lighting Research and Technology*, Vol. 13(4), pp.192–198.

Moon P, Spencer DE. 1942. Illumination from a non-uniform sky. *Illumination Engineering (N.Y.)*, Vol. 37, pp. 707–726.

Mahdavi A, Dervishi S. 2010. An empirically-based global luminous efficacy model for Vienna, Austria. Internal Report. Department of Building Physics and Building Ecology. Vienna University of Technology, Austria.

Mahdavi A, Dervishi S. 2010. Approaches to computing irradiance on building surfaces. *Journal of Building Performance Simulation*, Vol. 3 (2); pp. 129 - 134.

Mahdavi A, Dervishi S. 2009. A new model-based approach to lighting systems control in buildings. 4th International Building Physics Conference, Istanbul; 15.06.2009 - 18.06.2009; in: "Energy Efficiency and New Approaches", ISBN: 9789755613505; S. 719 - 723.

Mahdavi A, Dervishi S, Orehounig K. 2008. A feed forward scheme for building systems control"; ECPPM - eWork and eBusiness in architecture, Engineering and Construction, Sophia Antipolis, Frankreich; 10.09.2008 - 12.09.2008; in: "ECPPM 2008 eWork and eBusiness in Architecture, Engineering and Construction", (2008), ISBN: 978-0-415-48245-5; S. 381 - 387.

Mahdavi A, Dervishi S, Spasojevic B: "Computational Derivation of incident irradiance on building facades based on measured global horizontal irradiance data"; in: "BauSIM2006 (IBPSA) "Energieeffizienz von Gebäuden und Behaglichkeit in Räumen"", R. Koenigsdorff, C. van Treeck (Hrg.); Eigenverlag TU München, München, 2006, ISBN: 3-00-019823-7, S. 123 - 125.

Mahdavi, K. Orehounig, C. Pröglhöf, S. Dervishi. 2009. A new approach to passive cooling via natural ventilation"; Vortrag: Healthy Buildings 2009,

Syracuse, USA; 13.09.2009 - 17.09.2009; in: "Healthy Buildings 2009", E.A. Bogucz et al. (Hrg.); Eigenverlag, - Paper-Nr. 37, 4 S.

Mahdavi A, Schuss M, Suter G, Metzger A.S., Camara S., Dervishi S. 2009. Recent advances in simulation-powered building systems control, Vortrag: Building Simulation 2009, University of Strathclyde, Glasgow; 27.07.2009 - 30.07.2009; in: "Building Simulation 2009", L.B. McElroy, J.S. Turley (Hrg.); 7 S.

Mahdavi A. 2008. Predictive simulation-based lighting and shading systems control in buildings. Building Simulation, Vol. 1 (1), pp. 25–35.

Mahdavi A, Dervishi S, and Spasojevic B. 2006. Computational derivation of incident irradiance on building facades based on measured global horizontal irradiance data. In: R. Koenigsdorff and C. van Treeck, eds. Energieeffizienz Gebäuden und Behaglichkeit in Räumen, BauSIM2006 (IBPSA). München: Eigenverlag TU München, pp. 135–137.

Mahdavi A. 2004. Self-organizing models for sentient buildings. In: Malkawi A, Augenbroe G (eds), Advanced Building Simulation, New York: Spon Press, pp. 159 – 188.

Mahdavi A. 2003a. Computational building models: Theme and four variations (keynote). In Building Simulation '03: Proceedings of the Eighth International IBPSA Conference, Vol.1, pp. 3-18.

Mahdavi A. 2003b. Modell-basierte Steuerungsstrategien für selbstbewusste Gebäude. Gesundheits Ingenieur. Vol. 5, pp. 234-244. Oldenbourg Industrieverlag, Munich.

Mahdavi A. 2001a. Aspects of self-aware buildings. International Journal of Design Sciences and Technology. Vol.9 (1), pp. 35-52.

Mahdavi A. 2001b. Simulation-based control of building systems operation. *Building and Environment*, Vol. 36 (6), pp. 789 – 796.

Mahdavi A, Spasojević B, Brunner K. 2005. Elements of a simulation-assisted daylight-responsive illumination systems control in buildings. In *Building Simulation 2005: Proceedings of the Ninth IBPSA Conference*, Vol. 2, pp. 693-699.

Mahdavi A, Spasojević B. 2007. Incorporating Simulation into Building Systems Control Logic. In: Zhao B et al. (eds), *Proceedings of the 10th International Building Performance Simulation Association Conference and Exhibition (BS2007)*, Beijing, China, pp. 1175 – 1181.

Mahdavi A, Icoğlu O, Camara S. 2007. Vision-Based Location Sensing and Self-Updating Information Models for Simulation-Based Building Control Strategie. In: Zhao B et al. (eds), *Proceedings of the 10th International Building Performance Simulation Association Conference and Exhibition*, Beijing, China, pp. 1291 – 1298.

Mahdavi A, Tsiopoulou C, Spasojević B (2006). Generation of detailed sky luminance maps via calibrated digital imaging, In: Koenigsdorff R, van Treeck C (eds), *Energieeffizienz von gebäuden und Behaglichkeit in Räumen, BauSIM2006 (IBPSA)*, Eigenverlag TU München, München, pp. 135 – 137.

Mahdavi A, İçoğlu O, Camara S. 2007. Vision-Based Location Sensing and Self-Updating Information Models For Simulation-Based Building Control Strategy. *Proceedings of the 10th International Building Performance Simulation Association*", B. Zhao et al. (Editors), Beijing, China.

Mahdavi A, Chang S, Pal V. 1999. Simulation-based integration of contextual forces into building systems control. In *Building Simulation '99: Proceedings of the Sixth International IBPSA Conference*, Vol 1, pp. 193-199

Temps RC, Coulson KL. 1997. Solar radiation incident upon slopes of different orientations. *Solar Energy*, Vol. 19(2), pp. 179–84.

Mardaljevic J. 2004. Daylight simulation: validation, sky models and daylight coefficients. Thesis (PhD). De Montfort University, Leicester, UK.

Mardaljevic J. 1999. Daylight Simulation: Validation, Sky Models and Daylight Coefficients. PhD Dissertation. Institute of Energy and Sustainable Development, De Montfort University, Leicester, UK.

Moon P. and Spencer D.E. 1942. Illumination from a nonuniform sky. *Illumination Engineering*, Vol. 37 (10), pp. 707–726.

Munier T, Kinghorn D. 1997. Luminous efficacy of solar irradiance: improved models. *Lighting Research and Technology*, Vol. 29, pp. 185.

Nabil A, Mardaljevic J. 2005. Useful daylight illuminance: a new paradigm for assessing daylight in buildings. *Lighting Research Technology*, Vol. 37: pp. 41 – 57.

Nakamura H, Oki M, Hayashi Y. 1985. Luminance distribution of intermediate sky. *Journal of Light and Visual Environment*, Vol. 9(1), pp. 6–13.

Perez R, Seals R, Michalsky J. 1993. All Weather Model for sky luminance distribution—preliminary configuration and validation. *Solar Energy*, Vol. 50 (3), pp. 235–45.

Perez R. Seals R. and Michalsky J. 1993. All-weather model for sky luminance distribution—preliminary configuration and validation. *Solar Energy*, Vol. 50 (3), pp. 235–245.

Perraud M. 1988. Luminance models. National Lighting Conference, Cambridge, p. 291–292.

Perez R, Ineichen P, Seals R, Michalsky J, Stewart R. 1990. Modeling daylight availability and irradiance components from direct and global irradiance. *Solar Energy*, Vol. 44, pp. 271-289.

Rea MS, Bullough JD, Figueiro MG. 2001. Human melatonin suppression by light: a case for scotopic efficiency, *Neuroscience Letters*, Vol.299, pp.45–48.

Reindl D.T, Beckam W.A, Duffie J.A. 1990. Diffuse fraction correlations. *Solar Energy*, Vol. 45 (1), pp. 1–7.

Robledo L, Soler A. 2000. Luminous efficacy of global solar radiation for clear skies. *Energy Conversion and Management*, Vol. 41, pp. 1769.

Robledo L, Soler A, Ruiz E. 2001. Luminous efficacy of global solar radiation on a horizontal surface for overcast and intermediate skies. *Theoretical and Applied Climatology*, Vol. 69, pp. 123–134.

Roisin B, Bodart M, D’Herdt P. 2008. Lighting energy savings in offices using different control systems and their real consumption. *Energy and Buildings*, Vol. 40, pp. 514–523

Roy G.G, Hayman S, and Julian W. 1998. Sky modelling from digital imagery. ARC Project A89530177. Final Report. The University of Sydney and Murdoch University, Australia.

Roy GG, Hayman S, Julian W. 1998. Sky Modeling from Digital Imagery. ARC Project A89530177, Final Report. The University of Sydney, Murdoch University, Australia, 72 pages.

Ruiz E, Soler A, Robledo L. 2001. Assessments of Muneer’s Luminous Efficacy Models in Madrid and a proposal for new models based on his approach. *J Sol Energy Eng, Trans ASME*, Vol. 123, pp. 220–224.

Spasojević B. and Mahdavi A. 2005. Sky luminance mapping for computational daylight modelling. In: Building Simulation, Proceedings of the Ninth international IBPSA conference, Vol. 3, pp. 1163–1169.

Spasojević B. and Mahdavi A. 2007. Calibrated sky luminance maps for advanced daylight simulation applications. In: Building Simulation 2007: Proceedings of the 10th International Building Performance Simulation Association Conference, Beijing, China. ISBN: 0-9771706-2-4.

Spasojević B, Mahdavi A (2007). Calibrated Sky Luminance Maps For Advanced Daylight Simulation Applications. In: Zhao B et al. (eds), Proceedings of the 10th International Building Performance Simulation Association Conference and Exhibition (BS2007), Beijing, China, pp.1205 – 1210.

Ward Larson, G. and Shakespeare, R., 2003. Rendering with radiance: the art and science of lighting visualisation. Revised Edition. CA, USA: Space and Davis.

Ward G. 1994. The RADIANCE lighting simulation and rendering system. In: Proceedings of the 21st Annual Conference on Computer Graphics and Interactive Techniques (SIGGRAPH '94), pp. 459 – 472.

Webb Ann. R. 2006. Considerations for lighting in the built environment: Non-visual effects of light Energy and Buildings, Vol. 38, pp. 721-727

Wright J, Perez R, Michalsky J.J. 1989. Luminous efficacy of direct irradiance: variations with insolation and moisture conditions. Solar Energy, Vol. 42, pp. 387–394.

7 Appendix

7.1 Measurement Equipments

7.1.1 External

A microclimatic monitoring station is placed on the tower of university building, Vienna University of Technology. Table 1 shows details of the weather station instrument which monitors the external climate parameters. Table 2 shows detail of the pyranometer instrument (*GSM 10.7*) measuring the vertical global irradiance for north, east, south and west respectively. Table 3 shows details of the sunshine pyranometer instrument (SPN1) which measures the diffuse and global horizontal irradiance. Note that the sensor information of the instruments includes the range and accuracy respectively.

Table A 1 Monitored external climate parameters together with sensor information

Parameter	Symbol	Unit	Sensor range	Accuracy of sensor
Outdoor air temperature	Θ_e	° C	-30 to +70	$\pm 0,2$ °C
Outdoor relative humidity	RH	%	0 to 100	$\pm 2\%$
Wind speed	V	m.s ⁻¹	0,5 to 50	$\pm 0,5$ m/s
Wind direction	VD	°	0 to 360	$\pm 5^\circ$
Global horizontal irradiance	$I_{e,global, hor}$	W.m ⁻²	0 to 1300	$\pm 10\%$
Global horizontal illuminance	$E_{e,global, hor}$	lm.m ⁻²	0 to 130	$\pm 10\%$
Water precipitation		mm/mi n	0 to 7	$\pm 0,1$ mm
Air pressure		hPa	800 to 1060	$\pm 1,5$ hPa

Table A 2 Monitored vertical irradiance together with sensor information

Parameter	Symbol	Unit	Sensor range	Accuracy of sensor
Global vertical irradiance	$I_{e,global, hor}$	$W.m^{-2}$	0 to 1300	$\pm 10\%$

Table A 3 Monitored diffuse and direct horizontal irradiance together with sensor information

Parameter	Symbol	Unit	Sensor range	Accuracy of sensor
Diffuse horizontal irradiance	$I_{d,diffusel, hor}$	$W.m^{-2}$	0 to 2000	$\pm 5\%$
Global horizontal irradiance	$I_{e,global, hor}$	$W.m^{-2}$	0 to 2000	$\pm 5\%$

7.1.2 Internal

For the monitoring of the illuminance levels inside the space, illuminance sensors are placed. Table A4 shows details of a Minolta instrument (T10) which monitors the inside illuminance in terms of sensor range and accuracy.

Table A 4 Monitored global horizontal illuminance together with the sensor information

Parameter	Symbol	Unit	Sensor range	Accuracy of sensor
Illuminance	E	$lm.m^{-2}$	20 to 20,000 lux	$\pm 2\%$

7.2 Reindl Algorithm

This algorithm considers the following parameters: clearness index (kt), sun altitude (a), outdoor air temperature (Ta) and the relative humidity (f). The measurements of global horizontal irradiance, outdoor air temperature and the relative humidity were obtained from the weather station of the Department of Building Physics and Building Ecology of Vienna University of Technology. Reindl et al. identified three characteristic intervals for clearness index, defined

as the ratio of global horizontal to extraterrestrial radiation. Depending on clearness index value, the diffuse fractions (I_d/I) are calculated as per equations 16-18 (Reindl et al. 1990):

i) $0 \leq k_t \leq 0.3$ Constraint: $I_d/I \leq 1.0$

$$I_d/I = 1.00 - 0.232 + 0.0239 \sin(\alpha) - 0.000682 + 0.0195 \phi \quad (\text{Eq A.1})$$

ii) $0.3 \leq k_t \leq 0.78$ Constraint: $I_d/I \geq 0.1$ $I_d/I \leq 0.98$

$$I_d/I = 1.329 - 1.716 + 0.267 \sin(\alpha) - 0.00357 + 0.106 \phi \quad (\text{Eq A.2})$$

iii) $0 \leq k_t \leq 0.3$ Constraint: $I_d/I \geq 0.1$

$$I_d/I = 0.426 - 0.256 \sin(\alpha) - 0.00349 + 0.0734 \phi \quad (\text{Eq A.3})$$

where

I global horizontal irradiance

I_d diffuse horizontal irradiance

k_t clearness index

α sun altitude

T_a outdoor air temperature

f relative humidity

After having calculated diffuse fractions, diffuse horizontal irradiance and normal direct irradiance, are calculated as follows:

$$k_{\text{diff}} = I_d / I \quad (\text{Eq A.4})$$

$$I_d = I \times k_{\text{diff}} \quad (\text{Eq A.5})$$

$$I_{\text{bh}} = I - I_d \quad (\text{Eq A.6})$$

$$I_{\text{bn}} = I_{\text{bh}} / \sin(\alpha) \quad (\text{Eq A.7})$$

Where

k_{diff} global horizontal irradiance

I_{bh} direct horizontal irradiance

I_{bn} direct normal (beam) irradiance

T_a outdoor air temperature

7.3 Comparison of the vertical irradiance data

Figures A 1-A 20 illustrate the relationship between the computationally derived vertical irradiance values for all methods (vertical axis) and the measured vertical irradiance values (horizontal axis) for each orientation. Their correlation coefficient of their linear regression is defined. Figures A 1-A 4 illustrate the relationship between the computationally derived vertical irradiance values for DG-I method. Figures A 5-A 8 illustrate the relationship between the computationally derived vertical irradiance values for DG-P method. Figures A 9-A 12 illustrate the relationship between the computationally derived vertical irradiance values for G-I method. Figures A 13-A 16 illustrate the relationship between the computationally derived vertical irradiance values for G-P method. Figures A 17-A 20 illustrate the relationship between the computationally derived vertical irradiance values for C method.

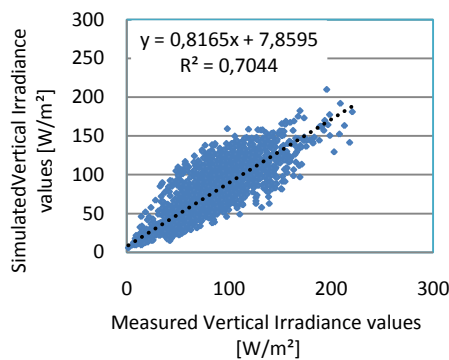


Figure A 1: Comparison of measured and simulated (method: DG-I) vertical irradiance values (North)

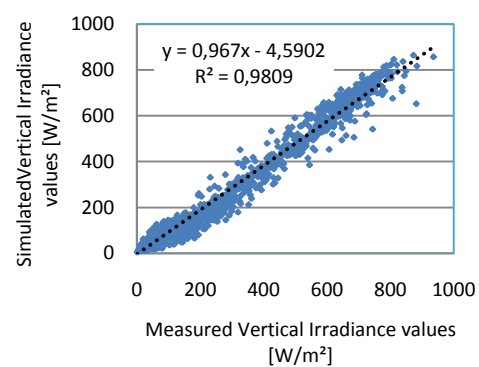


Figure A 2: Comparison of measured and simulated (method: DG-I) vertical irradiance values (East)

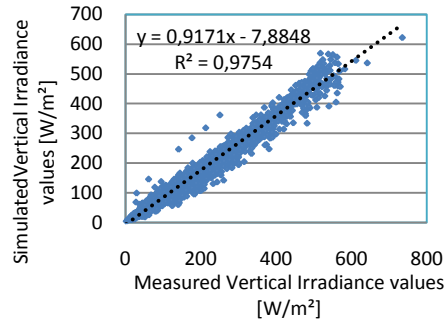


Figure A 3: Comparison of measured and simulated (method: DG-I) vertical irradiance values (South)

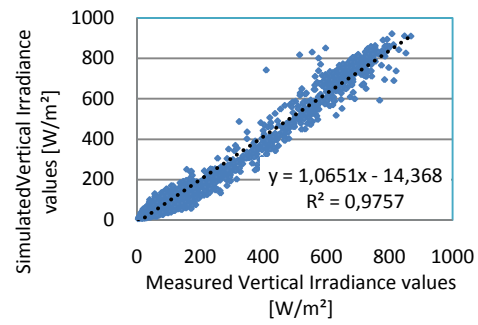


Figure A 4: Comparison of measured and simulated (method: DG-I) vertical irradiance values (West)

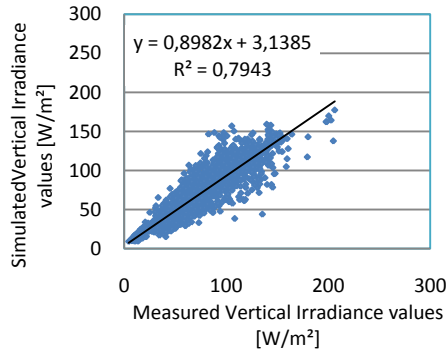


Figure A 5: Comparison of measured and simulated (method: DG-P) vertical irradiance values (North)

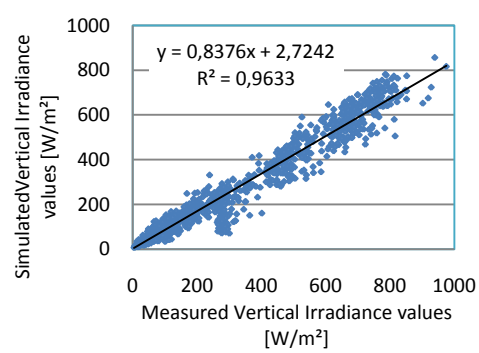


Figure A 6: Comparison of measured and simulated (method: DG-P) vertical irradiance values (East)

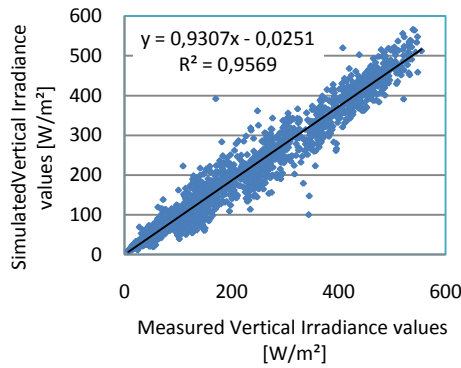


Figure A 7: Comparison of measured and simulated (method: DG-P) vertical irradiance values (South)

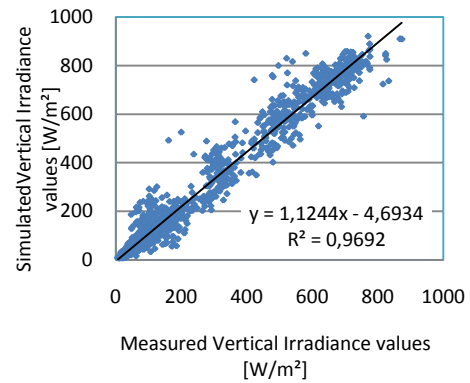


Figure A 8: Comparison of measured and simulated (method: DG-P) vertical irradiance values (West)

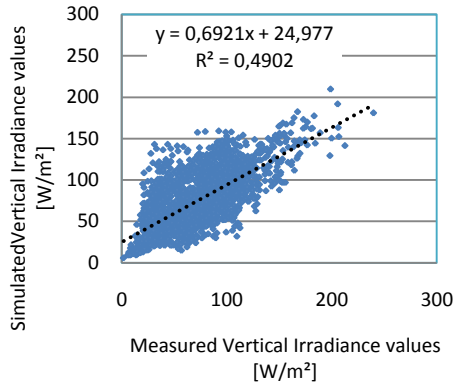


Figure A 9: Comparison of measured and simulated (method: G-I) vertical irradiance values (North)

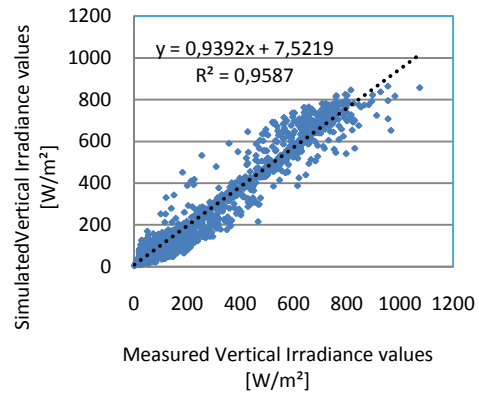


Figure A 10: Comparison of measured and simulated (method: G-I) vertical irradiance values (East)

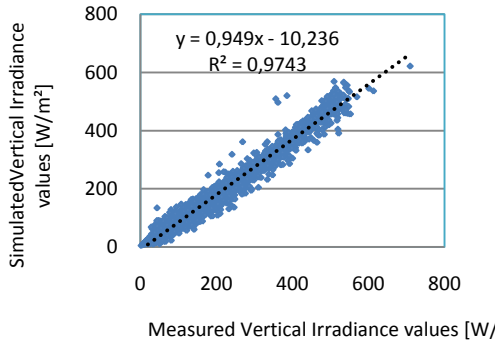


Figure A 11: Comparison of measured and simulated (method: G-I) vertical irradiance values (South)

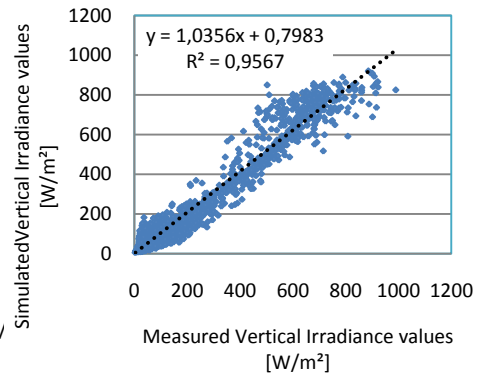


Figure A 12: Comparison of measured and simulated (method: G-I) vertical irradiance values (West)

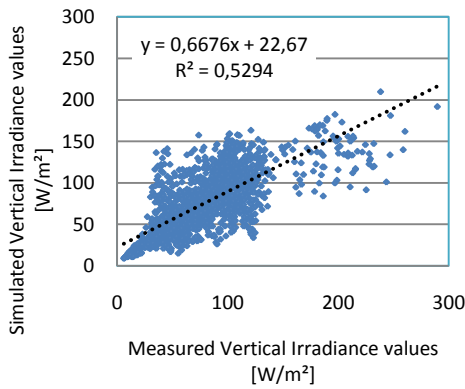


Figure A 13: Comparison of measured and simulated (method: C) vertical irradiance values (North)

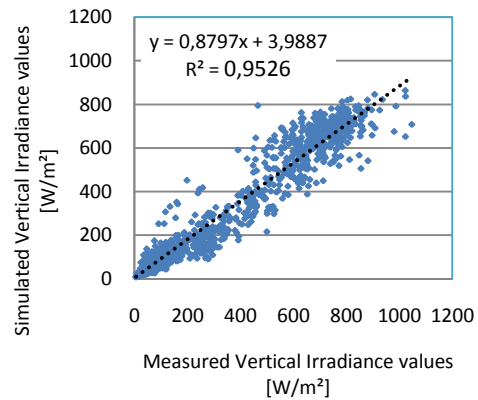


Figure A 14: Comparison of measured and simulated (method: C) vertical irradiance values (East)

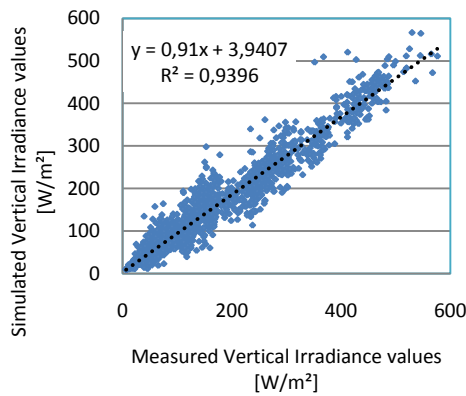


Figure A 15: Comparison of measured and simulated (method: C) vertical irradiance values (South)

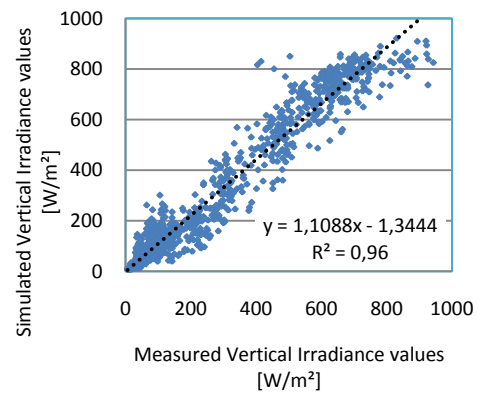


Figure A 16: Comparison of measured and simulated (method: C) vertical irradiance values (West)

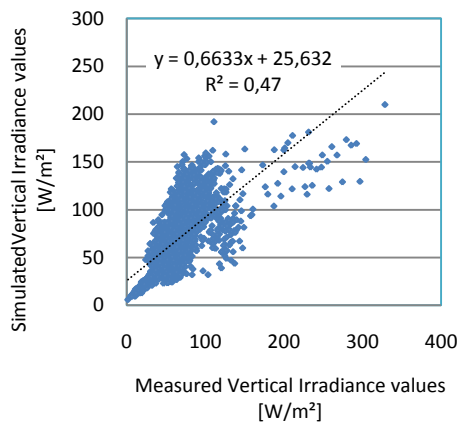


Figure A 17: Comparison of measured and simulated (method: C) vertical irradiance values (North)

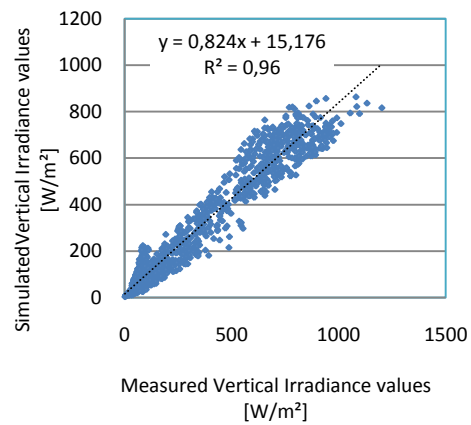


Figure A 18: Comparison of measured and simulated (method: C) vertical irradiance values (East)

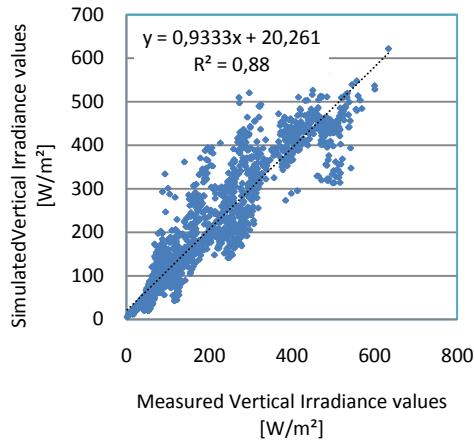


Figure A 19: Comparison of measured and simulated (method: C) vertical irradiance values (South)

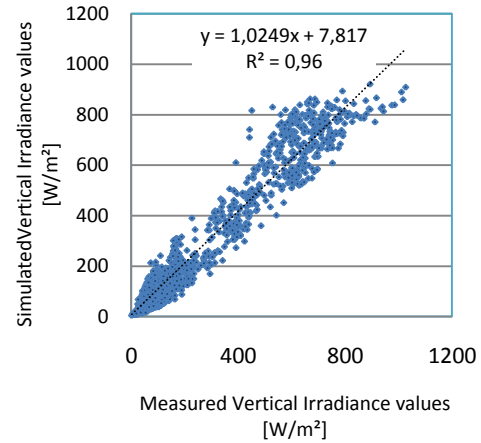


Figure A 20: Comparison of measured and simulated (method: C) vertical irradiance values (West)

7.4 Validation of the lighting system of the testbed

7.4.1 Validation due to the operation of Luminaires

As mentioned previously, it was possible to validate the predictions of the control system's embedded lighting simulator. Figure A 17-A 23 show a comparison of measured and simulated horizontal illuminance levels at 10 locations in the test room due to the operation of luminaire 1 and luminaire 2 for different dimming states (100%, 80%, 60% and 40%) respectively. Likewise, figure A 17, A 19, A 21, A 23 show a comparison of measured and simulated horizontal illuminance levels at the same 10 locations due to the luminaire 1 at different output levels (at 100%, 80%, 60%, 40%). Figure A 18, A 20, A 22, A 24 show a comparison of measured and simulated horizontal illuminance levels at the same 10 locations due to the luminaire 2 at different output levels (at 100%, 80%, 60%, 40%).

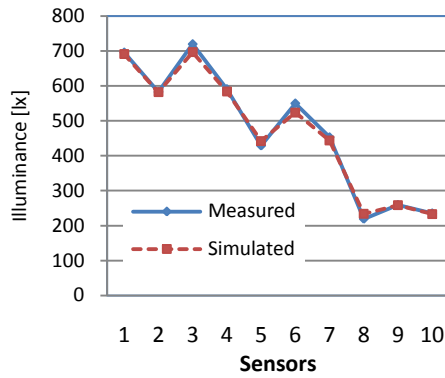


Figure A 21 Comparison of measured and simulated illuminance levels at 10 points in the test room due to the operation of luminaire 1 for light output level 100%.

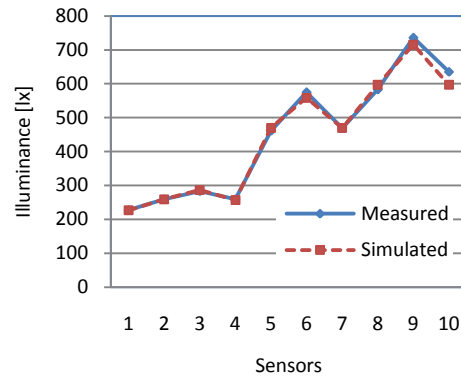


Figure A 22 Comparison of measured and simulated illuminance levels at 10 points in the test room due to the operation of luminaire 2 for light output level 100%.

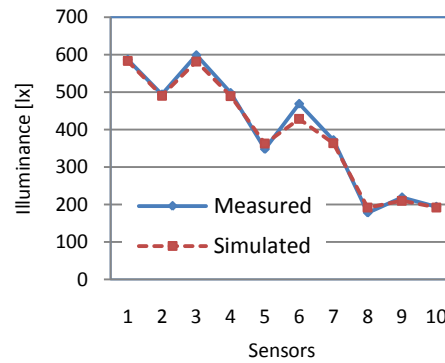


Figure A 23 Comparison of measured and simulated illuminance levels at 10 points in the test room due to the operation of luminaire 1 for light output level 80%.

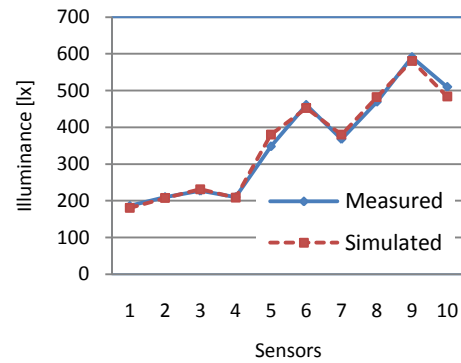


Figure A 24 Comparison of measured and simulated illuminance levels at 10 points in the test room due to the operation of luminaire 2 for light output level 80%.

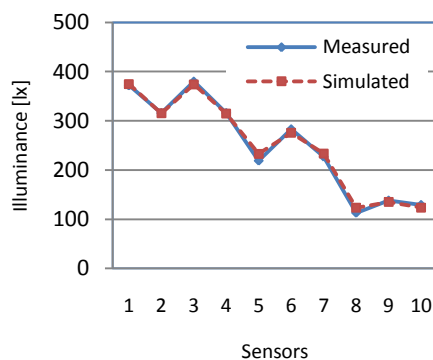


Figure A 25 Comparison of measured and simulated illuminance levels at 10 points in the test room due to the operation of luminaire 1 for light output level 60%.

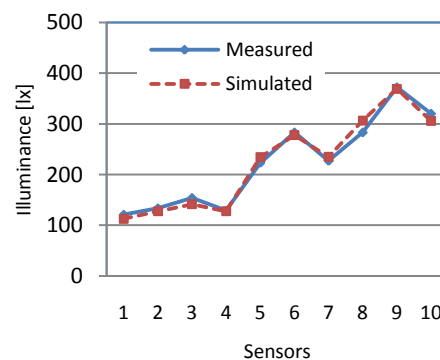


Figure A 26 Comparison of measured and simulated illuminance levels at 10 points in the test room due to the operation of luminaire 2 for light output level 60%.

output level 60%.

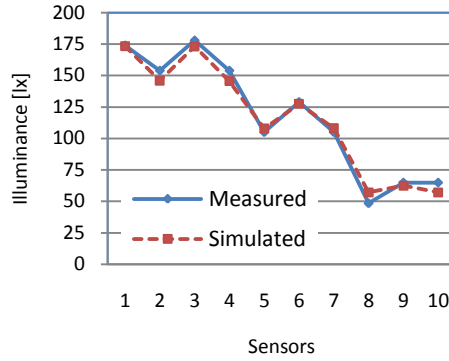


Figure A 27 Comparison of measured and simulated illuminance levels at 10 points in the test room due to the operation of luminaire 1 for light output level 40%.

output level 60%.

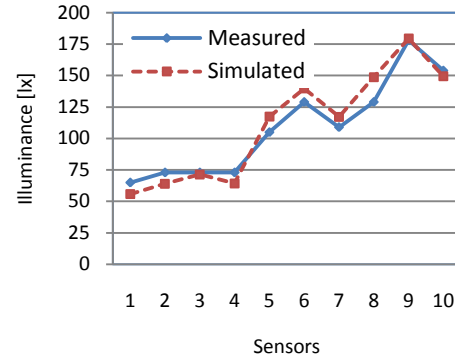


Figure A 28 Comparison of measured and simulated illuminance levels at 10 points in the test room due to the operation of luminaire 2 for light output level 40%.

7.4.2 Validation due to the operation of daylight emulator

Figure A 25-A 30 show a comparison of measured and simulated horizontal illuminance levels at 10 locations in the test room due to the operation of daylight emulator for two dimming states (100% and 50%) for different blind positions (100%, 80%, 60%, 40) respectively. Likewise, figure A 25, A 27, A 29, A 31 show a comparison of measured and simulated horizontal illuminance levels at the same 10 locations due to the daylighting emulator (at 100% output level) for different blind positions (100%, 80%, 60%, 40%). Figure A 26, A 28, A 30, A 32 show a comparison of measured and simulated horizontal illuminance levels at the same 10 locations due to the daylight emulator (at 50% output level) for different blind positions (100%, 80%, 60%, 40%).

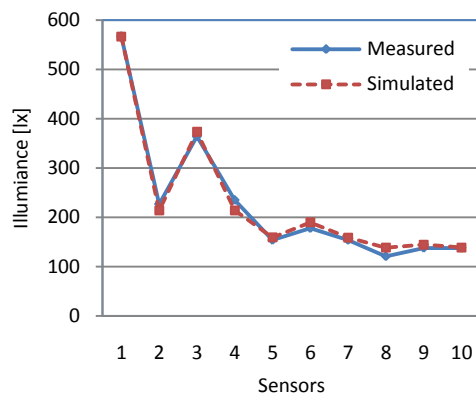


Figure A 29 Comparison of measured and simulated illuminance levels at 10 points in the test room due to the operation of Daylight Emulator for light output level 100%, blinds 100% open

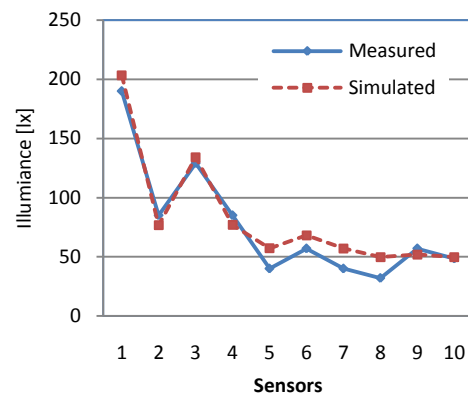


Figure A 30 Comparison of measured and simulated illuminance levels at 10 points in the test room due to the operation of Daylight Emulator for light output level 50%, blinds 100% open

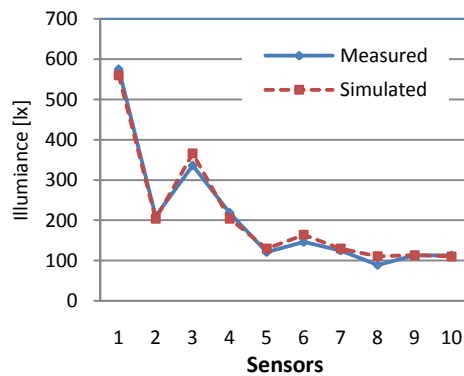


Figure A 31 Comparison of measured and simulated illuminance levels at 10 points in the test room due to the operation of Daylight Emulator for light output level 100%, blinds 80 % open

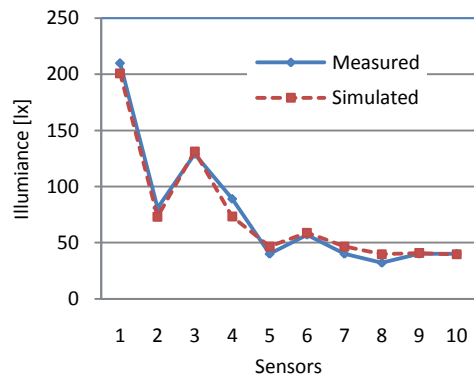


Figure A 32 Comparison of measured and simulated illuminance levels at 10 points in the test room due to the operation of Daylight Emulator for light output level 50%, blinds 80 % open

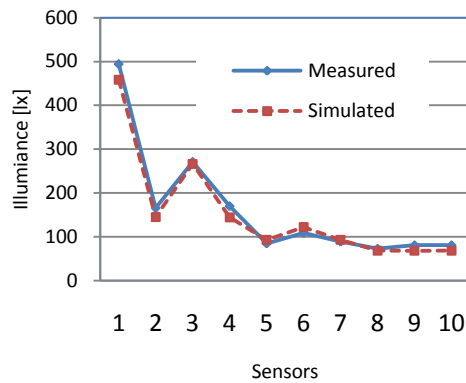


Figure A 33 Comparison of measured and simulated illuminance levels at 10 points in the test room due to the operation of Daylight Emulator for light output level 100%, blinds 60 % open

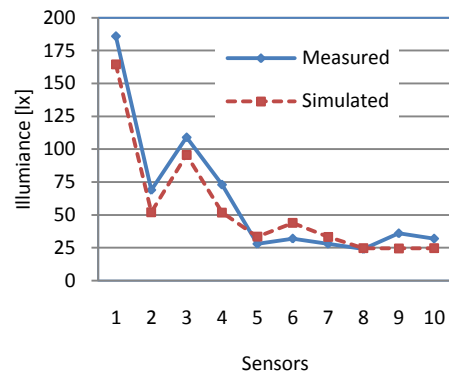


Figure A 34 Comparison of measured and simulated illuminance levels at 10 points in the test room due to the operation of Daylight Emulator for light output level 50%, blinds 60 % open

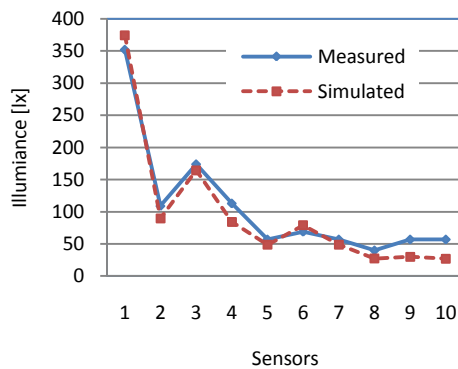


Figure A 35 Comparison of measured and simulated illuminance levels at 10 points in the test room due to the operation of Daylight Emulator for light output level 100%, blinds 40 % open

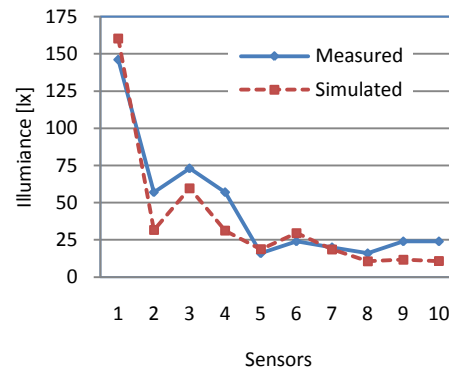


Figure A 36 Comparison of measured and simulated illuminance levels at 10 points in the test room due to the operation of Daylight Emulator for light output level 50%, blinds 40 % open

7.5 Ten-day operation of simulation-assisted lighting control in the testbed (scenario 1)

The following figure illustrates the performance of the prototypical implementation of simulation-assisted lighting systems control during 10 days of operation.

Figures A 37 shows the corresponding values of the external global illuminance and the values of the relevant control parameter (i.e., mean workstation illuminance level, derived as the arithmetical average of the illuminance at points E2, E3, and E4) over the course of the reference day for scenario 1. Figures A 38 shows the system's recommendations (the dimming position of the two luminaries and the deployment position of the blind) together with the resulting UF values over the course of the reference day (office hours) for scenario 1.

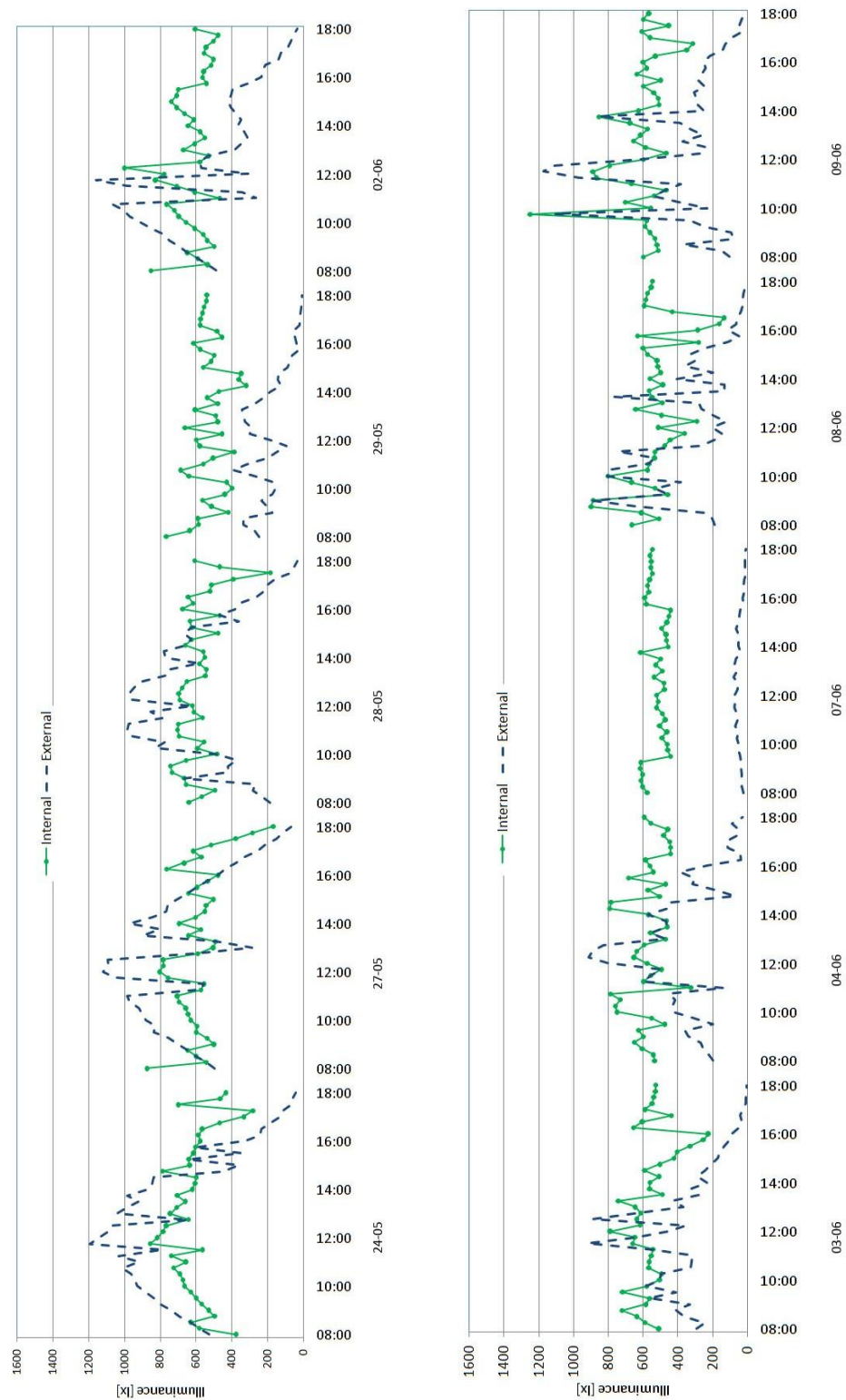


Figure A 37 Predicted values of the relevant control parameter (workstation illuminance level) together with the prevailing external global illuminance over a period of 10 days (Scenario 1)

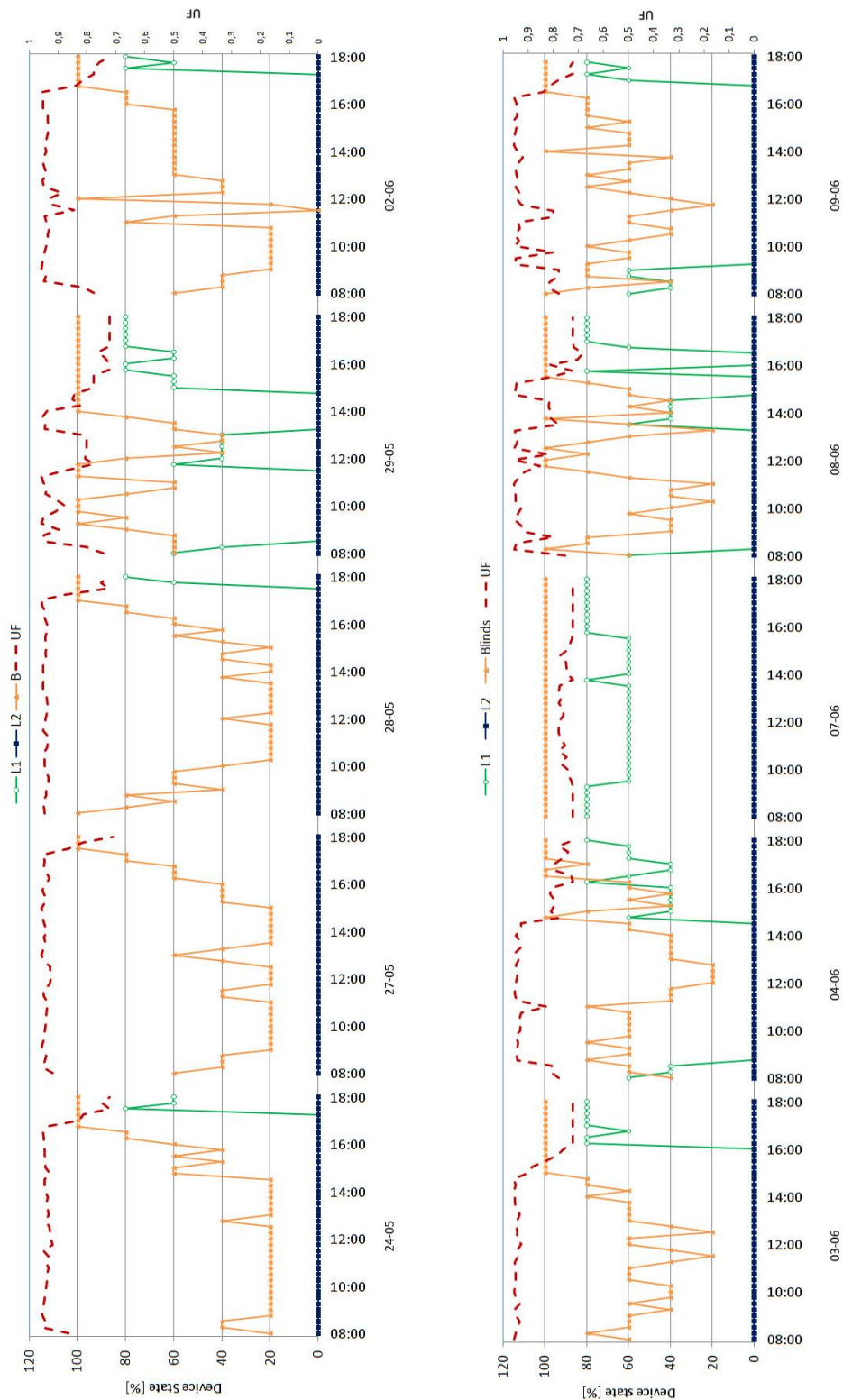


Figure A 38 Recommended states of lighting and shading devices together with the resulting UF values for a reference day over a period of 10 days (Scenario 1)

7.6 Example of sky radiance/luminance map

A typical .cal file describing the sky luminance distributions based on digital imaging for use within RADIANCE lighting simulation is described.

```
{ patchfile created by class bpi.sdbm.illuminance.SkyPatches on Fri May 21
12:26:11 CEST 2010}
{ 1174570176.jpg taken on Thu Mar 22 14:29:36 CET 2007
based on measured total luminance value: 70000
correction factor (CCF): 0.0
azimuth correction: 3.0 deg }
patchRad(i, j) = select (i*8 + j,

12.57114, 15.93833, 20.5916, 25.05738, 33.0272, 36.55085, 54.46453,
21.41117, 12.00424, 14.38721, 16.54963, 19.87235, 25.83789, 29.9979,
41.80765, 18.45344, 11.51016, 12.62391, 13.543, 16.01001, 21.33063,
23.90078, 30.44009, 18.7921,
10.78277, 11.06626, 11.40696, 13.0506, 16.29499, 18.18535, 23.98045,
19.28432, 10.20883, 10.19479, 9.95615, 10.64579, 13.45766, 15.10412,
20.80211, 20.55391, 9.88092, 8.95188, 8.62948, 9.40432, 12.11755, 14.62905,
19.38211, 20.53782,
9.62973, 8.26334, 8.02739, 8.41138, 10.54984, 15.1949, 19.55287, 24.89366,
8.9735, 7.56185, 7.10472, 8.08418, 9.70791, 16.67595, 26.3052,
22.64127, 8.63633, 7.34032, 6.54049, 7.19868, 8.86522, 16.00307, 45.63177,
22.62824,
8.37282, 6.89908, 6.41643, 7.14348, 8.8926, 15.08587, 36.68592, 22.21782,
8.24598, 6.65463, 6.31596, 6.8495, 9.07346, 20.40026, 32.07344,
26.07385, 0.01088, 6.57887, 6.11529, 6.88409, 10.80075, 34.62662, 36.06223,
33.75049,
8.00146, 6.93575, 6.40626, 7.49333, 10.05154, 18.31713, 33.79389, 34.44018,
8.04966, 6.86866, 6.91076, 7.96032, 11.01911, 16.54736, 29.94438,
35.12266, 8.1632, 6.98999, 7.20396, 8.16908, 11.5406, 17.67475, 35.16397,
32.77967,
8.46951, 7.418, 7.39642, 8.17308, 13.33537, 25.11252, 41.41372, 32.77265,
8.97761, 8.20637, 7.79119, 9.0515, 12.26701, 25.60808, 41.63596,
29.8725, 9.14113, 8.58153, 8.20874, 9.6272, 11.92992, 23.8619, 37.7656,
26.77656,
9.82611, 9.11526, 8.96124, 10.33292, 14.30576, 34.11056, 39.4161, 24.41844,
10.65241, 10.00294, 10.35979, 12.29431, 16.42332, 31.33861, 43.35088,
23.50666, 11.12467, 11.20257, 12.36684, 14.61513, 19.1041, 34.61468,
36.41724, 17.93389, 11.53083, 12.96535, 14.81848, 18.19931, 23.65232,
42.0827, 52.01908, 22.15017, 12.02725, 14.66664, 18.04362, 23.28294,
29.49062, 48.66361, 57.208, 23.56144, 12.65642, 16.64324, 22.19305,
30.32084, 36.91047, 50.83711, 69.12636, 20.23213,
13.05956, 18.81901, 27.22055, 39.55169, 48.80018, 58.2925, 74.78472,
30.86266, 13.36853, 20.52528, 32.48069, 48.50588, 64.55502, 72.02775,
```

```
82.27284, 27.16552, 13.72247, 21.59172, 36.41038, 54.92417, 75.25013,
89.09002, 91.7741, 35.60379,
13.75072, 22.07981, 38.12741, 61.75801, 97.41584, 19216.78312, 98.91491,
40.74786, 13.84746, 20.52731, 33.41499, 58.27445, 95.58284, 98.55037,
97.54668, 35.5992,
13.75959, 19.42335, 30.86732, 48.67552, 69.40524, 82.079, 94.29549,
31.46385, 13.07431, 18.53468, 27.92552, 43.74551, 56.81698, 68.2832,
86.55594, 27.33747, 12.60395, 17.33906, 25.03683, 34.04204, 45.68208,
48.95288, 69.58583, 21.7925,
0.0);
sectors = 32;
rings = 8;
sector_angle = 11.25; { angular width of a sector }
ring_angle = 11.25; { angular height of a ring }
azi_deg = min(359.999, Atan2(Dx,Dy) * 180/PI + 180); { azimuth measured
from south to west }
eta_deg = min(89.999, acos(Dz) * 180/PI); { eta measured from zenith }
sector_num = sectors - 1 - floor (azi_deg / sector_angle);
ring_num = floor (eta_deg / ring_angle) + 1;
skybr2 = patchRad(sector_num, ring_num);
```

CV Sokol Dervishi

Working Experience

- 2006- Project Assistant, Department of Building Physics and Building Ecology, Vienna University of Technology, Austria
- 2009- Visiting Lecturer, Faculty of Architecture and Engineering, Epoka University, Tirana-Albania
- 2006-2009 CEE Group, Vienna, Austria
- 2004 Istanbul Earthquake Masterplan Pilot Project in Zeytinburnu
In cooperation with Istanbul metropolitan initiative and in consultation with Earthquakes and Megacities initiative ("EMI")
- 2003 - 2004 Zambak Architecture office, Istanbul, Turkey

Research Area

Building physics, computational building performance simulation, sustainable design strategies.

Education

- 2006 - Doctoral Studies,
Department of Building Physics and Building Ecology, Vienna University of Technology, Austria
- 2004 -2006 MSc (Dipl.-Ing)
Building Science and Technology Master Program,
Department of Building Physics and Building Ecology, Vienna University of Technology, Austria
- 2000 -2004 Dipl. –Arch
Faculty of Architecture, Istanbul Technical University, Istanbul, Turkey

Awarded Honors

2004	High Honor Student Award Academic achievement. Sixth best ranked student (GPA 3.56 over 4.00) over 139 students, Faculty of Architecture, Istanbul Technical University, Istanbul- Turkey
2004	Rector's Award, ranking category Best foreign outstanding student, Istanbul Technical University, Istanbul-Turkey
2004	Istanbul Educational Institute (IEI) Award Best outstanding foreign student in universities-wide in Istanbul Istanbul-Turkey
2000	College Director Institution-Albanian National Biology Olympiad Award (excellent performance) Tirana- Albania